MITIGATION OF CO_2 GRAVITY OVERRIDE BY SOLVENT BLENDING

BY

KHALED HUSSEIN MUHAMMED AL-AZANI

A Thesis Presented to the
DEANSHIP OF GRADUATE STUDIES

KING FAHD UNIVERSITY OF PETROLEUM & MINERALS
DHAHRAN, SAUDI ARABIA

In Partial Fulfillment of the
Requirements for the Degree of

MASTER OF SCIENCE

In

PETROLEUM ENGINEERING

APRIL, 2019

KING FAHD UNIVERSITY OF PETROLEUM & MINERALS

DHAHRAN- 31261, SAUDI ARABIA

DEANSHIP OF GRADUATE STUDIES

This thesis, written by **Khaled Hussein Muhammed Al-Azani** under the direction of his thesis advisor and approved by his thesis committee, has been presented and accepted by the Dean of Graduate Studies, in partial fulfillment of the requirements for the degree of **MASTER OF SCIENCE IN PETROLEUM ENGINEERING.**

Dr. Sidqi Abu-Khamsin
(Advisor)

Dr. Dhafer Alshehri
Department Chairman

Dr. Abdullah Sultan
(Member)

Dr. Salam A. Zummo
Dean of Graduate Studies

Dr. Michael Fraim
(Member)

23/4/19

Date

© Khaled Hussein Muhammed Al-Azani

2019

DEDICATION

I dedicate this thesis with all my love to my father, my mother, my wife and my daughter Anhaar who always encourage me to work hard and continue the higher studies and whose prayers give me the strength and power throughout my life.

ACKNOWLEDGMENTS

In the name of Allah, Most Kind, Most Merciful. All Praise and thanks be to Allah alone, and His peace and blessings are upon his messenger and bondman our prophet Muhammed his family, his companions and his followers.

I would like to express my sincere gratitude to **my parents** who encouraged me to continue the Master's degree and whose prayers always give me the strength and power. I would like also to thank **my wife** and **my daughter Anhaar** for their patience on me to have the time to accomplish this work. I owe thanks to **my brother** Saddam and **my sisters** and other family members for their prayers and continuous support.

I would like also to express my deep appreciation to **Prof. Sidqi Abu-Khamsin**, who served as my major advisor, for his guidance and patience during the thesis work, and for his unforgettable and continuous encouragement and support. I am also grateful to **Dr. Abdullah Sultan**, who served as a committee member for this thesis work, for his assistance and support in all the aspects of this work especially support in getting the chemicals and making it easy for me to have the access to all the equipment used in this work. Sincere thanks are also due to thesis committee member **Dr. Michael Fraim** for his cooperation, comments and support. Special thanks are due to **Mr. Abdulsamad Idrisu**, whom I spent most of my time during my work in the laboratory, for training me on the PVT system and for assisting me in other aspects of this work. I am also thankful to **Mr. Lionel Fogang** who trained me on the core-flooding system.

I am also grateful **King Fahd University of Petroleum & Minerals (KFUPM)**, especially the **College of Petroleum Engineering and Geosciences (CPG)** for giving the opportunity and support to finish this research work and providing the required research facilities. Special thanks are due to the **Department of Petroleum Engineering** and the **Center for Integrative Petroleum Research (CIPR)** including Faculty, Staff, Fellow Graduate Students and friends who contributed directly or indirectly to accomplish this work. At the end, I am grateful to all my friends inside and outside KFUPM.

TABLE OF CONTENTS

ACKNOWLEDGMENTS ..... **V**

TABLE OF CONTENTS ..... **VII**

LIST OF TABLES ..... **XI**

LIST OF FIGURES ..... **XIII**

ABSTRACT ..... **XVII**

ملخص الرسالة ..... **XX**

CHAPTER 1 INTRODUCTION **1**

1.1 Stages of Oil Production **1**

1.2 Enhanced Oil Recovery Methods **2**

1.3 CO_2 Flooding for Enhanced Oil Recovery **4**

1.4 Carbon Dioxide Sources and Properties **5**

1.5 Minimum Miscibility Pressure **8**

1.6 CO_2 Displacement Mechanisms **10**

1.6.1 Miscible CO_2 Flooding **10**

1.6.2 Immiscible CO_2 Flooding **12**

1.7 Challenges in CO_2-EOR Process **13**

CHAPTER 2 LITERATURE REVIEW **15**

2.1 CO_2 Gravity Override Mitigation Techniques **15**

2.2 Studies on the Solubility of Different Chemicals with CO_2 ..... **18**

2.2.1 Studies on CO_2 Solubility with Different Solvents & Chemicals **19**

2.2.2 Studies on CO_2 Solubility with Ionic Liquids and Deep Eutectic Solvents 22

2.3 Laboratory Experiments to Evaluate CO_2 Flooding 29

CHAPTER 3 PROBLEM STATEMENT AND RESEARCH DESIGN 35

3.1 Problem Statement 35

3.2 Research Objectives 35

3.3 Research Project Methodology 36

3.4 Research Key Milestones 37

CHAPTER 4 EXPERIMENTAL WORK 38

4.1 Rocks and Fluids 38

4.1.1 Rock Core Samples 38

4.1.2 Gases 40

4.1.3 Crude Oil 40

4.1.4 Seawater 41

4.1.5 Selected Solvents 42

4.2 Solubility Measurement of CO_2 with the Selected Solvents 46

4.2.1 Experimental Apparatus 47

4.2.2 Experimental Procedure 49

4.3 Solvents Interaction Tests with Fluids and with Rocks 55

4.3.1 Oil and Water Miscibility Tests with the Solvents 55

4.3.2 Imbibition Test of Oil-Saturated Core Sample in TEC 57

4.4 Core-Flooding Experiments 57

4.4.1 Experimental Setup for Core-Flooding Experiments 58

4.4.2 Preparation of Live Oil 61

4.4.3 Estimation of CO_2 Minimum Miscibility Pressure 63

4.4.4 Core-Flooding Procedure 64

CHAPTER 5 RESULTS AND DISCUSSION 69

5.1 Results of CO_2 Solubility Measurement with the Solvents 69

5.1.1 Carbon Dioxide and Ethyl Benzoate 70

5.1.2 Carbon Dioxide and Triethyl Citrate 73

5.1.3 Discussion of Results from Solubility Measurements 78

5.2 Discussion of the Core Flooding Results 81

5.2.1 Run 1-DO: Displacing Dead Oil by Pure $scCO_2$ (Base Case) 81

5.2.2 Run 2-DO: Displacing Dead Oil by CO_2-TEC Blend 84

5.2.3 Run 1-LO: Displacing Live Oil by Pure $scCO_2$ 87

5.2.4 Run 2-LO: Displacing Live Oil by CO_2-TEC Blend 89

5.2.5 Comparison of the Results from All Flooding Runs 91

CHAPTER 6 CONCLUSIONS AND RECOMMENDATIONS 95

6.1 Conclusions 95

6.2 Recommendations 98

APPENDIX A DATA FROM SOLUBILITY EXPERIMENTS 99

A.1 CME Data for CO_2 - Ethyl Benzoate Systems 99

A.2 CME Data for CO_2 - Triethyl Citrate Systems 102

A.3 Prediction of Saturation Pressure Using PR-EOS 105

APPENDIX B DATA FROM CORE-FLOODING EXPERIMENTS 108

B.1 Data from Run 1-DO 108

B.2 Data from Run 2-DO 109

B.3 Data from Run 1-LO 110

B.4 Data from Run 2-LO 111

REFERENCES 112

VITAE 120

LIST OF TABLES

Table 2.1: Characteristics of Ionic Liquids (Adopted from Johnson [60]) 23

Table 2.2: Classifications of Ionic Liquids 28

Table 4.1: Properties of the Rock Samples Used in this Work 39

Table 4.2: Properties of the Crude Oil Used in this Work 41

Table 4.3: Results of SARA Analysis of the Used Crude Oil 41

Table 4.4: Composition of the Used Crude Oil 41

Table 4.5: Properties of the Seawater Used in this Work 42

Table 4.6: Ionic Composition of the Used Seawater 42

Table 4.7: Properties of CO_2 and Organic Solvents Used in this Work 43

Table 4.8: Composition of Associated Natural Gas with Saudi Arabian light Crude Oils versus the Composition of Gas Prepared in this Work 62

Table 5.1: CO_2-EB Saturation Pressure Results (Experimental and Predicted Using EOS) 70

Table 5.2: CO_2-TEC Saturation Pressure Results (Experimental and Predicted Using EOS) 74

Table 5.3: Summary of the Results Obtained from Flooding Run 1-DO 83

Table 5.4: Summary of the Results Obtained from Flooding Run 2-DO 85

Table 5.5: Summary of the Results Obtained from Flooding Run 1-LO 88

Table 5.6: Summary of the Results Obtained from Flooding Run 2-LO 90

Table 5.7: Summary of the Results from All Flooding Runs 94

Table A.1: Regressed Parameters Obtained after Best Prediction of Saturation Pressure Using PR-EOS 107

Table B.1: Recovery Data from Run 1-DO 108

Table B.2: Recovery Data from Run 2-DO 109

Table B.3: Recovery Data from Run 1-LO..... 110

Table B.4: Recovery Data from Run 2-LO..... 111

LIST OF FIGURES

Figure 1.1: Different EOR Techniques (adopted from Taber et al. [7]) 3

Figure 1.2: Range of Oil Gravity for Different EOR Methods [7] 4

Figure 1.3: Pressure-Temperature Phase Diagram of CO_2 7

Figure 1.4: Density (Left) and Viscosity (Right) of CO_2 versus Pressure at Different Temperatures [18] 7

Figure 1.5: Illustration of the Molecular Structure of CO_2 8

Figure 1.6: A Comparison of the Density (Left) and Viscosity (Right) of H_2S, CO_2, N_2, and CH_4 at 100 ℃ [18] 8

Figure 1.7: 1-D Schematic Showing the CO_2 Miscibility Process with Oil [13] 12

Figure 3.1: Key Milestones of Research Work 37

Figure 4.1: Molecular Structure of Ethyl Benzoate 44

Figure 4.2: Pressure-Temperature Phase Diagram for CO_2-EB Binary Systems Using PR-EOS 44

Figure 4.3: Molecular Structure of Triethyl Citrate 45

Figure 4.4: Pressure-Temperature Phase Diagram for CO_2-TEC Binary Systems Using PR-EOS 46

Figure 4.5: PVT 300/700 FV EDU from Sanchez Technology 48

Figure 4.6: Experimental Set-up for CO_2 Solubility Measurement 48

Figure 4.7: Experimental Setup for CO_2 Solubility Measurement 49

Figure 4.8: Example of the Observation form the Inside of the PVT Cell 54

Figure 4.9: Pressure of the PVT Cell versus its Volume for Determining the Saturation Pressure 54
Figure 4.10: Miscibility Test between (a) Oil and EB and (b) Oil and TEC at Ambient Conditions 56
Figure 4.11: Miscibility Test between TEC and Oil, TEC and Distilled Water and TEC and Seawater at 90 ℃ 56
Figure 4.12: Imbibition Test of Oil-Saturated Core Sample in TEC at Ambient Conditions 57
Figure 4.13: Core Flooding System (CFS 700) Manufactured by VINCI Technologies . 59
Figure 4.14: Schematic Diagram of the Core-Flooding System 60
Figure 4.15: CO_2 Analyzer Model 906 from Quantek Instruments 60
Figure 4.16: Graduated Cylinder Used for Fluid Collection During CO_2 Flooding..... 60
Figure 5.1: Saturation Pressure of CO_2-EB Blend versus Temperature for Different CO_2 Concentrations 71
Figure 5.2: Saturation Pressure of CO_2-EB Blend versus CO_2 Molar Concentration at Different Temperatures 71
Figure 5.3: Saturation Density of CO_2-EB Blend versus Saturation Pressure at Different Temperatures for Different CO_2 Concentrations 72
Figure 5.4: Density of CO_2-EB Blend versus Pressure at 100 ℃ for Different CO_2 Concentrations 73
Figure 5.5: Saturation Pressure of CO_2-TEC Blend versus Temperature for Different CO_2 Concentrations 74

Figure 5.6: Saturation Pressure of CO_2-TEC Blend versus CO_2 Molar Concentration at Different Temperatures 75
Figure 5.7: Saturation Density of CO_2-TEC Blend versus Saturation Pressure at Different Temperatures for Different CO_2 Concentrations 76
Figure 5.8: Density of CO_2-TEC Blend as a Function of Pressure at 100 ℃ for Different CO_2 Concentrations 77
Figure 5.9: Viscosity of CO_2-TEC Blend versus Pressure at 100 ℃ with 85 mol% CO_2 77
Figure 5.10: Comparison between Density Results of CO_2-TEC and CO_2-EB blends at 100 ℃ 81
Figure 5.11: Oil Recovery Factor and Oil Flow Rate versus PV of Injected Pure scCO_2 (Run 1-DO) 83
Figure 5.12: Oil Recovery Factor and Oil Flow Rate versus PV of Injected CO_2-TEC Blend (Run 2-DO)..... 85
Figure 5.13: Comparison of Oil Recovery Factor Obtained from Run 1-DO and Run 2-DO..... 86
Figure 5.14: Comparison of Oil Flow Rate Obtained from Run 1-DO and Run 2-DO.... 86
Figure 5.15: Oil Recovery Factor and Oil Flow Rate versus PV of Injected Pure scCO_2 (Run 1-LO)..... 88
Figure 5.16: Comparison of Oil Recovery Factor Obtained from Run 1-DO and Run 1-LO 89
Figure 5.17: Oil Recovery Factor and Oil Flow Rate versus PV of Injected CO_2-TEC Blend (Run 2-LO) 90

Figure 5.18: Comparison of Oil Recovery Factor Obtained from Run1-LO and Run 2-LO 91
Figure 5.19: Comparison of Oil Recovery Factor from All Flooding Runs 92
Figure 5.20: Comparison of All Parameters from All Flooding Runs 93
Figure A.1: CME Data for CO_2-EB Blend with 90 mol% CO_2 99
Figure A.2: CME Data for CO_2-EB Blend with 85 mol% CO_2 99
Figure A.3: CME Data for CO_2-EB Blend with 80 mol% CO_2 100
Figure A.4: CME Data for CO_2-EB Blend with 75 mol% CO_2 100
Figure A.5: CME Data for CO_2-EB Blend with 70 mol% CO_2 101
Figure A.6: CME Data for CO_2-EB Blend with 65 mol% CO_2 101
Figure A.7: CME Data for CO_2-TEC Blend with 90 mol% CO_2 102
Figure A.8: CME Data for CO_2-TEC Blend with 85 mol% CO_2 102
Figure A.9: CME Data for CO_2-TEC Blend with 80 mol% CO_2 103
Figure A.10: CME Data for CO_2-TEC Blend with 75 mol% CO_2 103
Figure A.11: CME Data for CO_2-TEC Blend with 70 mol% CO_2 104
Figure A.12: CME Data for CO_2-TEC Blend with 65 mol% CO_2 104
Figure A.13: Saturation Pressure of CO_2-EB Blend versus Temperature 105
Figure A.14: Saturation Pressure of CO_2-EB Blend versus CO_2 Molar Concentration . 105
Figure A.15: Saturation Pressure of CO_2-TEC Blend versus Temperature 106
Figure A.16: Saturation Pressure of CO_2-TEC Blend versus CO_2 Molar Concentration 106

ABSTRACT

Full Name: KHALED HUSSEIN MUHAMMED AL-AZANI

Thesis Title: MITIGATION OF CO_2 GRAVITY OVERRIDE BY SOLVENT BLENDING

Major Field: PETROLEUM ENGINEERING

Date of Degree: April, 2019

Injecting supercritical carbon dioxide ($scCO_2$) into the oil reservoirs is a proven enhanced oil recovery (EOR) method. This is due to the ability of $scCO_2$ to swell the oil, to decrease oil viscosity, and to lower oil interfacial tension (IFT). Some observations have also shown that $scCO_2$ can alter the rock wettability towards more water wetness, especially in carbonate reservoirs. Moreover, CO_2 gas is abundant all over the globe and its sources can be natural from underground reservoirs or anthropogenic resulting from human industrial activities.

Although carbon dioxide's density and viscosity are much higher than those of other gases employed in EOR operations, such as methane and nitrogen, especially at reservoir conditions, these properties of $scCO_2$ are still not high enough compared with those of reservoir fluids (e.g. oil and water). The contrast in the fluids' density leads to gravity segregation and the contrast in their viscosity leads to viscous fingering. Gravity segregation causes CO_2 gas to rise to the top of the reservoir and flow towards the producing wells especially in thick reservoirs with good vertical communication. Known as gravity override, this phenomenon is considered as the major factor resulting in poor reservoir sweep efficiency, early breakthrough and low oil recovery.

Many techniques have been proposed and tested for their effectiveness in CO_2 mobility and conformance control such as introducing a blocking agent such as foam, cross-linked polymers, and gels. However, such techniques are more effective in preventing fingering and thief zones than reducing gravity override. Also, no foaming agent has been identified to withstand the high temperatures and high salinities of Saudi Arabian reservoirs. Therefore, we have chosen densifying agents to add to the $scCO_2$ to reduce the gravity override effects.

After a scoping study of commercial solvents, two different solvents, namely triethyl citrate (TEC) and ethyl benzoate (EB), were identified and tested for their ability to blend with CO_2 for the purpose of producing blends with high densities, and, hence, minimizing the effect of gravity override. Solubility experiments between CO_2 and the selected solvents showed the ability of these solvents to blend with CO_2 at conditions close to typical reservoir conditions with resulting saturation pressures close to normal reservoir pressures at the reservoir temperatures. The results also showed that the densities of the resulting blends are close to those of resident reservoir fluids. Since TEC showed no or negligible solubility in crude oil or water, it was selected for the core flooding experiments.

High-permeability Indiana limestone core sample saturated with dead light crude oil from Saudi Arabia at irreducible water saturation was flooded vertically upwards with about one pore volume of pure $scCO_2$. The flood was carried out at 3,500 psia and 212 °F. The oil recovery at $scCO_2$ breakthrough was 14.82% of the initial oil in place and the final oil recovery was 60.14%. When the experiment was repeated with a CO_2-TEC blend of 85-mole percent (mol%) CO_2, the oil recovery at CO_2 breakthrough increased to 31.99% and the final oil recovery to 72.67%. The two experiments were then repeated with the same

crude oil but saturated with hydrocarbon gas at the same conditions. The pure scCO_2 flood yielded breakthrough and final oil recoveries of 15.19% and 49.13%, respectively, while the CO_2-TEC blend flood yielded breakthrough and final oil recoveries of 27.06% and 67.89%, respectively.

The results of these experiments demonstrate the ability of CO_2-TEC blend to minimize the effect of gravity override as shown by delayed gas breakthrough and higher oil recovery. This is true for both dead and live oils. The results also show how natural gas dissolved in the oil can diminish the effectiveness of a CO_2 flood.

ملخص الرسالة

الاسم الكامل: خالد حسين محمد العِزَّاني

عنوان الرسالة: تخفيف الإمتطاء الثقلي لغاز ثاني أكسيد الكربون عن طريق المزج بالمذيبات

التخصص: هندسة البترول

تاريخ الدرجة العلمية: ابريل 2019

يعتبر غمر مكامن الزيت بغاز ثاني اكسيد الكربون من التقنيات المعتبرة لتحسين الإنتاج بما لها من تطبيقات واسعة. يعود السبب في ذلك لما يتمتع به ثاني أكسيد الكربون من خواص كالكثافة واللزوجة العاليتين مقارنة بالغازات الأخرى المستخدمة لهذا الغرض كالميثان والنيتروجين وغيرها. إلا أن هاتين الخاصيتين ليستا عاليتين بالقدر الكافي مقارنة بتلك التي تتمتع بها موائع المكمن. يتسبب الفارق في هذه الخواص خصوا الكثافة في حدوث ظاهرة الامتطاء الثقلي والتي تلعب دورا سلبيا في كفاءة العملية خاصة في المكامن السميكة والتي تتمتع بتواصل عمودي جيد. وبالرغم من أن هناك العديد من الطرق المتبعة لتحسين الإنتاج من ثاني أكسيد الكربون، إلا أن هذه الطرق لا تهتم بمشكلة الامتطاء الثقلي أو لم تظهر كفاءتها في حل هذه المشكلة.

في هذا العمل البحثي، ولغرض تخفيف ظاهرة الامتطاء الثقلي لثاني أكسيد الكربون، تم اختبار قابلية مذيبين مختلفين، هما سترات ثلاثي الإيثيل (triethyl citrate) وبنزوات الإيثيل (ethyl benzoate)، في المزج مع ثاني أكسيد الكربون وفاعليتهما في انتاج مزيج ذي كثافة ولزوجة عاليتين بما يسهم في خفض ظاهرة الامتطاء الثقلي. في هذا الشأن، تمت الاختبارات عن طريق تحديد ضغط التشبع للمزيج عند درجات حرارة مختلفة ولتراكيز مختلفة من ثاني أكسيد الكربون. أظهرت النتائج القدرة العالية لهذين المذيبين على المزج مع ثاني أكسيد الكربون تحت ظروف مقاربة لظروف المكامن. كما أظهرت النتائج أن ضغوط التشبع لكل مزيج كانت منخفضة عند درجات الحرارة المُختَبَرة. بالنسبة لكثافة الخليط، فقد أظهرت النتائج أنها مقاربة لتلك التي تتمتع بها موائع المكمن. ولكن لسبب أن بنزوات الإيثيل أظهر قابليته للامتزاج الكلي مع النفط، وبسبب أن الحصول على مزيج ذي كثافة مقاربة لتلك التي تتمتع بها موائع

المكمن يتطلب كمية عالية من بنزوات الإيثيل، مقارنة بتلك التي يتطلبها السترات ثلاثي الإيثيل فقد تم استثناء بنزوات الإيثيل من تجارب غمر الأقوار.

لتقييم كفاءة وفاعلية المذيبات المستخدمة وخليطها مع ثاني أكسيد الكربون في خفض مشكلة الامتطاء الثقلي، تم اجراء أربع تجارب غمر الأقوار بشكل عمودي من الأسفل إلى الأعلى. لإجراء هذه التجارب، تم استخدام عينات حجر جيري من صخور إنديانا بعد نقعها وتشبيعها بالزيت العربي السعودي الخفيف وتمت جميع التجارب عند درجة حرارة 100 درجة مئوية. في التجربة الأولى تم حقن القور بثاني أكسيد الكربون ليقوم بإزاحة الزيت الخام عند أقل مستوى تشبع بالماء، وتم اعتبار هذه التجربة كمرجع لمقارنة النتائج من التجارب الأخرى. في هذه التجربة، تم استخراج حوالي 14.82% من حجم الزيت الموجود في القور تزامنا مع ظهور أول فقاعة لثاني أكسيد الكربون وكانت النسبة النهائية للزيت المستخرج بعد حقن قرابة مسام حجمي واحد ما يقارب 60.14%. تم في التجربة الثانية حقن خليط مكون من ثاني أكسيد الكربون وسترات ثلاثي الإيثيل بتركيز يحتوي على 85 مول في المئة لإزاحة الزيت الخام من القور؛ حيث تم استخراج حوالي 31.99% من حجم الزيت الموجود في القور تزامنا مع ظهور أول فقاعة لثاني أكسيد الكربون وكانت النسبة النهائية للزيت المستخرج بعد حقن قرابة مسام حجمي واحد ما يقارب 72.67%. لمحاكاة ظروف مقاربة أكثر لظروف المكامن، ولدراسة تأثير الميثان في عملية الحقن والامتزاج بين ثاني أكسيد الكربون والزيت الخام، تم تكرار هاتين التجربتين بنفس الزيت الخام ولكن بعد إعادة تركيبه عن طريق مزجه بخليط غاز يحتوي على مركبات الميثان، الإيثان، والبروبان، والبيوتان بنسب مقاربة لتلك التي يحتويها أي غاز مصاحب لمكامن النفط العربي السعودي الخفيف. تزامن ظهور أول فقاعة من ثاني أكسيد الكربون مع انتاج حوالي 15.19% من حجم الزيت الموجود في وكانت النسبة النهائية للزيت المستخرج بعد حقن قرابة مسام حجمي واحد ما يقارب 49.13% في تجربة الازاحة بثاني أكسيد الكربون بينما كانت هاتان النتيجتان حوالي 27.06% و 67.89% على التوالي في تجربة حقن خليط مكون من ثاني أكسيد الكربون وسترات ثلاثي الإيثيل بتركيز يحتوي على 85 مول في المئة.

من خلال هذه التجارب تبين فعالية الخليط المكون من ثاني أكسيد الكربون وسترات ثلاثي الإيثيل في خفض مشكلة الامتطاء الثقلي حيث نتج عنه تأخير في ظهور أول فقاعة لثاني أكسيد الكربون وكذلك كمية الزيت الناتج النهائي كانت أعلى وذلك في حالتي الزيت الخام والزيت المركب. أظهرت النتائج أيضاً مدى تأثير الميثان في خفض كفاءة عملية الإنتاج بثاني أكسيد الكربون.

CHAPTER 1

INTRODUCTION

1.1 Stages of Oil Production

An oil reservoir is generally developed in three recovery stages: primary, secondary and tertiary. In the primary stage, oil is produced by natural drive mechanisms through the utilization of the natural energy stored within the reservoir rocks and fluids in the form of pressure. The source for this natural energy can be from either the solution-gas drive, gas-cap drive, water drive, expansion of rocks and fluids, the effect of gravity or combinations of these mechanisms. However, with continuous production, the reservoir pressure drops and some of the stored fluid energy is lost. Therefore, it is necessary for the operator to boost or maintain the reservoir pressure through water or gas injection. This process is referred to as the secondary recovery stage. The recovery from primary and secondary recovery stages is usually low because of high remaining oil saturation left behind in which a large amount of oil remains as isolated and trapped droplets in the pores or as films around the rock particles. This residual saturation typically ranges from 20% to 35% in the water-flooded regions [1]. Finally, according to Sandrea and Sandrea (2007), the typical recovery factor after these recovery stages ranges from 45% to 50% of the original oil in place (OOIP) leaving a high amount of oil trapped in the reservoir. This level of recovery may vary from reservoir to another depending on the properties of the reservoir fluids and the characteristics of the reservoir rocks [2].

Due to the marked decline in the discoveries of new hydrocarbon reservoirs and the continuous increase in demand for more oil and gas, most of the world oil comes from mature fields. The production rates from these fields are steadily deteriorating, which makes the targeted oil production rate unachievable [3]. Therefore, the need for new techniques to increase the recovery led the industry to develop tertiary or enhanced oil recovery (EOR) methods and the selection of the best EOR method becomes highly important to petroleum engineers.

1.2 Enhanced Oil Recovery Methods

Previous applications and studies have proven that EOR can effectively recover the remaining oil from the reservoirs where the drive from primary recovery mechanisms has weakened. For instance, it has been shown that 7 to 23% of the original oil in place can be recovered by applying the EOR techniques [4, 5]. To achieve this additional recovery, many techniques can be applied such as gas injection, chemical injection, microbial injection or using steam injection. These techniques are categorized as mobility-control, chemical, thermal and other techniques including microbial EOR [1, 6] and they are summarized in **Figure 1.1**.

The selection of any of these methods depends on many factors including reservoir characteristics and economics. Alvarado and Manrique (2010) presented a comprehensive review of EOR status and the related opportunities to increase ultimate recovery factors in reservoirs ranging from extra heavy oil to gas condensate. Their review also organized the EOR opportunities based on lithology type and the locations of the fields (i.e. offshore or onshore) [3]. Taber et al. (1997) also proposed screening criteria for eight different EOR

techniques (i.e. three gases (Nitrogen (N_2), hydrocarbon, and carbon dioxide (CO_2)), three different waters and three thermal/mechanical techniques (combustion and surface mining)) based on field results and oil recovery mechanisms [7, 8] The criteria they presented included many factors such as crude oil properties (e.g. ˚API gravity, viscosity, and composition), reservoir characteristics (e.g. oil saturation, formation type, average permeability, reservoir depth, and reservoir temperature, … etc.) and economic considerations. As an example, **Figure 1.2** shows the range of ˚API gravity for different EOR techniques. The sizes of the methods shown in the figure indicate the importance of each of these methods in terms of oil recovery increase [7]. Economically, they stated that some of the EOR techniques have been proven to be technically successful but have relatively few economic successes and these methods are expected to be profitable with high oil prices [7].

Finally, although the most widely applied EOR techniques are thermal-based, which include the steam drive, cyclic steam and in-situ combustion [1], the EOR through the injection of hydrocarbons and CO_2 flooding is increasing [7].

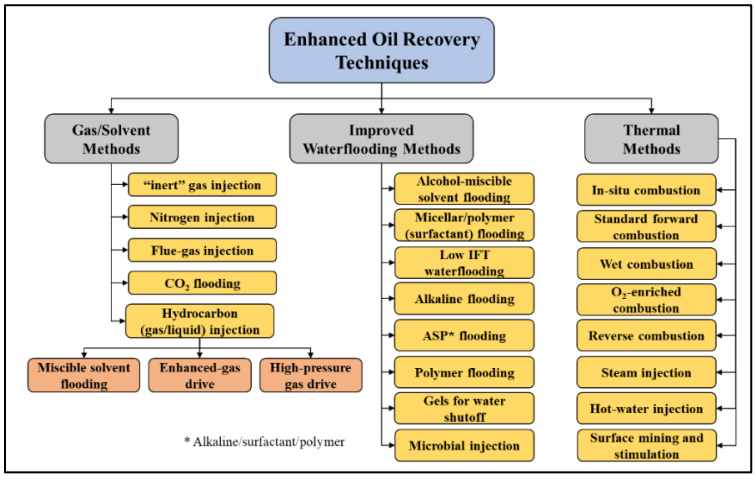

Figure 1.1: Different EOR Techniques (adopted from Taber et al. [7])

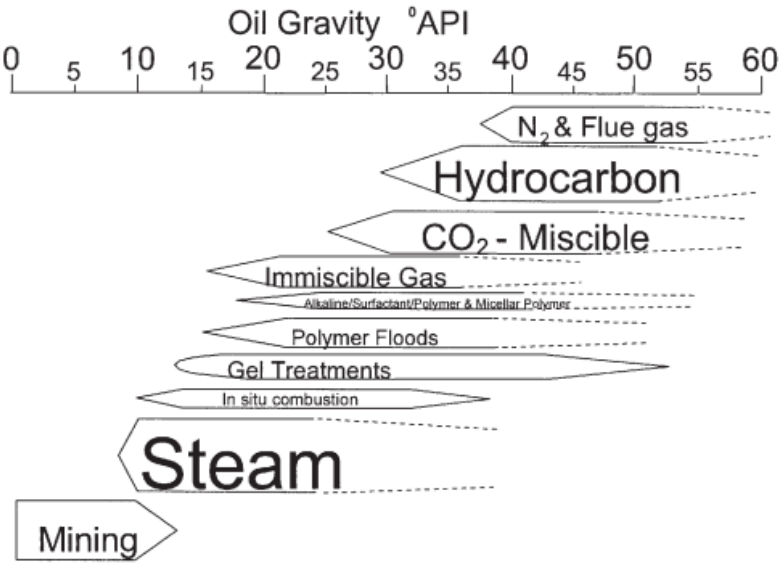

Figure 1.2: Range of Oil Gravity for Different EOR Methods [7]

1.3 CO_2 Flooding for Enhanced Oil Recovery

One of the most effective EOR techniques involves injecting CO_2 into the reservoir. The viability of this technique has been proven both experimentally and in the field. Also known as CO_2-EOR, the technique is considered as the second major EOR process in the world after thermal techniques [9]. Taber et al. [7] showed that oil production from CO_2 flooding is the only EOR technique that has continuously increased in the US despite the different declines in oil prices with time. CO_2 was first used as an EOR technique in the 1930s and in the 1970s there was a considerable advancement in this technique [10]. Grigg and Schechter (1997) showed that further and continuous developments over the years have led this recovery mechanism to become a leading technique for light and medium oils [11]. However, due to the deficiency in understanding the mechanism of the process, in heterogeneous reservoirs only CO_2-flooding projects have been economically successful though there is a great opportunity of integrating EOR with CO_2 sequestration [12].

1.4 Carbon Dioxide Sources and Properties

Carbon dioxide is abundant all over the globe and it exists either as a natural source in underground reservoirs or from anthropogenic sources (i.e. as an artificial source resulting from industrial operations) through the advances in carbon capture and storage (CCS) technology [13]. Example of CO_2 natural sources include the natural CO_2 reservoirs in the McElmo Dome and Sheep Mountain both in Bravo dome in New Mexico and in Colorado where the CO_2 gas is transported via pipeline networks to the Permian Basin fields [14]. Saudi Aramco's first CO_2-EOR demonstration project represents an example of anthropogenic sources of CO_2 in which CO_2 is being captured at the Hawiyah Gas Plant and transported through an 85-kilo-meter (85-km) pipeline to the pilot site in the Uthmaniyah Field where almost 800,000 tons of CO_2 is stored per year (0.8 Mtpy) at a rate of approximately 40 million standard cubic feet of pure CO_2 per day (MMscf/d) [15, 16].

CO_2 has been studied widely due to its outstanding properties. For example, CO_2 is a colorless, odorless, non-toxic, non-combustible and non-reactive gas. Also, CO_2 is cheaper than any other solvent and is easy to obtain at high purity. In addition, from a thermodynamics point of view, carbon dioxide has a mild critical point where its critical pressure, P_c, and critical temperature, T_c, are 1070.7 pounds per square inches (psia) (7.38 megapascals (MPa)) and 87.9 °F (31.1 °C), respectively, as illustrated by the pressure-temperature phase diagram presented in **Figure 1.3**. When CO_2 exists at pressures and temperatures above its critical pressure and temperature it is referred to as supercritical carbon dioxide ($scCO_2$). The viscosity of carbon dioxide at its critical point is 0.0335 centi-Poise (cP) and its density is about 0.36 grams per cubic centimeters (g/cm^3 or g/cc). At

typical reservoir temperatures (e.g. 100 ℃), the density of CO_2 ranges from around 0.1 g/cm^3 at low pressures to around 0.6 g/cm^3 at higher pressures, which is close to that of typical light crude oil [17]. The densities and viscosities of carbon dioxide as function of pressure at different temperatures are shown in **Figure 1.4** [18]. Moreover, CO_2's linear molecular structure, **Figure 1.5**, and small molecular weight (i.e. 44.01 grams per mole (g/mol)) provide it with faster diffusivity than any other conventional liquid solvent, which makes it a good solvent for sensitive solutes under extreme conditions. At its supercritical state, CO_2 can be used as a solvent for hydrocarbons because it is miscible with different kinds of organic materials and, hence, can be used in extracting many nonpolar materials [19] such as crude oil. $ScCO_2$ also has a higher ability to extract hydrocarbon components from oil than if it were in the gaseous phase [20].

Carbon dioxide has many other properties that make it an effective agent for oil displacement. Because of these special properties, CO_2 can improve the oil recovery by swelling the oil, reducing oil's viscosity, lowering the interfacial tension (IFT) and altering oil's density. Compared with other gases used in EOR operations, namely nitrogen and methane (CH_4), the minimum miscibility pressure (MMP) (discussed later) of CO_2 with oil is much lower than that for these gases and is usually close to reservoir conditions that the miscibility between oil and CO_2 is easily achieved [7]. Another advantage of CO_2 over these gases is illustrated in **Figure 1.6**, which shows a much larger density and viscosity of CO_2 at reservoir pressures than the other gases.

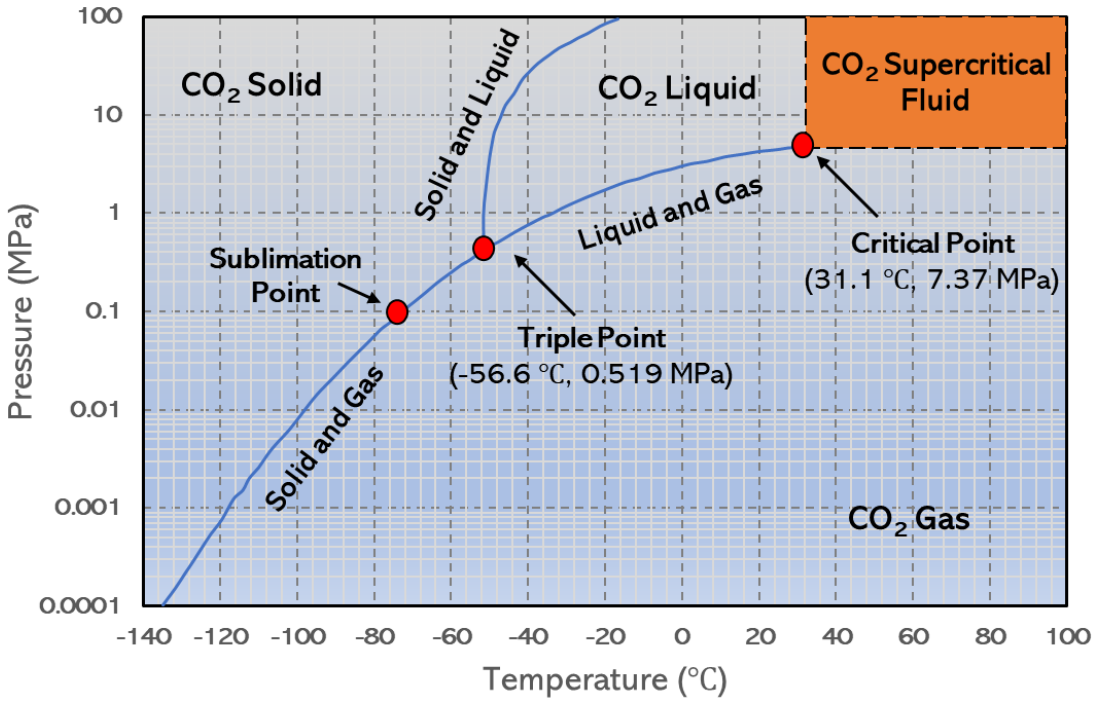

Figure 1.3: Pressure-Temperature Phase Diagram of CO_2

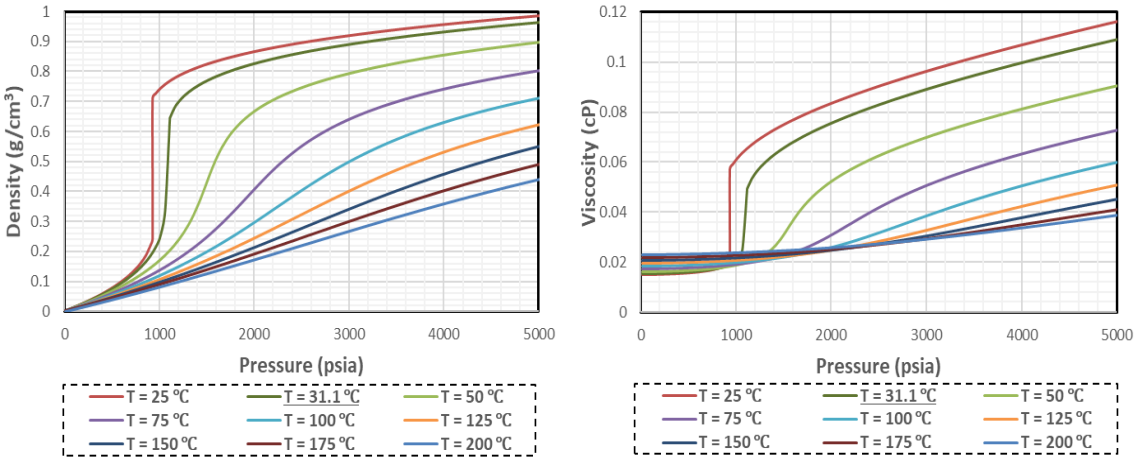

Figure 1.4: Density (Left) and Viscosity (Right) of CO_2 versus Pressure at Different Temperatures [18]

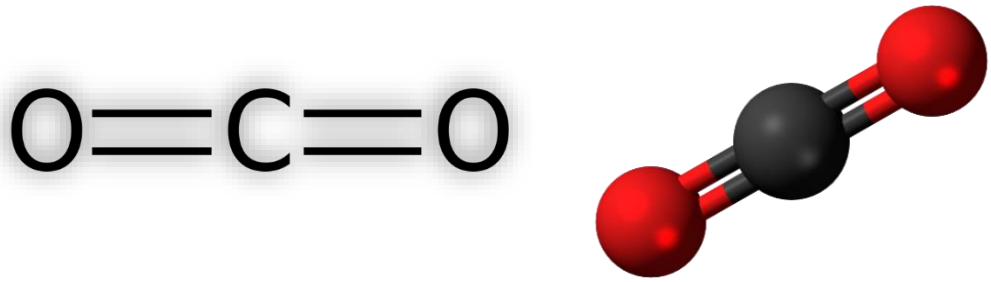

Figure 1.5: Illustration of the Molecular Structure of CO_2

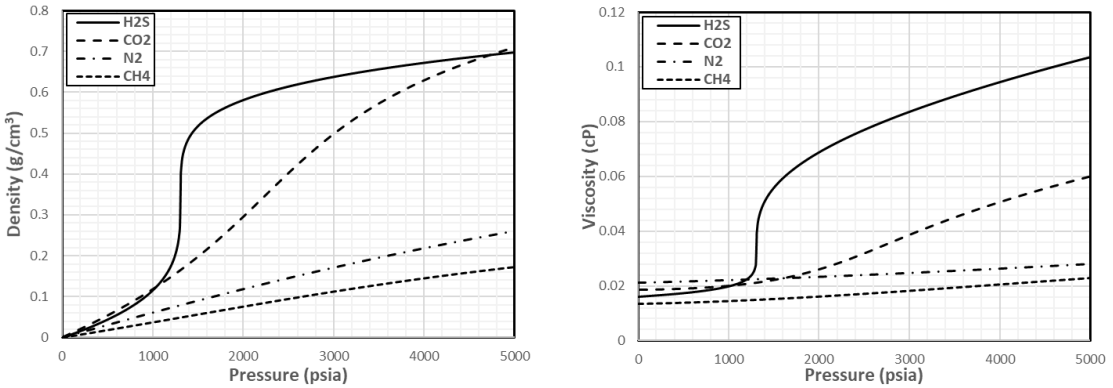

Figure 1.6: A Comparison of the Density (Left) and Viscosity (Right) of H_2S, CO_2, N_2, and CH_4 at 100 °C [18]

1.5 Minimum Miscibility Pressure

When considering injecting CO_2 (or any other gases) into an oil reservoir, the MMP is a very important factor to be considered and determined. This is because of the correlation between reducing production costs and improving oil recovery. To illustrate, the injected gas and the oil would still be in a two-phase mode if the injection pressure is too low and, hence, the desired recovery efficiency will not be achieved. By contrast, if the injection pressure is too high, the displacement will be multi-contact miscible and the costs of pressurizing the injected gas will be higher than what is needed, although the desired recovery efficiency has been achieved at lower pressures [21, 22].

The MMP is defined as the minimum pressure at which CO_2 becomes miscible with oil. It is influenced by many factors including the oil composition and the purity of the injected CO_2. The presence of methane and nitrogen as CO_2 contaminants, for example, can significantly increase the minimum miscibility pressure while the presence of hydrogen sulfide (H_2S) and light hydrocarbons other than methane in the injected CO_2 have the opposite effect [13].

The MMP is usually determined either experimentally either using the slim tube test (STT) [23] or the rising-bubble apparatus (RBA) [24]. In a comparative study by Elsharkawy and Christiansen [25], the RBA gave faster and more reliable results than the STT methods. Recently, the magnetic resonance imaging (MRI) technique was applied to estimate the MMP of CO_2 in n-Decane [26, 27]. Mathematical correlations and models can also be used to estimate the MMP. Al-Netaify (2008) presented comprehensive literature reviewing the experimental methods and mathematical models to determine the MMP [28].

Using the Slim-Tube Displacement tests, Oskay et al. (1989) conducted experimental work to determine the minimum miscibility pressure for three different Saudi Arabian Crudes: Arab Light, Arab Medium, and Arab heavy. Their results showed that the MMP for Arab Light increased from 2,450 psig to 2,760 psig when the temperature was raised from 170 °F to 195 °F while for Arab Medium crude it increased from 2,675 psig to 3,050 psig. For Arab Heavy crude, the MMP was 3,100 psig at 170 °F. Since these results were obtained for stock tank oil samples, they stated that the MMP values obtained could be slightly higher if live crude oil (recombined oil with methane-rich gas) was used. Finally, it was concluded that the heavier the fraction of Heptane-plus (C_{7+}) in the oil requires higher MMP to be in the single phase. Five different MMP correlations were tested to determine

their accuracy in estimating the MMP of Saudi Arabian crudes. They found that the tested correlations did not show satisfying results except that of Cronquist [29] which gave the least error [30].

1.6 CO_2 Displacement Mechanisms

Carbon dioxide flooding can be carried out either in the miscible or immiscible mode [31]. Under miscibility conditions, the miscible/vaporizing mode dominates oil recovery while solubility dominates the immiscible mode [32]. Therefore, miscibility conditions play a vital role in the recovery process during CO_2 flooding; that is, the oil recovery and the overall recovery performance through the injection of CO_2 are greatly influenced by the presence or lack of CO_2-oil miscibility. Whether the flooding process is miscible or immiscible depends on the conditions of the targeted reservoir.

In the literature, many researchers have investigated CO_2 flooding under different miscibility conditions. The following subsections briefly describe the difference between the two displacement mechanisms.

1.6.1 Miscible CO_2 Flooding

As stated above, the flooding process can be either miscible or immiscible depending on the conditions of the reservoir. For instance, miscible CO_2 flooding occurs only under specific conditions including mainly the reservoir temperature, reservoir pressure, injected gas composition, and oil chemical composition [33]. However, for isothermal reservoirs, the miscible or multi-contact miscible conditions are only achieved when the injection pressure is above the thermodynamic minimum miscibility pressure (MMP) given that it is below the reservoir fracture pressure.

Oil and CO_2 are not miscible on a first contact, which necessitates many contact stages in a process defined by Zick (1986) as a condensing/vaporizing mechanism. In this process, components from oil and CO_2 are transferred back and forth until there is difficulty in distinguishing the oil-enriched CO_2 from the CO_2-enriched oil phases (**Figure 1.7**) [34]. Therefore, under miscible flooding, CO_2 and oil form a single-phase liquid which results in swelling the oil and reducing its viscosity and its surface tension (ST). As a result, the ability of the oil to flow is improved and, hence, the oil recovery is increased.

For miscible CO_2 flooding to be achieved at the field scale, many criteria need to be fulfilled. For example, reservoirs with higher than 25 ˚API gravities and located at depths greater than 915 meters (3002 feet) are typically selected for miscible oil recovery [32]. Based on these criteria, Saudi Arabian Arab light reservoirs can be good candidates for miscible CO_2 flooding.

According to Holm and Josendal [20], flooding CO_2 under miscible conditions is considered the most efficient utilization of CO_2 in EOR processes. However, there are some problems associated with miscible CO_2 flooding. For example, in light oils, the fluid flow is delayed, and the mobility is significantly reduced because of asphaltenes deposition within the porous medium. Formation damage may then be induced due to blocking the necessary flow paths [35].

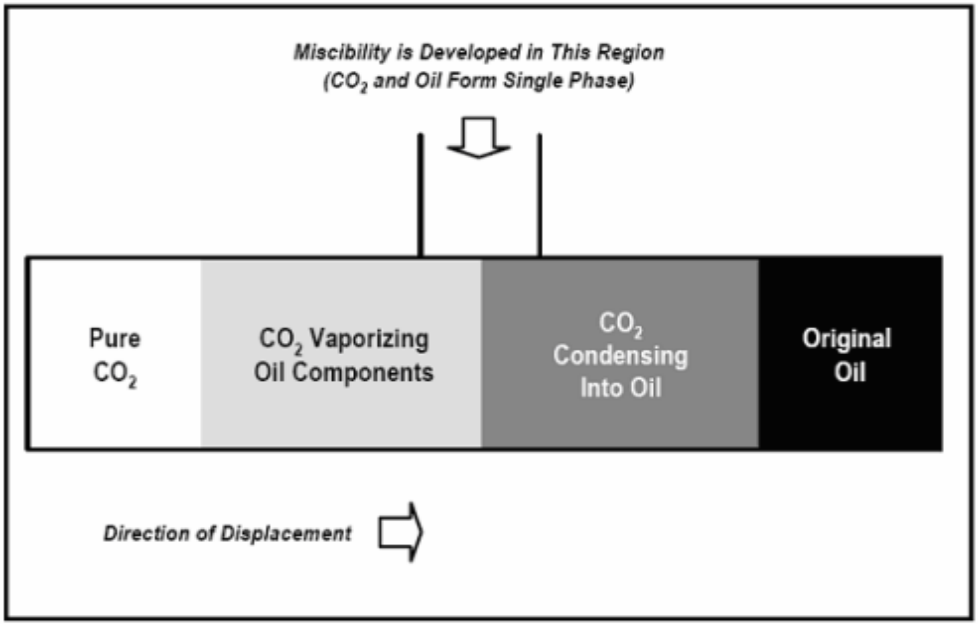

Figure 1.7: 1-D Schematic Showing the CO_2 Miscibility Process with Oil [13]

1.6.2 Immiscible CO_2 Flooding

On the other hand, immiscible flooding occurs when the reservoir pressure is less than the MMP. Under such pressures, the interchange between the oil and CO_2 is reduced. Perera et al. (2016) showed that immiscible oil recovery can be applied to reservoirs where the requirements for miscibility are not satisfied, e.g. relatively heavy oil reservoirs and shallow oil reservoirs. CO_2 displacement under immiscible conditions can enhance oil recovery particularly in low-pressure reservoirs in which CO_2 is injected for pressure maintenance purposes [32]. It can also be applied in heavy oil reservoirs since CO_2 can be partially dissolved in the oil [36].

Perera et al. (2016) also indicated that immiscible CO_2 flooding is dominated by the processes of oil swelling and viscosity reduction caused by the solubility of CO_2 in oil [32], which determines the degree of oil swelling and its viscosity reduction and, hence, the

effectiveness of CO_2-EOR. Therefore, the factors affecting the solubility of CO_2 in oil must be carefully taken into consideration when implementing immiscible CO_2-EOR. Han et al. (2016) showed that under immiscible conditions, oil production is limited by the volumetric sweep efficiency, the displacement efficiency of the injected fluid and how soluble CO_2 is in the oil, which decreases the viscosity and density of the oil phase [12].

Finally, this displacement technique is more attractive for capturing and storing CO_2 than miscible displacement since larger amounts of the injected gas can be stored compared to the miscible process, though it was experimentally shown that CO_2 flooding is ineffective under immiscible conditions in dipping reservoirs due to gravity override and the presence of CO_2 channels generated at the upper side of the reservoir [37].

1.7 Challenges in CO_2-EOR Process

Technically, the main challenge in continuous CO_2 flooding is how to reduce the mobility contrast [38] and the gravity override [39] of the injected CO_2. As stated earlier, the density and viscosity of $scCO_2$ are much higher than those of the other gases employed in EOR operations, such as methane and nitrogen, especially at reservoir conditions. However, these properties are not high enough compared with those of reservoir fluids (e.g. oil and water). For example, CO_2 is injected at the supercritical state where it shows a relatively low density compared to that of oil and brine which may vary from 0.8 to 1.230 g/cm^3 depending on the conditions of the targeted reservoir [40]. Consequently, the unfavorable viscosity ratio between CO_2 and resident fluids in the reservoir leads to viscous fingering. Also, the contrast in the density between reservoir fluids and CO_2 leads to gravity segregation, especially for thick reservoirs with a relatively high vertical permeability and

large spacing between the injection and producing wells. Known as gravity override, this phenomenon is considered as the major factor resulting in poor CO_2 reservoir sweep efficiency, early CO_2 breakthrough and low oil recovery. The problem is exacerbated when CO_2 extracts methane from the oil since gravity override can be correlated with methane absorption in the CO_2-rich phase, which reduces its density and diminishes its miscibility with the oil [41].

CHAPTER 2

LITERATURE REVIEW

This literature review includes three main parts: 1. previous attempts to mitigate CO_2 gravity override, 2. the various types of chemicals that have been studied as blending agents for carbon-capture purposes from which the effect of those agents on the density of CO_2 will be easily inferred and 3. the different laboratory studies that have been conducted for evaluating CO_2 flooding performance at different conditions.

2.1 CO_2 Gravity Override Mitigation Techniques

Mobility control of CO_2 aims at overcoming the contrast between the properties of CO_2 and those of resident reservoir fluids. Many attempts have been employed to mitigate gravity override. These techniques are either through the addition of chemicals or agents that increase the density of CO_2 and result in a minimum effect of gravity override or through the change in the flooding schemes. Enick et al. (2011) presented a comprehensive literature review on mobility and conformance control studies for CO_2-EOR process. Their review gives a detailed review of 40 years of research and pilot tests and mainly focuses on the thickeners of CO_2 and their history [42, 43].

One scheme for mobility control, for example, is the water alternating gas (WAG) in which a predetermined amount of CO_2 is injected in cycles with equal volumes of gas and water alternating at a constant gas-to-water ratio. Once the specified amount of CO_2 has been injected, a specific amount of water (a chase) follows [13]. In this technique, the injection

of brine with CO_2 results in increasing the saturation of brine and, hence, decreasing the saturation of CO_2 within the pores and it has nothing to do with the density or viscosity of CO_2. Investigations showed that this reduction in CO_2 saturation results in a reduction in the effective permeability to CO_2 which reduces the viscous fingering by lowering the mobility ratio. Although the recovery results of WAG are better than those of continuous CO_2 injection, the effects of gravity segregation are still present in this scheme [44] and approximately one-third to two-thirds of the oil is still left behind after WAG floods. The requirements for the WAG process are also high which include the installation of the facilities of water injection, production, separation, and collection. The contact between CO_2 and reservoir oil within the pores may also be curtailed in this scheme due to the large amounts of water injected which can also result in prolonging the life of the reservoir, delaying CO_2 injection and producing large volumes of water. Finally, this technique is not appropriate for tight reservoirs or water-sensitive reservoir where continuous CO_2 injection can be more effective than the WAG process [42]. An example of the WAG design is the Saudi Arabian first CO_2-EOR demonstration project. This project consists of four injectors, four producers and two observation wells. The injection pattern was selected as line-drive and two of the injection wells are selected for CO_2 injection into which CO_2 is being injected for a month. Water injection then alternates from the other two injection wells for the other month [16].

Other techniques that have been discussed in the literature to control the mobility of injected gas and delay gas breakthrough time include the surfactant-water-alternative gas (SWAG), foam-assisted-water-alternative gas injection (FAWAG), simultaneous water-alternative-gas injection (SimWAG), and profile improvement of CO_2 flooding [45].

However, the most common technique employed to minimize the CO_2 gravity override problem is by introducing a blocking agent such as foam, cross-linked polymers, and gels. These agents invade the high permeability zones of the reservoir and reduce their permeability to CO_2 significantly by gas trapping [46, 47]. However, each one of these agents has its limitations and disadvantages. For example, no foaming agent has been identified to withstand the high temperatures and high salinities of some Saudi Arabian reservoirs. Also, most of the agents used for CO_2 mobility and conformance control are not of practical use in field applications due to economic and technical limitations [42]. Finally, these techniques are more effective in preventing fingering and thief zones than minimizing the effect of gravity override.

According to Moortgat et al. (2013), injection of CO_2 with higher density than that of oil has a great interest in enhancing oil recovery from the largest oil fields in the world [41]. Therefore, many of the challenges present during CO_2 flooding can be alleviated by increasing its density and/or its viscosity which can lead to better recovery performance than oil recovery process by continuous injection of pure CO_2. In this regard, a technique of very high potential is to blend the $scCO_2$ phase with a solvent that increases its density and/or viscosity while minimizing the effect of methane absorption from the oil on its miscibility power.

Example of such work that used alcohol as a solvent to increase the density and viscosity of CO_2 include that of Djabbarah (1988) who showed that alcohol can be utilized to be mixed with $scCO_2$ for the purpose of modifying the MMP and reducing the density and viscosity contrasts between the injected CO_2 and the reservoir fluids. His method suggested either mixing $scCO_2$ with the selected alcohol prior the injection or a slug of $scCO_2$ can be

injected into the formation followed by a slug of the alcohol [48]. Recently, Al-Otaibi et al. (2018) addressed the density and viscosity challenge of $scCO_2$ by introducing a capsule-based carbon dioxide system. The capsules contain a dense liquid prepared using a hydrogel and each capsule has a capsule wall with an inner area and an outer side. These capsules are functionalized by adding CO_2-phillic molecules to the outer side of the capsule wall so that functionalized capsules are created. The functionalized capsules are then added to the $scCO_2$ such that a stable dispersion of capsules is created after which it is injected into the targeted reservoir. This dispersion of capsules has a density and viscosity higher than those of pure $scCO_2$ [49].

2.2 Studies on the Solubility of Different Chemicals with CO_2

In CCS operations and, depending on the conditions at which CO_2 is emitted, different methods are used for CO_2 capture including chemical absorption, physical adsorption, physical absorption, and cryogenic separation. Economic constraints can also be a factor in determining the CO_2 capturing method [50]. Amongst all these methods, the chemical absorption method is the most common and practical method due to its cost-effectiveness and simplicity [51, 52]. In this method, several chemicals and solvents can be used as summarized by Babamohammadi et al. [50].

This section involves two main groups of chemicals that have been used and studied for their solubility with CO_2 for carbon capture processes: general chemicals and solvents (e.g. polymers and amine solvents) and the ionic liquids (ILs) along with deep eutectic solvents (DESs).

2.2.1 Studies on CO_2 Solubility with Different Solvents & Chemicals

The following are highlights of a few studies that tested the solubility of CO_2 in various types of chemicals as well as different solvents.

Feng et al. (2001) generated the vapor-liquid equilibrium (VLE) data of three binary systems (i.e. CO_2+ethyl benzoate (EB), CO_2+diethyl succinate (DiES), and CO_2+isoamyl acetate (IAA)) by a semi-flow type apparatus at 35, 45, and 55 ℃ over the pressure range from 1 to 13 MPa (145 to 1885 psia). It is stated that ethyl benzoate has the structure with an aromatic group and, since the solubility of CO_2 in a compound with a ring aromatic group is difficult, the data showed that at a fixed pressure CO_2 is less soluble in ethyl benzoate than in the other two esters. The solubility of CO_2 in isoamyl acetate is the highest due to its lowest boiling point. At low pressures, there was no significant solubility of the ester compounds in the vapor phase. Conversely, at equilibrium pressures higher than the critical point of carbon dioxide, the solubility increased dramatically [53].

Shen et al. (2015) measured the density and viscosity of aqueous solutions of potassium lysinate (LysK) and potassium prolinate (ProK), both with and without dissolved CO_2, at temperatures from 25 to 75 ℃ with concentrations between 0.2 and 3.0 moles per liter (mol/L). They also measured the solubility of CO_2 in 2.5 mol/L amino-salt acid solutions at 40 ℃ and 60 ℃ with CO_2 partial pressures at flue gas conditions. They found that the density increased in the concentration of amino-acid in the solution. The density also increased greatly with an increase in the CO_2 loading. However, the density decreased with temperature rise for two solutions at a given concentration and CO_2 loading [54].

Chiu et al. (2016) used equilibrium analyzers to measure the VLE phase boundaries of CO_2 with mixed solvents of ethanol/water (9/1), dimethyl sulfoxide (DMSO)/water (9/1) and N, N-dimethyl formamide (DMF)/water (7.5/2.5) at a temperature range of 25 to 75 ℃ and pressures up to near critical values. The measurements were also conducted over a wide range of composition. The objective of this study was to investigate the changes of phase boundaries by introducing the phase modifier (i.e. water) into CO_2 + ethanol, CO_2 + DMSO, and CO_2 + DMF mixtures. The results were compared with those obtained with water-free binary systems. The authors concluded that introducing water into the CO_2/solvent mixture resulted in increasing the bubble, dew, and critical pressures and, hence, extended the superheated region. This shift enlarged the operable window to produce a micrometric particle through the SAS micronization process [55].

The high-pressure phase equilibrium of carbon dioxide-tristearin system was investigated by **Ilieva et al. (2016)** at 70, 80, 90 and 100 ℃ and pressures up to 250 bars (3625.94 psi). Solubility measurements were also carried out for carbon dioxide-rapeseed oil system at 40, 60 and 80 ℃ and pressures up to 310 bars. The viscosities of the CO_2-saturated tristearin and rapeseed oil mixtures were also measured at 70, 80, 90 and 100 ℃, and densities at 60 and 80 ℃ for pressures up to 200 bars. The results showed that the solubility of CO_2 in the liquids increased with increasing pressure and decreasing temperature. Viscosity measurements at atmospheric pressure showed Newtonian behavior for both systems. The viscosity of the rapeseed oil system at 80 ℃ decreased by about 94% from 1 to 200 bar. A linear increase in density was observed for both systems at all temperatures. It increased for the tristearin system at 80 ℃ from 867 kg/m^3 at 1 bar to 889.74 kg/m^3 at 200 bars. The smallest change was observed at 100 ℃ where the density of the tristearin

system increased from 849 kg/m^3 to 862.59 kg/m^3. For the rapeseed oil system at 60 ℃, the density increased from 888 kg/m^3 at atmospheric pressure to 915.65 kg/m^3 at 200 bars [56].

Li et al. (2016) studied the solubility and thermodynamic properties of CO_2 in five different biobased solvents (BBSs) including glyceryl triacetate (GT), glycerol formal (GF), DL-1,2-isopropyl-deneglycerol (GAK), triethyl citrate (TEC), and acetyl triethyl citrate (ATEC) at temperatures from 20 to 50 ℃ and pressures from 0 to 600 kilopascal (kPa). They compared their solubility data for these solvents with literature data of other solvents, including high boiling point solvents, and some new emerging ILs. Their results showed that the solubility of CO_2 increased with increasing pressure or decreasing temperature, meaning that CO_2 dissolves into the investigated BBSs through a physical process. They also showed that solubility in of the investigated BBSs follows the sequence of ATEC > TEC ≈ GT > GAK > GF at the same temperature. The comparison results showed that they were like polyethylene glycol dimethyl ether (NHD) which is an industrial CO_2 absorbent. However, the maximum reported solubility of CO_2 in TEC from this study was 0.1304 mol-fraction [57].

Kegl et al. (2017) determined the thermodynamic and transport properties of polyethylene glycols (PEG) 600/CO_2 and Brij52/CO_2 systems at different experimental conditions. The physical-chemical and mass transfer properties were studied under a pressure range from 0 bar to 300 bars at temperatures of 60 and 80 ℃. The results revealed that the solubility of CO_2 in PEG increased with increasing pressure and decreasing molecular weight. The solubility of CO_2 in the PEG 600 and Brij52 at 290 bars and 60 ℃ is 0.591 g/g and 0.766 g/g, respectively. The results also showed the solubility of binary systems to increase with

increasing pressure due to increasing the density of CO_2. This effect was more noticeable at pressures above the critical point of CO_2 because the density of CO_2 increased and, therefore, the interaction between molecules of CO_2 and polymer was even more intense. On the other hand, the diffusion coefficient was influenced mainly by the amount of CO_2 already present in PEG and less by the molecular weight of the PEG. A higher diffusion coefficient was obtained for the PEG/CO_2 system in the entire range of investigated conditions. The interfacial tension of the PEG/CO_2 system was also investigated. It decreased with increasing pressure; however, with increasing temperature, it decreased at lower pressures and increased slightly at pressures above 150 bars. With a binary system consisting of PEG and argon, the interfacial tension decreased with increasing temperature [58].

2.2.2 Studies on CO_2 Solubility with Ionic Liquids and Deep Eutectic Solvents

Bera and Belhaj (2016) presented an overview of the works that have been done on ILs and how effective they are in enhanced oil recovery operations. They also discussed the future challenges of ionic liquids in EOR operations. When considering the chemical enhanced oil recovery operations (CEOR), different chemicals such as alkali, surfactants, polymers, and organic solvents are used. However, due to the variations in oil prices, and because of the high costs and the environmental issues associated with using some of these chemicals, the oil industry is looking for cost-effective alternatives. Extensive and continuous research work has drawn toward the surface active ionic liquids as alternatives of surfactants [59].

To avoid defining ILs as “molten salts”, Bockris and Reddy (1974) described their nature as organic salts existing as a liquid at room temperature below 100 ℃. These chemicals

have also been defined later by Johnson [60] as volatile organic solvents in which their vapor pressure and specific conductivity are low and moderate, respectively. The properties of newly developed ionic liquids are those of organic salts with relatively large cations and anions. **Table 2.1** summarizes the characteristics of these liquids. As shown in the table, ionic liquids have a melting point of 100 ℃ and they exist in a liquid state at temperatures below 200 ℃. Ionic liquids are also highly thermally stable over a wide range of temperatures and their workable viscosity is normally less than 100 cP. Other unique properties include their nonflammability and solubility in many organic and inorganic compounds [59]. Moreover, ideal ionic liquids can be possibly designed for specific reservoir conditions including the fluid and rock properties [61]. Finally, in addition to all these features of ionic liquids, some of the newly developed ionic liquids are environmentally friendly. The ionic liquids have been used as alternatives to many harmful and polluting chemicals in different applications [62].

Table 2.1: Characteristics of Ionic Liquids (Adopted from Johnson [60]**)**

A salt	Cation and or anion quite large
Freezing point	Preferably below 100 ℃
Liquidous range	Often > 200°C
Thermal stability	Usually high
Viscosity	Normally < 100 cP, workable
Density	800-1500 kg/m^3 *(According to Ramdin et al. 2012* [63]*)*
Dielectric constant	Implied <30
Polarity	Moderate
Specific conductivity	Usually < 10 mScm-1, “Good”
Molar conductivity	< 10 Scm2 mol-1
Electrochemical window	> 2V, even 4.5 V, except for Brønsted acidic systems
Solvent and/or catalyst	Excellent for many organic reactions
Vapor pressure	Usually negligible

Another class of solvents that share some of the promising characteristics of the ionic liquids is the deep eutectic solvents (DESs). DESs are classified as ionic solvents, which are formed from a eutectic mixture of acids and bases. They can contain a variety of anionic and/or cationic ions, and they display special properties especially the melting point, which can be much lower than the melting points of the solvent's ingredients. Compared with conventional ionic liquids, DESs have the advantages of low cost, renewability, low-toxicity, and simplicity of preparation [64, 64].

Many researchers have investigated ILs and DESs as gas absorbents for CO_2. Some of those investigations are highlighted in this literature review.

Althuluth et al. (2012) experimentally investigated the solubility of CO_2 in 1-ethyl-3-methylimidazolium tris(pentafluoroethyl)trifluorophosphate ([emim][FAP]) at different temperatures ranging from 14.6 to 91 ℃ and at pressures up to 10.40 MPa. The tested CO_2 concentrations varied from 10.03 to 60.00 mol% with a water content of less than 200 ppm for all the prepared samples. The methodology followed for solubility determination was through the measurement of the bubble point of the CO_2+IL binary system. The purpose of their study was to investigate the effect of the anion of the IL solubility with CO_2. The results showed that the increase in the system temperature results in an increase the bubble point pressures of the binary systems and, hence, the solubility of CO_2 in the IL decreases with increasing the temperature at a specific amount of CO_2 in the tested IL. Increasing the mole fraction of CO_2 at given temperature results in a sharp increase in the bubble-point pressure of the system and, hence, the solubility of CO_2 in the IL decreased with increasing the molar ratio of CO_2. Comparing the solubility of CO_2 in the [FAP]-based IL to other

ionic liquids with the same cation showed that the [emim][FAP] has the highest absorption capacity than the others [66].

Nam & Lee (2013) presented results for the solubility measurements of CO_2 in two ammonium-based ILs (i.e. ([N4,1,1,1][Tf_2N]) and ([N1,8,8,8][Tf_2N])) for pressures up to 45 MPa and temperatures ranging from 30 ℃ to 70 ℃ and at different molar fractions of CO_2. In their study, solubility was determined from the measurement of bubble-point pressure of the CO_2+IL binary system using high-pressure equilibrium apparatus. The results showed that, at lower pressures, the solubility of CO_2 in the IL was very high, and, at higher CO_2 composition, the equilibrium pressure increased sharply. The results also showed that there is a substantial dependency of the solubility of CO_2 in the IL on the variation of the length of the alkyl anion chain attached to the ammonium-based cation of the IL. To illustrate, the solubility of CO_2 increased with the increase in the length of alkyl chains at low pressures and, at higher pressures, the solubility became more apparent [67].

Makino et al. (2013) measured the densities, viscosities and the electrical conductivities of an ionic liquid, N-(2-hydroxyethyl) pyridinium bis(trifluoromethanesulfonyl) amide ([Py_2OH][Tf_2N]), over a temperature range of 273.15 to 363.15 K at atmospheric pressure. The PVT/Composition relations in the CO_2 + [Py_2OH][Tf_2N] system was obtained under pressure conditions up to 5 MPa at 25 ℃ and 60 ℃. The volumetric properties showed ordinary dependencies with regards to temperature: the densities decreased as temperature increased. [Py_2OH][Tf_2N] had a higher density than [Py4][Tf2N]. They concluded that the present IL became denser and more viscous in the presence of the hydroxyl group compared with the nonfunctionalized one. CO_2 solubilities in [Py_2OH][Tf_2N] varied with pressure as a function of mole fraction or molarity that was typical for a physical absorbent.

The molar volume of the liquid [Py_2OH][Tf_2N] phase decreased with the dissolution of CO_2. The volume of the ionic liquid phase expanded with an increase in CO_2. As a result, the number of molecules per unit volume increased and the saturated liquid density slightly decreased over the conditions investigated [68].

Carvalho et al. (2014) studied the solubility of the CO_2 + 1-ethyl-3-methylimidazolium ethyl sulfate system at a temperature ranging from 0 to 140 ℃ and at pressure up to 5 MPa. The mole fraction of the CO_2 used in the study was ranging from 0.02 to 0.5 using the isochoric method. The authors also studied the system density at temperature ranges of 5 – 125 ℃ and a pressure ranging from 10 MPa to 120 MPa with CO_2 mole fractions of 0.2, 0.4, 0.7 and 0.8. For the solubility measurements, it was observed that the solubility of the system decreases with the temperature and increases with the pressure as expected. The results from density measurements showed that the density of the mixture increases as the pressure increases and decreases with the temperature. However, at CO_2 mole fractions up to 0.6, it was observed that there is no significant effect of pressure on the density. For higher mole fractions, they found that the pressure highly affects the density and attributed this effect to the presence of the liquid–liquid-like region [69].

Chen et al. (2014) measured the solubility of CO_2 in eutectic mixtures containing choline chloride (CC) and dihydric alcohols (including 1,4-butanediol, 2,3-butanediol, and 1,2-propanediol) with a molar ratio of choline chloride to dihydric alcohol of 1:3 and 1:4 at temperatures from 20 to 50 ℃ andd under pressures up to 600 kPa. The results showed that the DES composed of CC and 2,3-butanediol with the molar ratio of 1:4 have the largest ability to dissolve CO_2 among all the DESs [70].

The solubility of CO_2 was measured in three other types of DESs: choline chloride + phenol, choline chloride + diethylene glycol, and choline chloride + triethylene glycol by **Li et al. (2014).** The measurements were conducted at temperatures ranging from 20 to 50 ℃ under pressures up to 600 kPa. The mole ratios of choline chloride to phenol were selected as 1:2, 1:3 and 1:4, while it was 1:3 and 1:4 for the others. The results showed that the solubility of CO_2 increased with increasing pressure and decreased with increasing temperature [71].

Deng et al. (2016) studied the solubility of CO_2 in five DESs at temperatures from 30 to 60 ℃ with 10 ℃ intervals under pressures from 0 to 600 kPa. The DESs were prepared from levulinic acid and quaternary ammonium salts (QAS) with a mole ratio of 3:1. The results showed that the solubility of CO_2 in the DESs increased with increasing pressure or decreasing temperature. The solubility of CO_2 in the liquid phase was proportional to the equilibrium pressure in the gas phase. Changes in the densities of the DESs because of CO_2 dissolution were small and negligible [72].

A study conducted by **Ji et al. (2016)** presented phase equilibria data of binary mixtures of high-pressure CO_2 and DESs formed by quaternary ammonium salts and phenol at temperatures from 40 to 60 ℃, pressures from 1.71 to 13.3 MPa, and mole ratios of phenol to QAS from 2 to 4. The results showed the solubility of CO_2 in DES increases almost linearly with pressure up to 8 MPa with a slower increase at higher pressures. The solubility of phenol in supercritical CO_2 is much larger than that at low pressures because at or close to its critical point the density of CO_2 increases greatly with pressure, thus resulting in high solubility. On the other hand, the solubility of CO_2 in the DES decreases with increasing temperature within pressures ranging between 1.71 and 12.96 MPa. Increase in temperature

resulted in an increase in phenol volatility, which is beneficial for its solubility in high-pressure CO_2, while it caused a decrease in the density of high-pressure CO_2, which is unfavorable to its solubility [73].

Ponte and Zakrzewska (2016) experimentally studied the volumetric and phase behavior of mixtures of fluoroalkyl phosphate-based ionic liquids with high-pressure CO_2. They also measured the solubility of high-pressure CO_2 in those liquids at 40 °C temperature and pressures up to 10 MPa as well as the liquid phase volume expansion upon CO_2 dissolution. They concluded that the solubility of CO_2 in ionic liquids with fluoroalkyl phosphate anion is among the highest reported so far for ionic liquids where CO_2 is dissolved by "physical" means. They reached the same conclusion for the CO_2-induced volume expansion of the liquid [74].

To conclude this literature review showed that a lot of chemicals and solvents have the potential to blend with CO_2 at different conditions and with different concentrations including ionic liquids (ILs) which have the potential to dissolve CO_2 and increase its density. Moreover, there are different types and classes of ionic liquids. **Table 2.2** summarizes the various classes and types of ionic liquids.

Table 2.2: Classifications of Ionic Liquids

Cation Organic	Anion Organic	Anion Inorganic
Imidazolium	Alkylsulfate	bis(trifluoromethyl-sulfonyl)imide
Pyridinium	Tosylate	Hexafluoro-phosphate
Pyrrolidinium	Methanesulfonate	tetrafluoroborate
Phosphonium	Others	Halide
Ammonium		Others
Sulfonium		
Others		

2.3 Laboratory Experiments to Evaluate CO_2 Flooding

A lot of studies have also been conducted to evaluate CO_2 flooding performance. Most of these studies were based on experimental evaluations. This section presents some of the experimental studies that have been conducted on CO_2 core flooding for evaluating CO_2-EOR operations and the associated observations.

In general, **Orr et al. (1982)** showed that there are three experimental techniques for evaluating a CO_2-flooding prospect. These are the slim-tube displacements, core flooding displacements and high-pressure volumetric (PVT) and VLE experiments. Each of these techniques provides different information about the CO_2 flood. Of the three types, slim-tube displacement is the simplest method for evaluating the effectiveness of the phase-behavior during the displacement process in addition to eliminating the viscous fingering, gravity segregation, and rock heterogeneity. Though they are costly and inefficient, equilibrium phase-behavior experiments provide useful data for modifying the calculations of phase-behavior in a reservoir simulator. In contrast, it is most difficult to interpret CO_2 core floods because the displacement efficiency is influenced by the viscous fingering, gravity segregation, core heterogeneity which results in channeling and bypassing of oil. The presence of high-mobility water, which prevents/shields oil-CO_2 contact, also affects the displacement. All of this is further compounded by the complex phase behavior of CO_2 with crude oil [75].

Regardless of these difficulties, core flood experiments are the most appropriate type because important parameters for field-scale evaluation may be obtained from their results [41]. To illustrate, oil can be recovered through CO_2 injection under more realistic

conditions than those in slime-tube experiments. The ultimate oil recovery from a portion of a reservoir swept by CO_2 can also be estimated through examining the residual oil saturation in the swept zone after CO_2 injection. Core floods can also be used to investigate the influence of CO_2 flooding on the reservoir permeability and the problems associated with it (e.g. asphaltene deposition, relative permeability alteration, and dissolution of minerals in case of carbonate reservoirs). Finally, core flood experiments can be used to investigate the effect of CO_2 slug size on oil recovery as shown by Huang and Tracht [76] and Wang [77].

Sun et al. (2016) presented a systematic review of all the laboratory core flooding experiments and facilities that have been published and reported in the literature since 2006. Those studies investigated the interactions of scCO_2-brine-rock in a core-scale under reservoir conditions during CO_2 flooding. They also presented a tabulated summary of all the available studies on core flooding experiments for CO_2 geo-sequestration in deep saline aquifers which shows the details of the experimental conditions and the properties of the cores used in the experiments [78].

Wang (1982) developed a high-pressure glass-bead-packed transparent flow tube to visually examine the microscopic behavior of CO_2 flooding processes. The apparatus made it possible to observe the physical phenomena of displacement of oil by CO_2 under miscible and immiscible conditions. Depending on the test pressure range, it was observed that three types of displacement are present (i.e. immiscible, semi-miscible, and miscible) in which more than one type of these could coexist in the flooding system. During the experiments, the effect of CO_2 slug size and formation dip on oil recovery were also investigated. The results showed that it is not effective to inject a too large amount of CO_2 as it results in a

premature breakthrough. Finally, with downdip displacement, the oil recovery could be significantly increased due to the alleviation of CO_2 gravity override and the early miscibility development [77].

Tiffin and Kremesec (1988) conducted a series of vertical downward core flooding experiments of contact-miscible and multiple-contact-miscible CO_2 with recombined crude oil system at various operating conditions for evaluating gravity-assisted displacements. The core samples used were initially saturated with oil with no interstitial water saturation. Computer simulation models were also run for this evaluation. The results showed complex mechanisms present in gravity-assisted CO_2 flooding. They also showed that, during the core flooding, vertical downward displacement results in better performance than that obtained from horizontal displacement as it takes shorter core length for miscibility to happen in vertical flooding. In their conclusion, they also stated that, at lower injection rates, the efficiency of the vertical core flood improves since the gravity forces dominate and there is a minimum mixing of CO_2 and oil [79].

Ashgari and Torabi (2008) presented the outcomes of a series of experiments they conducted along with simulation studies to investigate the performance of oil drainage into a CO_2-filled matrix under miscible and immiscible conditions including the effect of gravity. The results showed that the oil recovery is almost negligible during the CO_2 injection at pressures much less than the MMP. As the pressure increased and approached the MMP, oil recovery increased substantially. Further increase in the pressure far above the MMP had a negative effect on the oil recovery because the density of CO_2 was higher than that of oil. The presence of connate water saturation in the core sample resulted in a decrease in oil recovery under immiscible conditions in contrast to that under miscible

conditions in which the oil recovery improved. The authors stated that these findings can be implemented in designing successful CO_2-EOR operations for naturally-fractured reservoirs [80].

To investigate the impact of gravity on the flow path and oil recovery during CO_2 injection, three core-flooding experiments along with simulation modeling investigating CO_2 injection were conducted by **Moortgat et al. (2013)** for both vertical (i.e. upward and downward) and horizontal systems. The test conditions (i.e. pressure and temperature) were much higher than those of the critical point of CO_2, thus the density of the injected CO_2 was higher than that of oil. The results showed that there was a noticeable gravity effect in the case of the horizontal flood due to the density difference between oil and CO_2 with an oil recovery of 92% after 2.6 hydrocarbon pore volume (HPV) of injected CO_2. For to the same reason, the results also showed that the oil recovered during the vertically downward flood was the least and it was gravitationally unstable resulting in fingering and the oil recovery was 84% after 2.6 HPV of injected CO_2. Finally, the most efficient flooding was in the case of vertically upward injection, which resulted in the highest oil recovery of 98% after 2.6 HPV of injected CO_2. Since the CO_2 density in this case of s higher than that of oil, a piston-like displacement may result [41].

Hamouda and Tabrizy (2013) experimentally investigated the performance oil recovery from sandstone and chalk for dead and live oil through CO_2 core flooding under miscible conditions. In the case of live oil, two samples were prepared: recombined oil with methane only and recombined oil with methane and propane. Their work showed that the oil recovery from sandstone was less than that from chalk and the recovery increased when the miscible conditions were approached. This is attributed to the higher permeability of

the sandstone sample compared to that of chalk, which caused fingering in the sandstone sample. The oil recovery with live oil was less than that with the dead oil while the oil recombined with methane and propane yielded less recovery than the recombined with methane only. This was due either to the decrease in CO_2 extraction efficiency by propane or due to the induced multiple contact miscibility resulting from pressure reduction within the core [81].

Han et al. (2014) and **Han et al. (2016)** designed a 2D CO_2 flooding apparatus mainly to simulate the conditions of gravity-segregation and to show its effects on oil production and CO_2 sequestration. The designed apparatus allows the flooding in different dipping angles (i.e. zero-degree for horizontal flooding and 90-degree for vertical flooding). In their study, a sandstone plate was used, and the experiments were conducted under both immiscible and near-miscible conditions at various injection rate to investigate the effect of injection rate on oil production and the volume of stored CO_2. The results showed that gravity greatly affects oil production under immiscible conditions in the vertical displacement, which is the effect of gravity in thick reservoirs. Furthermore, the oil recovery in the vertical system was less than that for the horizontal system due to gravity segregation regardless of the injection rate. This observation indicates that the reservoir thickness should not be highly considered during CO_2 flooding. For immiscible conditions, the results also showed that, increasing the CO_2 injection rate results in insufficient time for the contact between oil and CO_2 and, hence, decreasing the ultimate oil recovered. For near-miscible conditions, however, the phenomenon of gravity override was not noticeable. The oil recovered was three times greater than that recovered under immiscible conditions and it was most

efficient in the horizontal system. Finally, variation in the injection rate did not have much effect on the ultimate oil recovered [37, 12].

CHAPTER 3

PROBLEM STATEMENT AND RESEARCH DESIGN

3.1 Problem Statement

The gravity override phenomenon in CO_2 flooding is well documented in the petroleum literature by reports of laboratory and field observations. However, none of these have attempted to investigate the use of liquid organic solvents such as triethyl citrate (TEC) and ethyl benzoate (EB) as agents to blend $scCO_2$ for improving the flooding performance. Therefore, this work proposed blending the CO_2 phase with these organic solvents that would produce blends with desirable density and/or viscosity and could result in a better flood sweep efficiency with a minimum effect of methane absorption from the oil on the CO_2 miscibility power.

3.2 Research Objectives

The primary objectives of this research work were:

1. Identify different solvents that can blend with $scCO_2$ and produce blends with densities close to those of crude oil and water.
2. To test the ability of the selected solvents to blend with CO_2 and examine the effectiveness of the blends to minimize the effect of CO_2 gravity override through core-flooding experiments.

3.3 Research Project Methodology

Based on the research objectives, this project involved four phases:

- **Phase I** involved a literature survey to identify the different solvents that can blend with CO_2 and produce blends with desirable densities.
- **Phase II** involved solubility experiments between CO_2 and each selected solvent for different CO_2 concentrations to test the ability of each solvent to blend with CO_2 and to test the blends' densities. These experiments were carried out in a windowed PVT apparatus. From these experiments, the optimum solvent concentration that results in a blend density close to those of reservoir fluids was selected. The blends' saturation pressures and, hence, the injection pressure at which the core-flooding experiments were conducted were also measured.
- **Phase III** involved flooding vertically upwards Indiana limestone core samples saturated with dead Saudi Arabian light crude oil at irreducible water saturation. Recombined crude oil was also tested. In all core floods, the displacing fluid was either pure $scCO_2$ or a CO_2-solvent blend. All the experiments were conducted at typical Saudi Arabian reservoir conditions under a constant confining pressure of 4,000 psi with a constant back pressure of 3,500 psi at reservoir temperature of 100 °C (212 °F).
- **Phase IV** involved evaluating the effectiveness of the selected blends on minimizing the effect of gravity override and improving oil recovery.

3.4 Research Key Milestones

To meet the objectives of this research project, there were several key milestones that had to be fulfilled and they are shown in **Figure 3.1**.

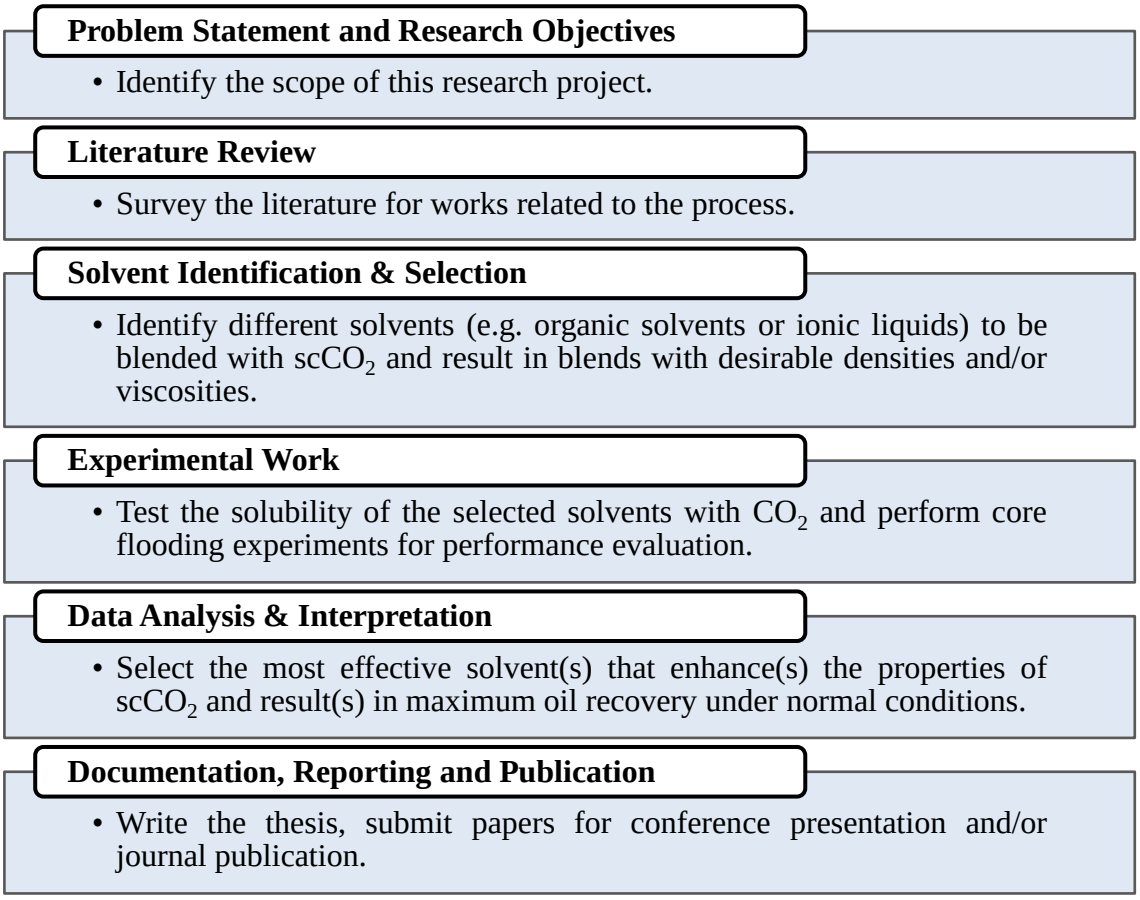

Figure 3.1: Key Milestones of Research Work

CHAPTER 4

EXPERIMENTAL WORK

This work was aimed at reducing the effect of gravity override during $scCO_2$ flooding for enhanced oil recovery purposes. Two different solvents were tested for their ability to blend with $scCO_2$ and the resulting blends' densities. Core flooding experiments were then conducted to evaluate the effectiveness of the selected solvents in improving oil recovery by reducing $scCO_2$ gravity override. This chapter presents the materials and fluids used, the experimental equipment used, and procedures followed to carry out the solubility and core-flooding experiments.

4.1 Rocks and Fluids

4.1.1 Rock Core Samples

Four Indiana limestone core samples with dimensions of 1.5 inches in diameter and 12 inches in length were used in the core flooding experiments. Limestone was selected over sandstone because the majority of Saudi Arabia's oil reserves are present in carbonate reservoirs.

The porosity of each sample was measured by saturating the core with distilled water by first drying it under vacuum at 60 ℃, left overnight to cool, then measuring its dry weight (m_{dry}). Then, two samples at a time were placed in a saturation accumulator where they were first vacuumed for around five hours to remove any air. Distilled water was then

injected into the accumulator and the accumulator was then pressurized to 2,000 psi at ambient temperature and left overnight. The weight of each sample ($m_{saturated}$) was then measured. The porosity of each sample was then estimated from the difference between the weights of the sample before and after saturation and its pore volume was calculated.

The permeability of each sample was measured by steady-state flooding with distilled water at three different flow rates and the pressure drop across the sample was noted. The flow rates were then plotted against the pressure drop and the permeability of the sample was calculated from the slope of the line using Darcy's equation. The setup used for permeability measurement is the same core-flooding setup described in section 4.4.1. The samples were found to have an average porosity and an average permeability of 18.91% and 267.99 mD, respectively, with an average pore volume (PV) of 64.81 cm^3. All properties of the core samples are summarized in **Table 4.1**.

Once the porosity and permeability were measured, the samples were then dried off to prepare them for oil saturation.

Table 4.1: Properties of the Rock Samples Used in this Work

Sample No.	Diameter, D (in)	Length, L (in)	Pore Volume, V_P (cc)	Porosity, φ $(\%)$	Permeability, k (mD)
3	1.4915	12.00	63.97	18.62	237.17
4	1.4920	12.01	64.87	18.85	297.55
5	1.4860	12.00	65.20	19.12	253.88
6	1.4878	12.03	65.20	19.03	283.34

4.1.2 Gases

The gases used in this work include 99.999% pure CO_2 that was used for solubility and flooding experiments. Other gases used were industrial grade methane, ethane, propane and butane, which were mixed to simulate a solution gas for recombining with dead oil.

4.1.3 Crude Oil

Saudi Arabian dead crude oil was used in this work. Before any analysis of the properties of the crude oil, it was first filtered to remove any debris or sand grains. The density and viscosity of the crude oil were then measured over a wide range of temperatures at atmospheric pressure using the OSTWALD method [82]. The results were then extrapolated to the test temperature of 100 ℃. The density results showed that the crude has 30.33 °API gravity. Other properties of the used crude oil are listed in **Table 4.2**.

SARA analysis was also conducted on an oil sample by High-Performance Liquids Chromatography (HPLC). HPLC separates the oil sample into four chemical groups (Saturates, Aromatics, Resins, and Asphaltenes) and expresses the concentration of each group in weight percent (wt%). The results of the SARA analysis are presented in **Table 4.3**. These results are close to those obtained by Hassan and Al-Hashim [83] who worked on the same oil; their results are also presented in **Table 4.3**. Hassan and Al-Hashim's [83] gas chromatography (GC) analysis of the oil are shown in **Table 4.4**. These are presented along with those of Oskay et al. [30] for Arab Light dead crude oil.

Table 4.2: Properties of the Crude Oil Used in this Work

°API Gravity	Specific Gravity @ 25 ℃	Density @ 25 ℃ (g/mL)	Specific Gravity @ 100 ℃	Dead Oil Viscosity @ 25 ℃ (cP)	Dead Oil Viscosity @ 100 ℃ (cP)
30.33	0.870	0.867	0.823	15.4	2.69

Table 4.3: Results of SARA Analysis of the Used Crude Oil

Crude Oil	**°API**	**Saturates (wt.%)**	**Aromatics (wt.%)**	**Resin (wt.%)**	**Asphaltenes (wt.%)**
Our work	30.33	39.9	41.9	12.7	5.55
Literature [83]	30.77	42.2	36.10	16.2	5.51

Table 4.4: Composition of the Used Crude Oil

Taken from Hassan and Al-Hashim [83]		Taken from Oskay et al.[30]	
Component	**Concentration (mole%)**	**Component**	**Concentration (mole%)**
C_5	1.23	CO_2	0.16
C_6	4.23	C_3	0.08
C_7	10.67	i-C_4	0.22
C_8	15.81	n-C_4	2.28
C_9	14.51	i-C_5	1.90
C_{10}	14.43	n-C_5	4.00
C_{11}	11.15	C_6	6.26
C_{12+}	27.98	C_{7+}	85.10
C_{5+}	**100%**	**C_{5+}**	**97.26**

4.1.4 Seawater

Natural Arabian Gulf water obtained from a coastal area near Dhahran was used in this study. The collected quantity of seawater was filtered, and its properties were measured as listed in **Table 4.5**. Ion Chromatography (IC) was also used to determine the water's ionic composition; this is shown in **Table 4.6**.

Table 4.5: Properties of the Seawater Used in this Work

Specific Gravity @ 25 ℃	Density @ 25 ℃ (g/mL)	Seawater Viscosity @ 25 ℃ (cP)	Electrical Conductivity (mS/cm)
1.03	1.02	1.09	64.5

Table 4.6: Ionic Composition of the Used Seawater

Ions	Concentration (mg/L)
Sodium (Na^+)	13903.5
Potassium (K^+)	502.5
Magnesium (Mg^{2+})	1819
Calcium (Ca^{2+})	794.5
Florine (F^-)	*ND*
Chlorine (Cl^-)	22289
Bromine (Br^-)	322
Nitrate (NO_3^-)	173
Sulfate (SO_4^{2-})	3362
Phosphate (PO_4^{3-})	*ND*
TDS	**43165.5**

ND = Not Detected
TDS = Total Dissolved Solids

4.1.5 Selected Solvents

Based on the literature survey and since many solvents show the ability to blend with CO_2, we had to set selection criteria to select right solvents to be used. For example, the solvent should be commercially available at low prices with no or with low solubility in both crude oil and water. Most importantly, the solvent should be able to blend with the highest possible amount of CO_2 and the solvent's density should be high enough so that when it is blended with CO_2 the resulting blend's density is close to that of dead crude oil and water at typical reservoir conditions. Other criteria involve that the solvent should have low vapor

pressure, should have no or low flammability and its boiling temperature should be high so that it can withstand high ambient temperatures. Based on these criteria, two organic solvents were selected to be studied in this work; namely ethyl benzoate (EB) and triethyl citrate (TEC) whose properties along with those of CO_2 are presented in **Table 4.7**. These solvents are briefly described next.

Table 4.7: Properties of CO_2 and Organic Solvents Used in this Work

Component	Molecular Weight (g/mol)	Chemical Formula	Critical Pressure (psia)	Critical Temperature (°C)	Acentric Factor
Carbon Dioxide	44.01	CO_2	1,071	31.1	0.228
Ethyl Benzoate (EB) [84]	106.2	$C_9H_{10}O_2$	411.9	425	0.769
Triethyl Citrate (TEC) [85]	276.3	$C_{12}H_{20}O_7$	322.4	708	0.414

4.1.5.1 Ethyl Benzoate

Ethyl benzoate (EB) is an ester with the molecular structure shown in **Figure 4.1** and is formed by condensing benzoic acid and ethanol. It is a colorless liquid with a density of 1.05 g/cm^3 at ambient conditions. It has a melting point of -34 °C (-29 °F) and a boiling point of 211-213 °C (412-415 °F). Such a high boiling point makes it of great interest since it stays in the liquid phase at extreme ambient temperatures. The advantage of using EB is that it is insoluble in water though it is miscible with many organic solvents. The purity of EB used in this work is higher than 99%.

Since the thermodynamic properties of EB are available (mainly the critical pressure, the critical temperature and the acentric factor) [84], it was possible to construct the pressure-

temperature phase diagram for binary systems consisting of CO_2 and EB at different CO_2 molar concentrations using WinProp software from CMG group that implements the Peng-Robinson Equation of State (PR-EOS) [86] as shown in **Figure 4.2**.

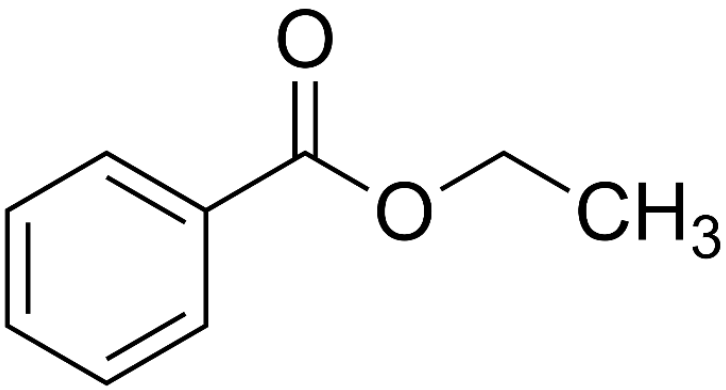

Figure 4.1: Molecular Structure of Ethyl Benzoate

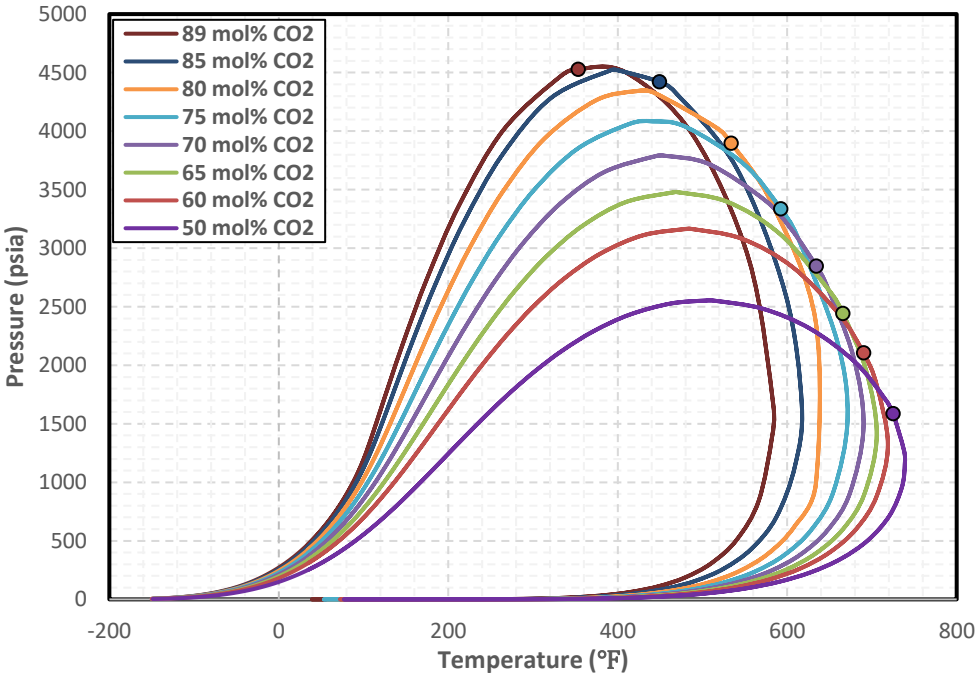

Figure 4.2: Pressure-Temperature Phase Diagram for CO_2-EB Binary Systems Using PR-EOS

4.1.5.2 Triethyl Citrate

Triethyl citrate (TEC) is an ester of citric acid that is used in many applications in the food industry, foam stabilization, pharmaceutical applications, and plastics and its molecular structure is shown in **Figure 4.3**. At ambient conditions, TEC is a colorless and odorless liquid with a density of 1.137 g/cm^3. It has a melting point of -55 ℃ (-67 ℉) and a boiling point of 294 ℃ (561 ℉) at atmospheric pressure, which is high enough to keep it in the liquid phase at extreme ambient temperatures. Unlike EB, TEC is slightly soluble in water with a solubility of around 60 g/L but shows negligible solubility in crude oil. The purity of TEC used in this work is 99%.

It was also possible to construct the pressure-temperature phase diagram for binary systems consisting of CO_2 and TEC at different CO_2 molar concentrations using WinProp software as shown in **Figure 4.4.**

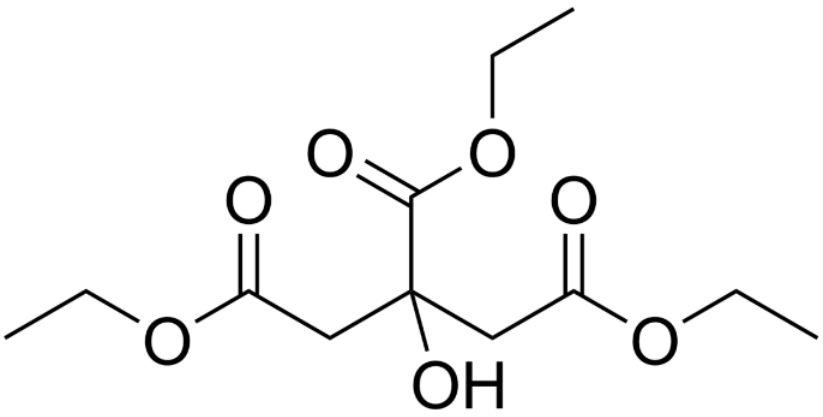

Figure 4.3: Molecular Structure of Triethyl Citrate

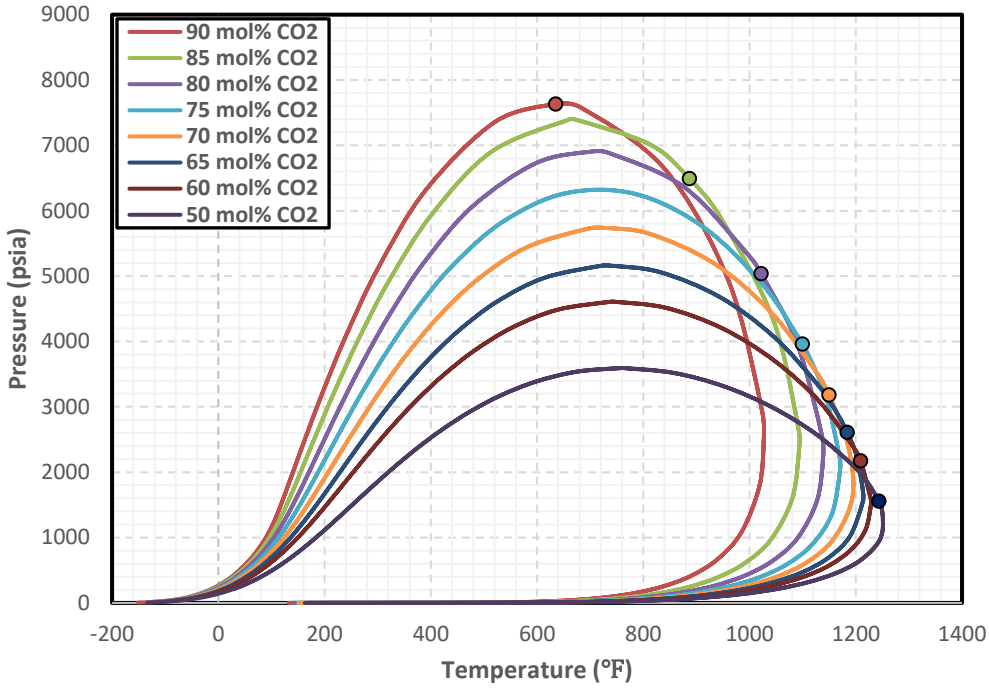

Figure 4.4: Pressure-Temperature Phase Diagram for CO_2-TEC Binary Systems Using PR-EOS

4.2 Solubility Measurement of CO_2 with the Selected Solvents

Prior to the core flooding experiments, the ability of CO_2 to blend with the selected solvents had to be determined and the resulting blends' densities had to be tested. This was done through measurement of the saturation pressure of CO_2-Solvent blend. It was necessary to determine this pressure to show the conditions at which blending is achieved and whether these pressures are reasonable for reservoir applications. Knowing the saturation pressure prior to a core flood is also important to avoid significant changes in the composition of the blend that could result if the pressure of the flooding experiment drops below this pressure. Therefore, a blend is maintained as a single-phase fluid by keeping the flood pressure above the blend's saturation pressure. The following subsections present the experimental set-up and the procedures followed.

4.2.1 Experimental Apparatus

The PVT 300/700 FV EDU system manufactured by Sanchez Technology was used for conducting the solubility experiments between CO_2 and the selected organic solvents. Photographs of the system are shown in **Figure 4.5**. The system's operating limits are 700 bar (10,152.6 psi) and 180 ℃ (356 ℉) with a maximum PVT cell volume of 300 mL, and its measurement accuracy is 0.1 bar (1.45 psi) for pressure, 0.1 ℃ (±32.2 ℉) for temperature and ± 0.35 bar for bubble/dew point repeatability. It is also resistive for corrosive gases such as CO_2 and H_2S. The main feature of this system is that it keeps the cell's contents at constant composition during the experiment. The cell's volume can be varied through the movement of the piston and, hence, pressurizing or depressurizing the cell's contents isothermally. Heating the PVT cell is achieved by an automatically controlled electric heating system. The cell's sapphire window allows visual observation of its contents via a high-resolution camera connected to a monitor. For mixing the cell's contents, a magnetic stirring system driven by an electric motor provides the stirring action [87].

Figure 4.6 and the schematic diagram shown in **Figure 4.7** illustrate the experimental setup used to prepare the CO_2-solvent mixture and to transfer the solvent into the PVT cell. The setup consists mainly of VPA syringe pump from DCI Test Systems, a CO_2 cylinder, a 100-cm^3 floating-piston accumulator (also from DCI Test Systems) and stainless-steel connection tubing.

Figure 4.5: PVT 300/700 FV EDU from Sanchez Technology

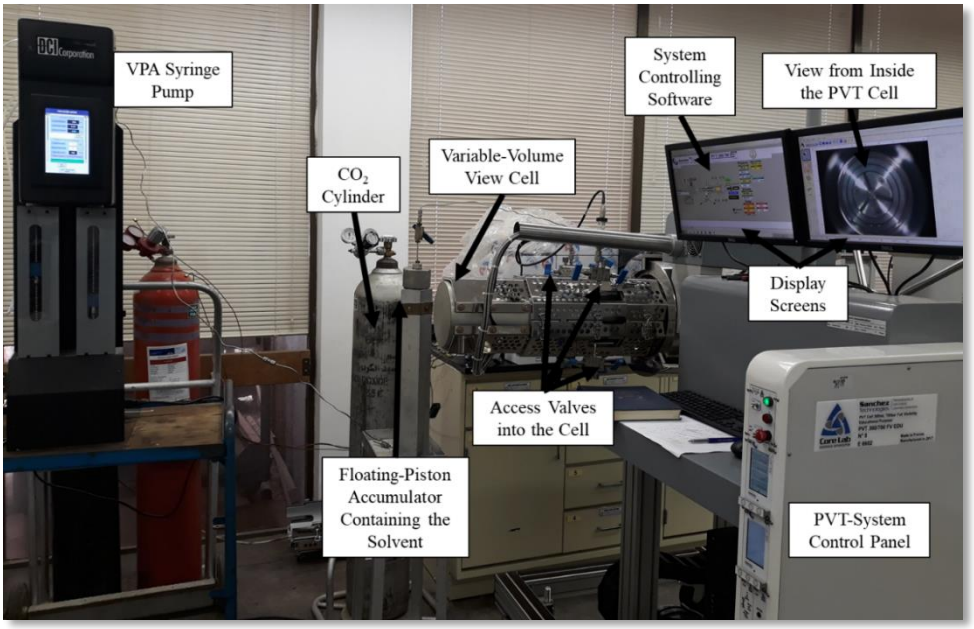

Figure 4.6: Experimental Set-up for CO_2 Solubility Measurement

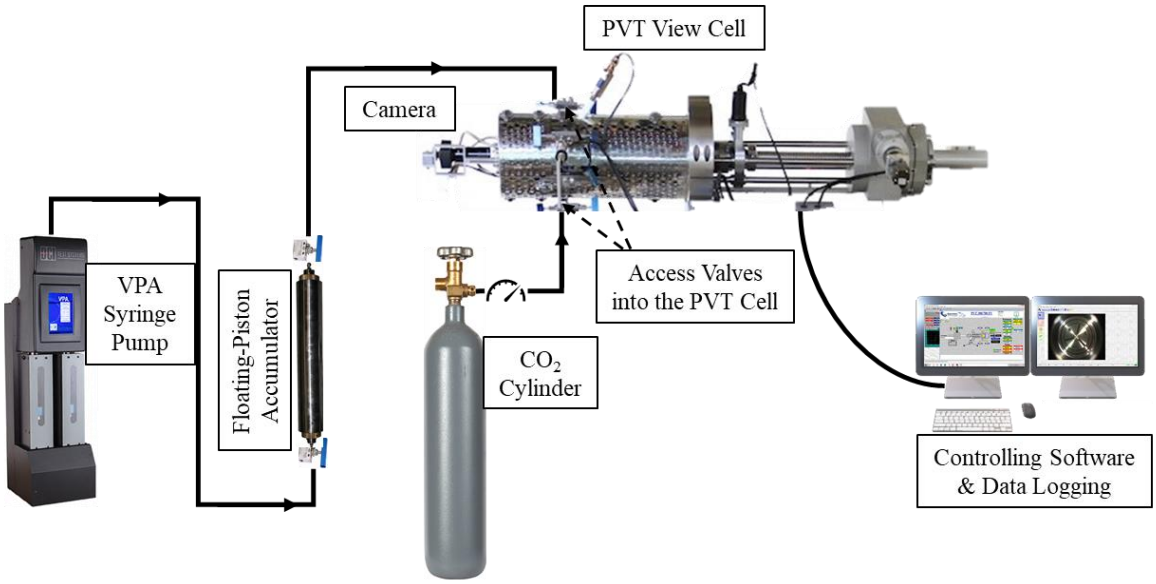

Figure 4.7: Experimental Setup for CO_2 Solubility Measurement

4.2.2 Experimental Procedure

The experimental procedure for solubility measurements involves the preparation of a CO_2-solvent blend with a specific CO_2 molar concentration that is held constant during the experiment at a given temperature. Once the blend is prepared, its bubble-point pressure, P_b, or saturation pressure, P_{sat}, is measured at different temperatures before the next concentration is prepared. The detailed experimental procedure is described in the following subsections and it is similar to that described by Hassan et al. [88] and elsewhere [89].

4.2.2.1 Preparation of CO_2- Solvent Blend

For a specific solvent, the PVT cell was first cleaned with cleaning solvents (i.e. toluene and acetone) and then vacuumed for a specific period. The cell's volume was then adjusted to a specific value at room temperature after which CO_2 was allowed into the cell from the

gas cylinder until the pressure in the cell became in equilibrium with that in the CO_2 cylinder.

Since no gas flow meter was used to measure the amount of injected CO_2, the amount of gas inside the cell was estimated by the real gas law. This was realized by first enlarging the cell's volume to reduce its pressure below the CO_2 liquefication pressure so that the real gas law could be applied as follows:

$$PV = ZnRT \tag{4-1}$$

where P is the cell pressure (psia), V is the cell volume (mL or cm^3), Z is the gas compressibility factor, R is the gas constant, T is the cell temperature (K) and 'n' is the number of moles of CO_2 in the cell.

The gas compressibility factor was estimated by the Peng-Robinson Equation of State (PR-EOS) expressed by the following equation [86]:

$$P = \frac{RT}{V_m - b} - \frac{\alpha(T)}{V_m(V_m + b) + b(V_m - b)} \tag{4-2}$$

where P is the absolute pressure, V_m is the gas's molar volume, T is the absolute temperature, $\alpha(T)$ is the temperature-dependent attractive parameter, 'b' is the co-volume and. The parameters 'b' is independent of temperature and it is a function of the gas's critical properties. It is calculated as follows:

$$b = 0.07780\frac{RT_c}{P_c} \tag{4-3}$$

where T_c and P_c are the gas's critical temperature (K) and critical pressure (psia), respectively.

The attraction parameter is calculated using the following equation:

$$\alpha(T) = a\left[1 + m\left(1 - \sqrt{T_r}\right)\right]^2 \tag{4-4}$$

in which the parameter 'a' is calculated by:

$$a = 0.45724\frac{(RT_c)^2}{P_c} \tag{4-5}$$

and the parameter 'm' is related to the acentric factor as follows:

$$m = 0.37464 + 1.54226\omega - 0.26992\omega^2 \tag{4-6}$$

For acentric factors greater than 0.49, Peng and Robinson [90] proposed the following equation for the parameter 'm':

$$m = 0.3796 + 1.485\omega - 0.1644\omega^2 + 0.01667\omega^3 \tag{4-7}$$

The PR-EOS can be expressed in terms of the compressibility factor (Z-factor) as follows:

$$Z^3 - (1 - B)Z^2 + (A - 3B^2 - 2B)Z - (AB - B^2 - B^3) = 0 \tag{4-8}$$

where:

$$A = \frac{\alpha(T)P}{(RT)^2} \tag{4-9}$$

$$B = \frac{bP}{RT} \tag{4-10}$$

The values of the roots obtained by solving equation (4-8) depend on the state of the fluid [91]; that is:

- For the two-phase region, the equation yields three different real roots in which the largest positive root corresponds to the Z-factor for the vapor phase (Z_{vap}) and the smallest positive root corresponds to that of the liquid phase (Z_{liq}).
- At the single-phase region (i.e. either gas or liquid phase), the equation yields one real root.
- At some points within the supercritical region, the equation can yield three real roots in which only the largest root has a physical meaning and is the value of the compressibility factor.

Once the Z-factor was estimated, the number of moles of CO_2 in the cell were calculated. The amount of solvent (in moles and, hence, in grams and milliliters) required for a specific CO_2 mole fraction in the blend was then determined by:

$$n_{Solvent} = \frac{n_{CO_2} - x_{CO_2} n_{CO_2}}{x_{CO_2}} \qquad (4\text{-}11)$$

where x_{CO2} is the mole fraction of CO_2 and $n_{Solvent}$ is the moles of the solvent.

The floating-piston accumulator was then filled with the solvent and the syringe pump was used to transfer the required amount of solvent for each composition into the PVT cell.

For that composition, the saturation pressure was then measured at different temperatures as described next. To test another blend with a lower CO_2 mole fraction, an additional amount of solvent was charged into the cell as determined by material balance. The procedure for determining the saturation pressure was then repeated for the new blend.

4.2.2.2 Measurement of the Saturation Pressure of the CO_2-Solvent Blends

For each prepared blend, its saturation pressure was determined by first pressurizing and agitating the cell until the cell's content became a single-phase fluid. To ensure a single-phase condition, the blend was pressurized to a pressure higher than its expected saturation pressure. The cell's pressure was then gradually reduced isothermally by expanding the cell volume at a constant expansion rate of 0.33 cc/min. The total volume of the blend, V_t, was measured and automatically recorded along with the corresponding pressure every 5 seconds. The continuous reduction in pressure was performed following the constant composition (or mass) expansion (CCE or CME) method in which no gas or liquid were removed from the PVT cell during the test [91]. The appearance of the first CO_2 bubble indicated that the saturation pressure of the blend at that specified temperature had been reached as shown in **Figure 4.8**. At this point, the cell's pressure was recorded as the saturation pressure of the blend of that composition at the given temperature. The cell's volume at this pressure was also recorded and noted as, V_{sat}.

To confirm the visual determination of the saturation pressure, the volume of the cell was plotted against its pressure as shown in **Figure 4.9**. The saturation pressure is then read from the intersection point of the two lines drawn through the data. The corresponding cell volume at the saturation pressure became the reference volume to compute the relative volume (i.e. V_t/V_{sat}).

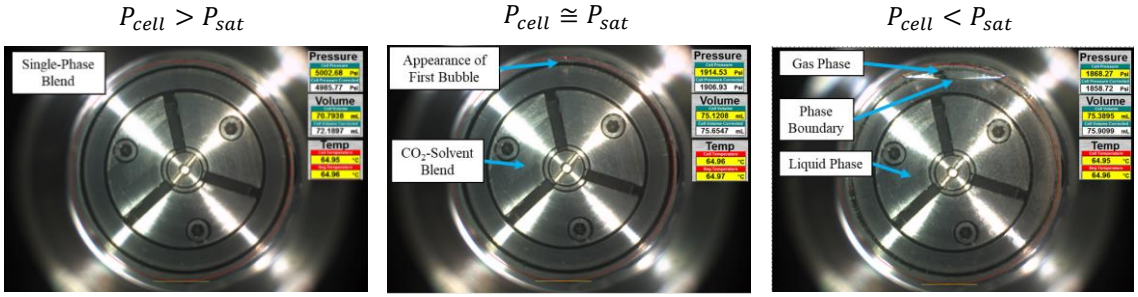

Figure 4.8: Example of the Observation form the Inside of the PVT Cell

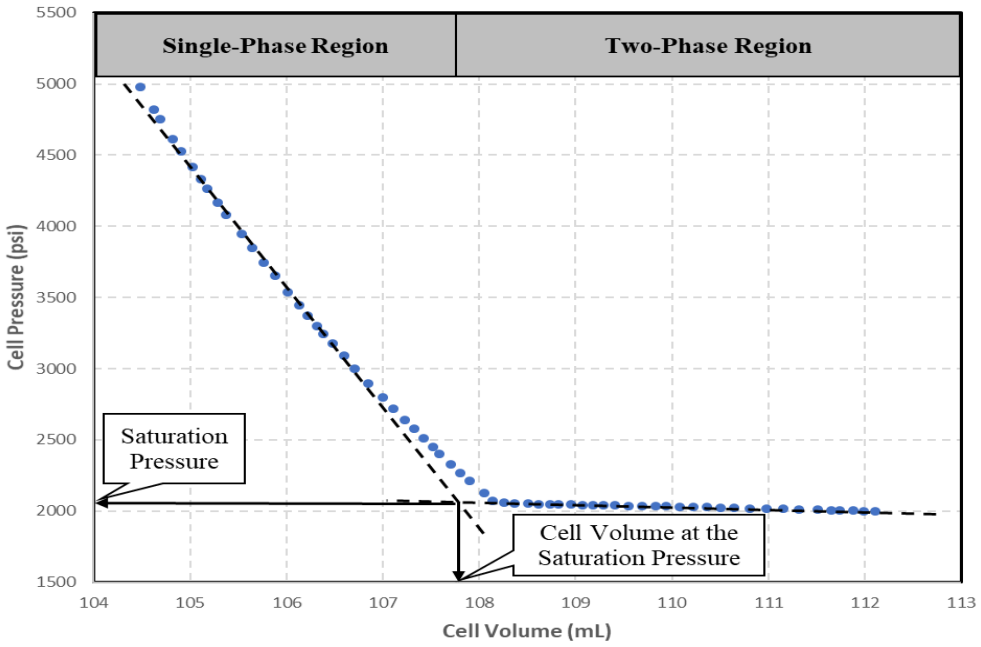

Figure 4.9: Pressure of the PVT Cell versus its Volume for Determining the Saturation Pressure

4.2.2.3 Calculation of the Density of the CO_2-Solvent Blends

The objectives of this research work involve the determination of the density of the blends containing CO_2 and the solvents. Since the mass of the blend is known, its density at its saturation pressure is given by:

$$\rho_{sat} = \frac{m_{blend}}{V_{sat}} \qquad (4\text{-}12)$$

where ρ_{sat} is the density of the blend at the saturation pressure, m_{blend} is the total mass of the charged fluid into the cell (equals $m_{co_2} + m_{solvent}$), m_{co_2} is the mass of CO_2 charged into the cell and $m_{solvent}$ is the mass of solvent charged into the cell.

For pressures above the saturation pressure, the blend's density is estimated by:

$$\rho = \frac{\rho_{sat}}{V_{rel}} \tag{4-13}$$

4.2.2.4 Measurement of the Viscosity of the CO_2-TEC Blend

The Rolling-Ball viscometer (RBV) was connected to the PVT system and was used to measure the viscosity of the 85 mol% CO_2 blend's viscosity which was selected for the core-flooding experiments. The measurement was conducted at 100 ℃ and at different pressures above its saturation pressure.

4.3 Solvents Interaction Tests with Fluids and with Rocks

4.3.1 Oil and Water Miscibility Tests with the Solvents

To investigate the interaction between the selected solvents and the oil, a quick miscibility test was conducted. The test was conducted in two ways: the first involved adding a few droplets of the oil to a few milliliters (mL) of solvent while the second involved mixing 0.5 mL of the solvent with 1 mL of the oil. The test was conducted at ambient conditions and the results showed that oil is completely miscible with EB but slightly miscible with TEC as shown in **Figure 4.10**. Therefore, it was decided not to use EB in the core flooding experiments since its miscibility with the oil could degrade the integrity and properties of

the blend. Therefore, only TEC will be tested as a blending solvent in the core-flooding experiments.

For TEC, the test was extended and conducted at 90 °C and between TEC and oil, between TEC and distilled water and TEC and seawater. The results are presented in **Figure 4.11** and showed that there is also a slight miscibility between Oil and TEC and that there is no solubility of TEC in either distilled water or seawater.

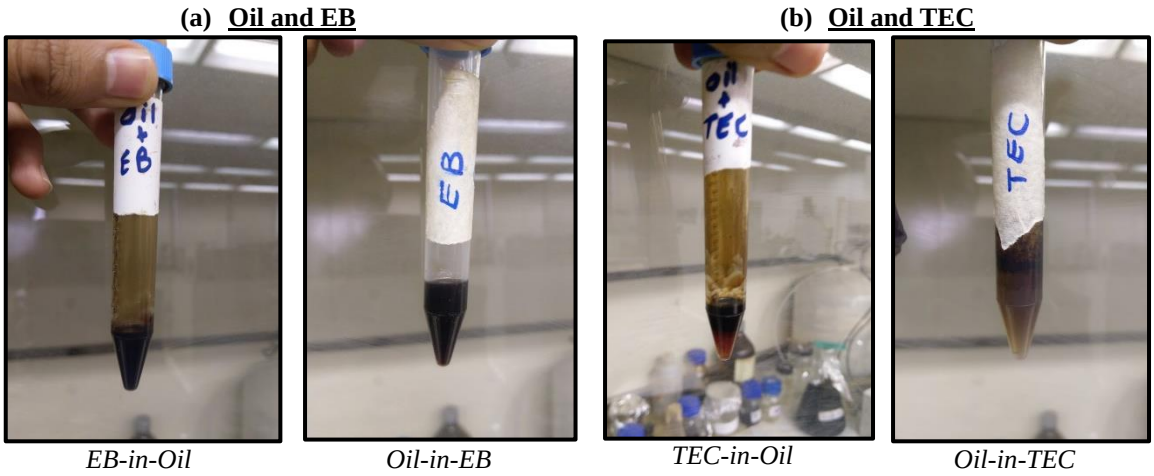

Figure 4.10: Miscibility Test between (a) Oil and EB and (b) Oil and TEC at Ambient Conditions

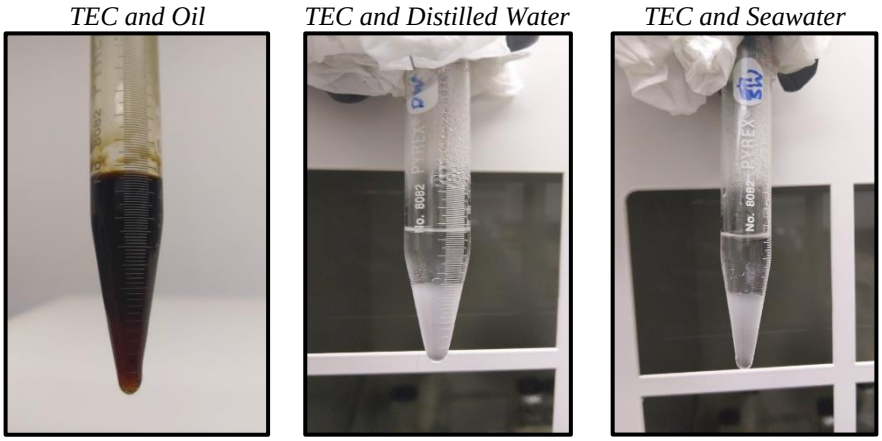

Figure 4.11: Miscibility Test between TEC and Oil, TEC and Distilled Water and TEC and Seawater at 90 °C

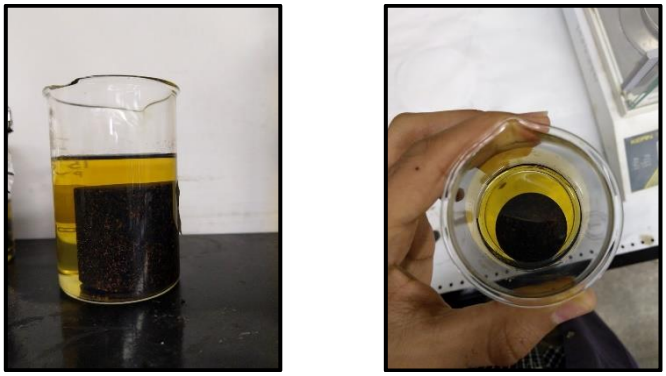

Figure 4.12: Imbibition Test of Oil-Saturated Core Sample in TEC at Ambient Conditions

4.3.2 Imbibition Test of Oil-Saturated Core Sample in TEC

Imbibition test was conducted at ambient conditions by immersing an oil-saturated core sample in TEC. The sample was observed for almost one week to see if TEC will imbibe into the rock. From the test, we did not observe any imbibition of TEC into oil-saturated core. The objective of this test was to show if any improvement in the oil recovery will happen by CO_2-TEC blend it will be because of the density improvement of the injected blend not because of any alteration of the rock properties cause by TEC.

4.4 Core-Flooding Experiments

To test the effectiveness of triethyl citrate on minimizing the effect of gravity override and improving the vertical sweep efficiency of CO_2, core-flooding experiments were conducted. This section provides a detailed description of the experimental setup, the fluid samples preparation, the estimation of the MMP, the core samples preparation, saturation with the crude oil and seawater, and the flooding experimental procedure.

4.4.1 Experimental Setup for Core-Flooding Experiments

The setup for conducting the flooding experiments was the Core Flooding System (CFS 700) manufactured by VINCI Technologies shown in **Figure 4.13** and illustrated schematically in **Figure 4.14**. The system consists of an oven, 2 double pumps, 4 floating-piston accumulators, a hydrostatic core holder, a back-pressure regulator (BPR), pressure measurement system and data acquisition system. The system can operate at confining and pore pressures up to 10,000 psi and temperatures up to 150 ℃ (302 ℉). The system's operation is controlled through a computer interface which allows for automated pump control and data acquisition. The core holder is made of Hastelloy and can hold cylindrical core samples with varying lengths and diameters up to 30.5 cm and 3.8 cm, respectively. Its orientation can be modified such that the flooding can be conducted either horizontally or vertically. The floating-piston accumulators are used to store the fluids to be injected into the core sample and are made of either Hastelloy or stainless-steel. Accumulators A and C are made of stainless steel and are used to inject dead oil and live oil, respectively, which are not corrosive. On the other hand, accumulators B and D are made of Hastelloy and are used to inject CO_2 (or CO_2-TEC blend) and brine, respectively, which are corrosive. The fluids are transferred from these accumulators through stainless steel tubing into the core sample through the dual-injection automated syringe pumps. These pumps are capable of continuously injecting fluids at predetermined flow rates ranging from 0.01 cc/min to 50 cc/min. The confining pressure on the core sample is provided by another automated syringe pump while the back-pressure is provided by a fourth syringe pump. The differential pressure across the core sample is measured by high-resolution differential

pressure transducers (i.e. ±50psi, ±500 psi and ±1,500 psi) with a resolution of ±0.1% of full scale [92]. The system has also been described elsewhere [93, 94].

The gas produced from the core sample was passed through a CO_2 analyzer to detect CO_2 breakthrough. The analyzer is the model 906 from Quantek Instruments (**Figure 4.15**), which uses a solid-state infrared sensor that has no moving parts, a compact optical cell, and microprocessor-based calibration factors using a 6^{th} order polynomial equation to linearize the full range measurement up to 100% [95]. The graduated cylinder used for collecting the produced oil was set in a way that all effluent fluids had to pass through distilled water at the bottom of the cylinder (**Figure 4.16**). This allowed quick separation of gas from liquid. Produced gas was then diverted into the CO_2 analyzer. The analyzer's reading at the start of the flood was zero and it increased gradually after CO_2 breakthrough. This change in the reading allowed accurate detection of CO_2 breakthrough. In the case of dead oil, CO_2 breakthrough was also detected by visual inspection of the effluent.

Figure 4.13: Core Flooding System (CFS 700) Manufactured by VINCI Technologies

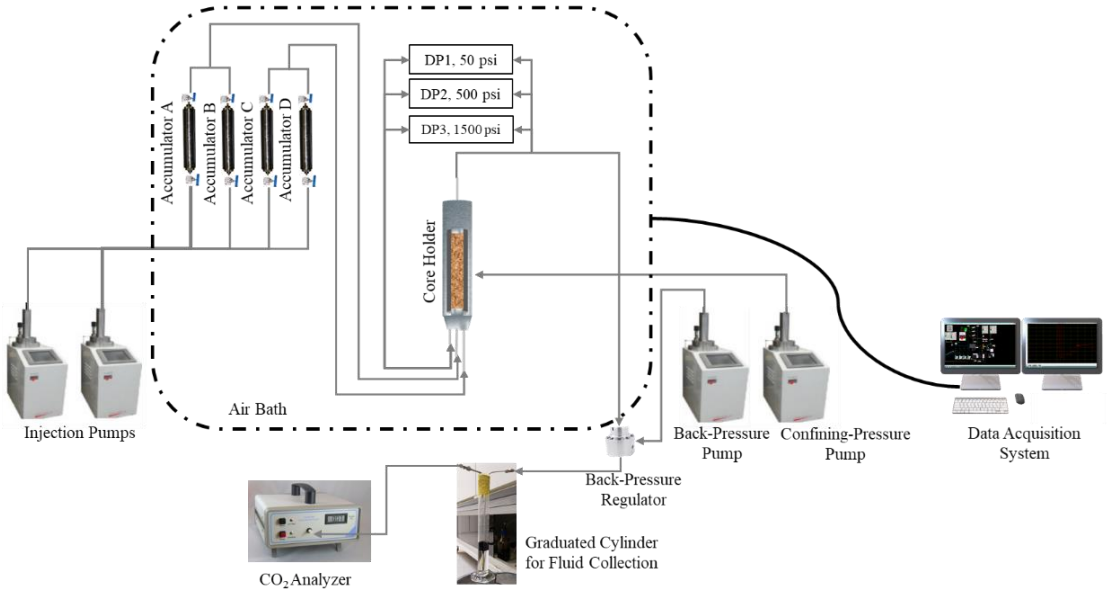

Figure 4.14: Schematic Diagram of the Core-Flooding System

Figure 4.15: CO_2 Analyzer Model 906 from Quantek Instruments

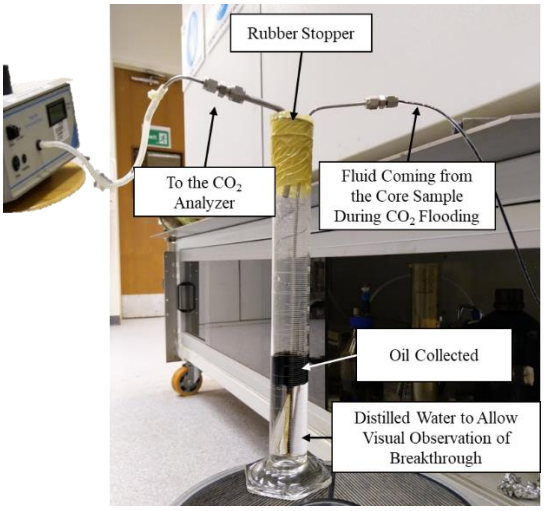

Figure 4.16: Graduated Cylinder Used for Fluid Collection During CO_2 Flooding

4.4.2 Preparation of Live Oil

As previously stated, in case of live oil, which represents the real reservoir conditions, the injected CO_2 extracts the light gases especially the methane and this results in a phase that has a density less than that of pure CO_2 which exacerbates the effect of gravity override. Also, the resulting phase is rich in methane which reduces the diffusivity of the injected CO_2 into the oil phase and affects the recovery performance of CO_2 displacement. To demonstrate the effect of methane and to test the effectiveness of the blends under the real reservoir conditions and to introduce the effect of methane, live oil had to be used in some displacement experiments. The gas used to prepare the recombined oil should have a composition close to that associated with light crude oils in Saudi Arabia. The typical composition of such associated gas is shown in **Table 4.8**. Since real samples of the gas were not available, a similar gas mixture had to be first prepared. The composition of the prepared gas mixture (listed in Table 4.8) was close enough to the real gas composition (also listed in Table 4.8) as found in the literature. Once the gas mixture had been prepared, a sufficient quantity of the crude oil was added to the gas mixture to produce a gas-in-oil solubility (R_s), or solution gas-oil ratio (GOR), of 600 standard cubic feet gas per stock-tank barrel oil (SCF/STB), which is also close to the typical GOR for Saudi Arabian light oil reservoirs.

Table 4.8: Composition of Associated Natural Gas with Saudi Arabian light Crude Oils versus the Composition of Gas Prepared in this Work

Gas Component	Composition (mol%)	
	Typical Composition	This Work
Methane (CH_4)	55.45	57.67
Ethane (C_2H_6)	18.30	27.56
Propane (C_3H_8)	10.15	13.29
Butane (C_4H_{10})	3.85	1.48
Pentane and Heavier (C_{5+})	2.41	0.00
Hydrogen Sulphide (H_2S)	0.77	0.00
Carbon Dioxide (CO_2)	8.68	0.00
Nitrogen (N_2)	0.39	0.00
Total	**100.00**	**100.00**

The procedure of mixing the gas with the crude was as follows:

- Knowing the pressure and temperature (which was the room temperature in this case) of the gas mixture in the vessel, the gas expansion factor, E_g, (in SCF/ft^3) of the gas mixture could be estimated by:

$$E_g = 35.37\frac{P}{ZT} \tag{4-14}$$

- From the gas expansion factor, the volume of the gas mixture in SCF, $V_{gas_{sc}}$, was calculated from:

$$V_{gas_{sc}} = V_{gas_{P,T}} E_g \tag{4-15}$$

- Knowing the volume of the gas mixture at standard conditions, the amount of oil, V_{oil}, a recombined gas with the required GOR is calculated as:

$$V_{oil} = \frac{V_{gas_{sc}}}{GOR} \tag{4-16}$$

- The required amount of oil was then added into the gas-containing accumulator the same way the solvent was added to the PVT cell during the CO_2 solubility experiments.
- The mixing vessel was then pressurized and agitated and left for several days to ensure that the gas is dissolved in the oil.

The bubble-point pressure of the live oil was estimated using Al-Marhoun's correlation [96] and was found to be approximately 2,700 psi at 100 ℃. The density of the live oil was also estimated at the same temperature using the Standing Correlation [97] and it was found to be 44.5 lb/ft^3 (0.7129 g/cm^3). The viscosity of the live oil at the bubble-point pressure and at 3,500 psi could be calculated using Abu-Khamsin and Al-Marhoun correlation [98] and Khan et al. correlation [99], respectively. These values were found to be 0.6499 cP and 0.6549 cP, respectively.

4.4.3 Estimation of CO_2 Minimum Miscibility Pressure

As described earlier, the minimum miscibility pressure (MMP) can be estimated either by conducting laboratory experiments or using the correlations. Since it is not the objective of this work to estimate the MMP experimentally, the MMP of CO_2 with dead crude oil used in this work was estimated by extrapolating the MMP results obtained by Oskay et al. [30]. The results of their work were used in this work because they used the same dead crude oil that has a very close pentane plus (C_{5+}) fraction to that of the crude oil used in this work.

The estimated MMP was found to be around 3,098 psia at the flooding temperature of 100 ℃. The MMP was also estimated using Cronquist correlation [29] in which the molecular weight of the C_{5+} was calculated from the API gravity of the oil [100]. The

estimated MMP from this correlation was 3,126 psia which is close enough to the extrapolated MMP. For the case of live oil, the MMP could be slightly higher than this pressure due to the presence of methane in the live oil.

4.4.4 Core-Flooding Procedure

In this work, a total of four flooding runs were conducted. The first run was a base-case experiment in which pure $scCO_2$ was injected to displace the dead oil at irreducible water saturation (Run 1-DO). The second flooding run involved injecting CO_2-TEC blend to also displace dead oil at irreducible water saturation (Run 2-DO). In the third run, pure $scCO_2$ was injected to displace live oil, also at irreducible water saturation (Run 1-LO). Finally, in the last run, CO_2-TEC blend of the same concentration used in the second run was injected to displace live oil at irreducible water saturation (Run 2-LO). All the experiments are described in detail as follows.

4.4.4.1 Core Samples Saturation and Aging

To prepare the core samples for the flooding experiments, two samples at a time were placed in a saturation vessel in which they were first vacuumed for around five hours to remove any air. Saturating crude oil with the properties previously outlined was then injected into the vessel to saturate the core samples and was then pressurized to 3,000 psi at ambient temperature. The core-containing vessel was then placed in an oven for three days at 60 ℃. This reduced the viscosity of the oil and helped achieve 100% saturation. Thereafter, since pressure has little effect in aging process and wettability alteration [101], the pressure was released to atmospheric pressure after which the samples were left for aging (curing) at 100 ℃ for three weeks to mimic real reservoir conditions and restore their

wettability. The three weeks of aging has been suggested to be sufficient for maximum wettability change [102].

4.4.4.2 Flooding Conditions and Procedure

After aging a core sample, the oil-saturated core sample was loaded into the core holder and placed inside the air bath (oven). The four accumulators were already filled with enough quantities of the respective fluids: Accumulator A with the live oil, B with pure CO_2 or the CO_2-TEC blend, C with dead oil and D with seawater, and were loaded inside the air bath. All the necessary connections to the core holder were then made including those to the fluid accumulators, those to the pressure transducers, that to the confining pressure pump and that to the back-pressure regulator (BPR) and the outlets. A confining pressure of 4,000 psi was then gradually applied on the sample inside the core holder and the BPR was set to a constant pressure of 3,500 psi at the core outlet (i.e. the net confining pressure on the sample was 500 psi). The air bath temperature was then set to 100 ℃ (212 ℉) with pressure control on the core holder and the accumulators, and the system was left overnight to reach stabilized conditions at this temperature. The reason for applying these pressures (i.e. confining pressure and back pressure) was to have the selected CO_2-TEC blend above its saturation pressure, which is about 2, 923 psi so that it remains as a single-phase. Also, to allow miscibility to develop between the oil and CO_2. As stated in section 4.4.3, the MMP between CO_2 and the dead oil was estimated to be 3,098 psia at 100 ℃.

Dead crude oil was then flowed through the sample at a constant flow rate of 1 cc/min. Several pore volumes of the dead oil were continuously injected until the pressure drop across the sample was stabilized, after which the absolute permeability to oil was measured at different flow rates (i.e. 0.25, 0.5 and 1 cc/min). Seawater was then continuously injected

to displace dead oil from the sample at flow rates alternating between 0.5 and 1 cc/min until no more oil was produced and the pressure drop across the sample stabilized. The oil produced by seawater displacement was collected and its volume was measured to determine the residual oil saturation, S_{or}, by mass balance. After that, continuous injection of dead oil was started to displace the seawater at alternating flow rates of 0.5 and 1 cc/min. After injecting several pore volumes of oil, the pressure drop across the sample stabilized and no more seawater was produced. The produced seawater was collected, and its volume was measured to determine the irreducible water saturation, S_{wi}.

In the case of a live-oil run, live oil was injected into the core after the displacement of seawater by dead oil. The injection of live-oil was at a constant rate of 0.25 cc/min and the injection was continued until the pressure drop across the sample stabilized, which was reached usually after injecting almost one pore volume of live oil.

4.4.4.3 Base-Case Flooding: Dead oil by Pure scCO$_2$ (Run 1-DO)

The objective of this run is to have as a reference comparison purposes with other runs. Core sample No. 4 was used. During the preparation, accumulator B was first vacuumed for several minutes to remove any air and was then filled with 850 psi of pure CO_2. During the flooding run, scCO_2 was displaced from the accumulator into the core holder at a constant flow rate of 0.25 cc/min, which was equivalent to almost 1 ft/day under field conditions. The produced oil was collected in a graduated cylinder and the volume of oil produced was continuously recorded manually. The injection was continued until one pore volume of pure scCO_2 was injected. Thereafter, injection was stopped, and the system was shut off and left to cool down for cleaning.

4.4.4.4 Dead Oil Displacement by CO_2-TEC Blend (Run 2-DO)

In this run, a CO_2-TEC blend consisting of 85 mol% CO_2 was used to flood core sample No. 5. The concentration of the mixture was selected based on the phase behavior study, which revealed a blend saturation pressure of 2,923 psi. This pressure is moderate and close to typical reservoir pressures at 100 ℃. Also, the selection was based on the blend's density, which was close to those of the fluids saturating the core sample, yet at a reasonably low concentration of TEC.

The blend was prepared by first injecting CO_2 into accumulator B. Knowing the conditions (pressure, temperature, and volume) of CO_2 in the accumulator, the required amount of TEC was then injected into the accumulator to produce the required concentration. The accumulator was then pressurized and agitated to ensure that the CO_2 is properly blended with TEC. During the core flooding phase, the blend was injected at 0.25 cc/min into the core holder. The oil produced was collected in a graduated cylinder and its volume was continuously noted and recorded manually. The injection was continuous until no more oil was produced, which occurred after injecting about 1 PV of CO_2-TEC blend. Thereafter, the injection was stopped, and the system was shut off and left to cool down for cleaning.

4.4.4.5 Live Oil Displacement by Pure $scCO_2$ (Run 1-LO)

The objective of this run was to demonstrate the effect of saturating the oil with a methane-rich gas on the CO_2 recovery process. In this run, core sample No. 3 was used. Accumulator B was filled with pure CO_2 following the same procedure as flooding run 1-DO. $ScCO_2$ was then injected in the core holder at a constant flow rate of 0.25 cc/min. The oil produced was collected in a graduated cylinder and the volume of oil produced was continuously recorded manually. The injection was continued until about one pore volume of pure CO_2

was injected. Thereafter, the injection was stopped, and the system was shut off and left to cool down for cleaning.

4.4.4.6 Live Oil Displacement by CO_2-TEC Blend (Run 2-LO)

In this run, sample No. 5 was used. This run is similar to the previous run except that the core sample was flooded with the CO_2-TEC blend of the same concentration as that of flooding run 2-DO and at the same rate. The oil produced was collected in a graduated cylinder and the volume of oil produced was continuously recorded manually. The injection was continued until about one pore volume of the blend had been injected. Thereafter, the injection was stopped, and the system was shut off and left to cool down for cleaning.

CHAPTER 5

RESULTS AND DISCUSSION

This chapter presents the results of the experimental work described in Chapter 4. The results of CO_2-solvents blend phase behavior study are reported first with comparisons between the predicted and measured parameters. The results of the core flooding experiments are then presented, discussed and compared.

5.1 Results of CO_2 Solubility Measurement with the Solvents

As shown in chapter 4, the solubility tests between CO_2 and the selected solvents were examined by measuring the saturation pressure of different blends at different temperatures. From the volume of the cell and the mass of the blend inside it, the density of the blends could be calculated at and above the blends' saturation pressures.

The results of the solubility measurements are presented graphically where the blends' saturation pressures are plotted versus temperature for each tested composition. Also, for each temperature, the blends' saturation pressures are plotted versus the corresponding CO_2 molar concentration. The results of the density of the blends are also presented in two ways. First, for each temperature, the density of the blend at the blend's saturation pressure is plotted versus the corresponding saturation pressure. Second, the density of each blend is plotted versus pressure for pressures at and above the blends' saturation pressures at 100 °C. The results are presented in the following subsection.

5.1.1 Carbon Dioxide and Ethyl Benzoate

The solubility between ethyl benzoate and CO_2 was determined for different CO_2 molar concentrations ranging from 90 mol% CO_2 to 65 mol% with a decrement of 5 mol% at four temperatures; these were 25 ℃, 50 ℃, 75 ℃, and 100 ℃.

5.1.1.1 Saturation Pressure Results

Table 5.1 presents the measured saturation pressures of the CO_2-EB blends for different CO_2 molar concentration and at different temperatures. These results are also shown in **Figure 5.1** in which the saturation pressures for different concentrations are plotted versus their corresponding temperatures. Also, the saturation pressure is plotted versus the CO_2 molar concentration for different temperatures in **Figure 5.2**.

The PR-EOS was also used to predict these pressures and the results are also listed in **Table 5.1** and are plotted (dashed lines) in **Figures 5.1 and 5.2**.

Table 5.1: CO_2-EB Saturation Pressure Results (Experimental and Predicted Using EOS)

Temperature (℃)	Saturation Pressure (psi)		Saturation Pressure (psi)	
	Experimental	PR-EOS	Experimental	PR-EOS
	90 mol% CO_2		**85 mol% CO_2**	
25	890	843	870	829
50	1410	1425	1400	1400
75	2220	2214	2190	2157
100	2850	2809	2800	2780
	80 mol% CO_2		**75 mol% CO_2**	
25	850	811	820	785
50	1320	1351	1250	1283
75	2050	2037	1850	1892
100	2650	2644	2430	2459
	70 mol% CO_2		**65 mol% CO_2**	
25	796	751	780	709
50	1200	1203	1120	1115
75	1700	1741	1530	1588
100	2210	2257	1980	2051

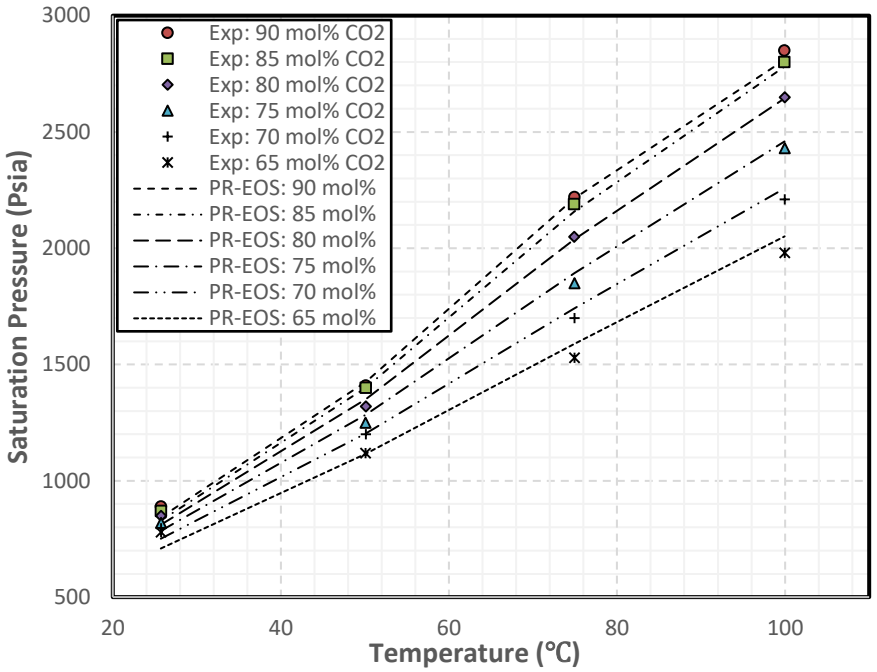

Figure 5.1: Saturation Pressure of CO_2-EB Blend versus Temperature for Different CO_2 Concentrations

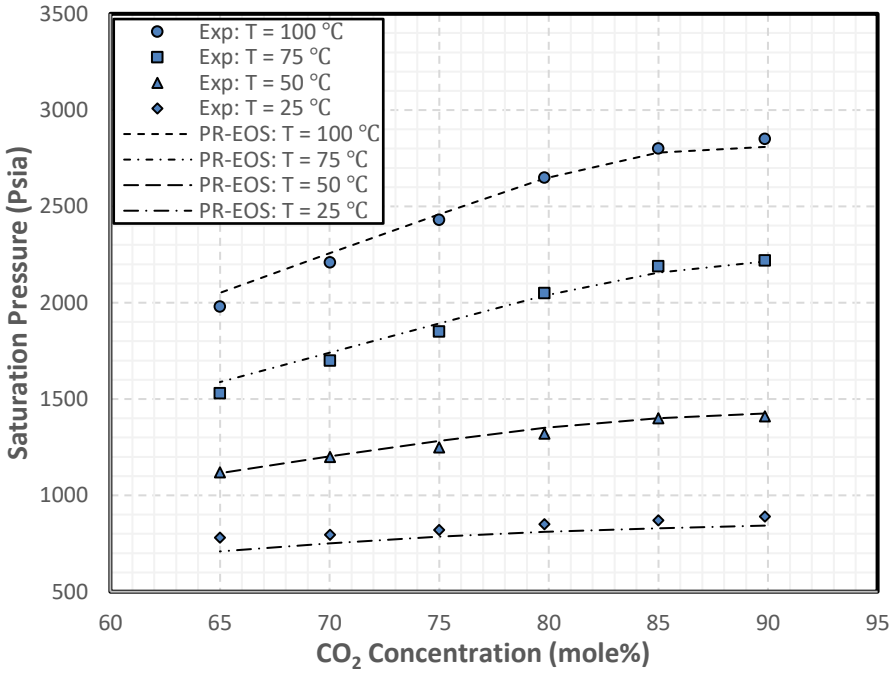

Figure 5.2: Saturation Pressure of CO_2-EB Blend versus CO_2 Molar Concentration at Different Temperatures

5.1.1.2 Density Results

The calculated densities of the different CO_2-EB blends at their saturation pressures are plotted versus the corresponding saturation pressure as shown in **Figure 5.3**. On the same figure, the dashed lines show the prediction of those densities using the PR-EOS. Because we are targeting a reservoir temperature of 100 ℃, the densities of the blends are plotted versus pressure for pressures above and at the blends' saturation pressures at 100 ℃ in **Figure 5.4**.

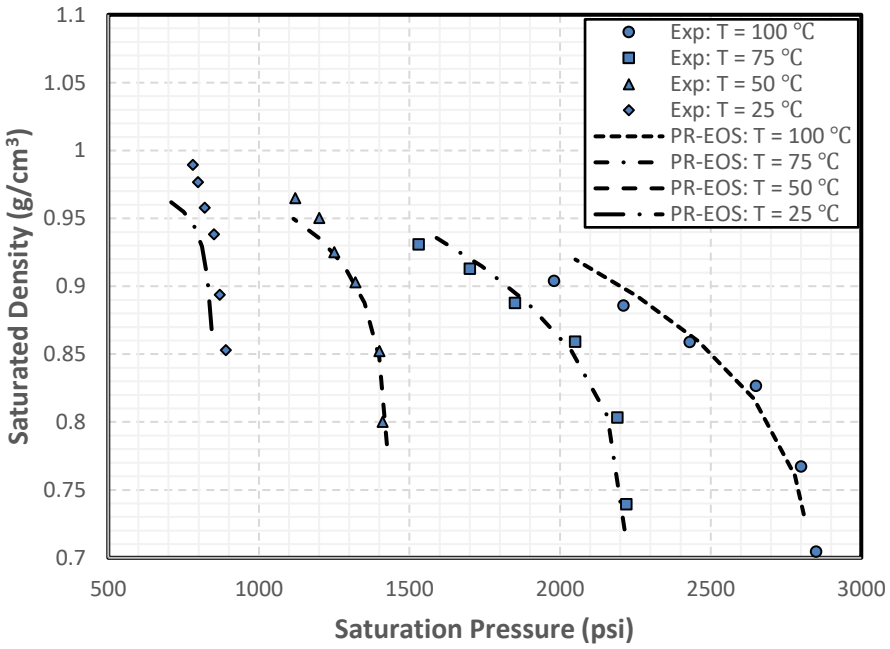

Figure 5.3: Saturation Density of CO_2-EB Blend versus Saturation Pressure at Different Temperatures for Different CO_2 Concentrations

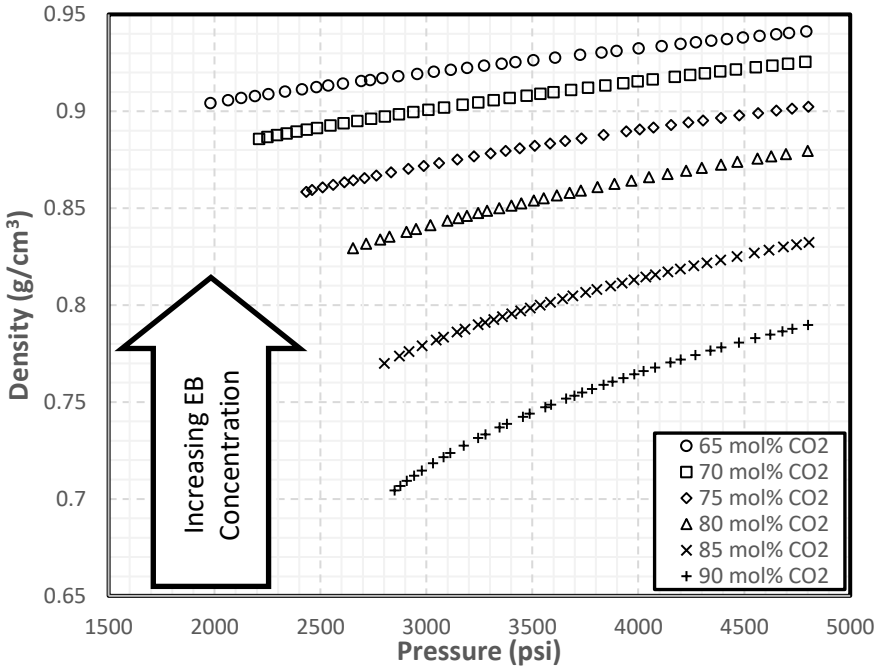

Figure 5.4: Density of CO_2-EB Blend versus Pressure at 100 ℃ for Different CO_2 Concentrations

5.1.2 Carbon Dioxide and Triethyl Citrate

The solubility tests between triethyl citrate and CO_2 were determined for different CO_2 molar concentrations ranging from 90 mol% CO_2 to 65 mol% with a decrement of 5 mol% and at three temperatures; these were 25 ℃, 65 ℃, and 100 ℃.

5.1.2.1 Saturation Pressure Results

The saturation pressures of CO_2-TEC blends with different CO_2 molar concentrations at various temperatures as obtained from this work are presented in **Table 5.2**. The results in this table are also shown in **Figure 5.5** in which the saturation pressures for different concentrations are plotted versus their corresponding temperatures. Also, the saturation pressures are plotted versus the CO_2 molar concentration for different temperatures as shown by the symbols in and **Figure 5.6**.

The PR-EOS was also used to predict these pressures and the results of this prediction are listed in **Table 5.2** and are plotted as shown by the dashed lines in **Figures 5.5 and 5.6**.

Table 5.2: CO_2-TEC Saturation Pressure Results (Experimental and Predicted Using EOS)

Temperature (°C)	Saturation Pressure (psi)		Saturation Pressure (psi)	
	Experimental	PR-EOS	Experimental	PR-EOS
	90 mol% CO_2		**85 mol% CO_2**	
25	810	833	790	774
65	2060	2008	1863	1755
100	3251	3189	2923	2809
	80 mol% CO_2		**75 mol% CO_2**	
25	737	714	700	655
65	1592	1544	1380	1366
100	2505	2461	2072	2158
	70 mol% CO_2		**65 mol% CO_2**	
25	650	597	580	542
65	1110	1213	950	1077
100	1704	1896	1385	1666

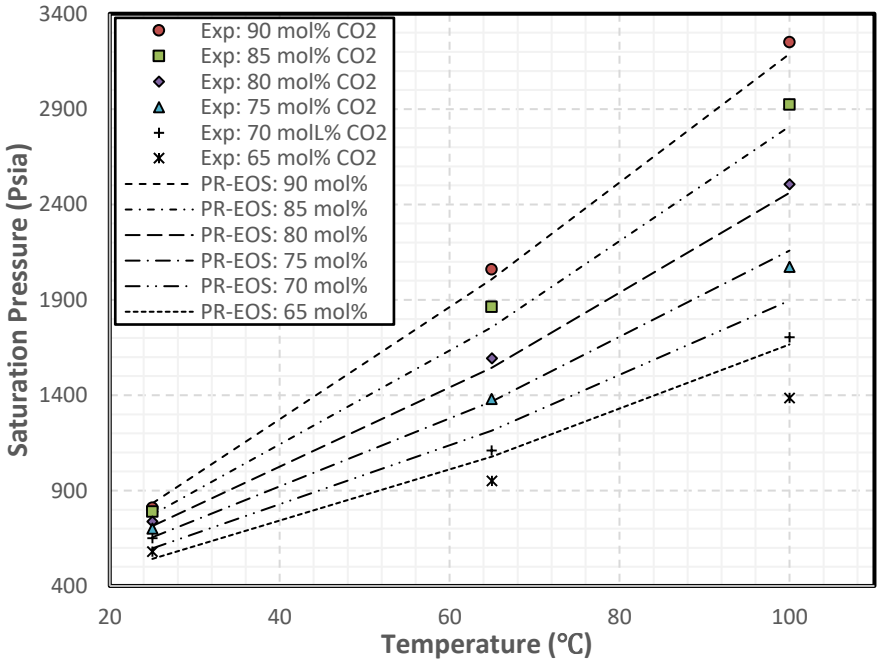

Figure 5.5: Saturation Pressure of CO_2-TEC Blend versus Temperature for Different CO_2 Concentrations

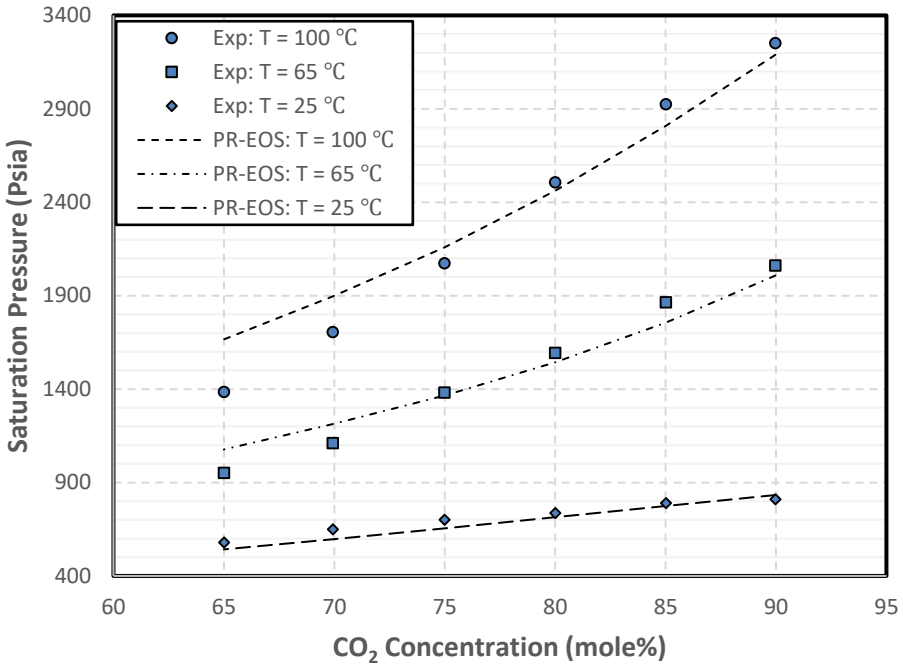

Figure 5.6: Saturation Pressure of CO_2-TEC Blend versus CO_2 Molar Concentration at Different Temperatures

5.1.2.2 Density Results

The calculated densities of the different CO_2-TEC blends at their saturation pressures are plotted versus those pressures as shown in **Figure 5.7**. These results were also estimated using PR-EOS as shown by the dashed lines on the same figure. Because we are interested in the density profile of the blend at the reservoir temperature, the densities of the blends are plotted versus pressure at and above the blends' saturation pressures at 100 ℃ as shown in **Figure 5.8**.

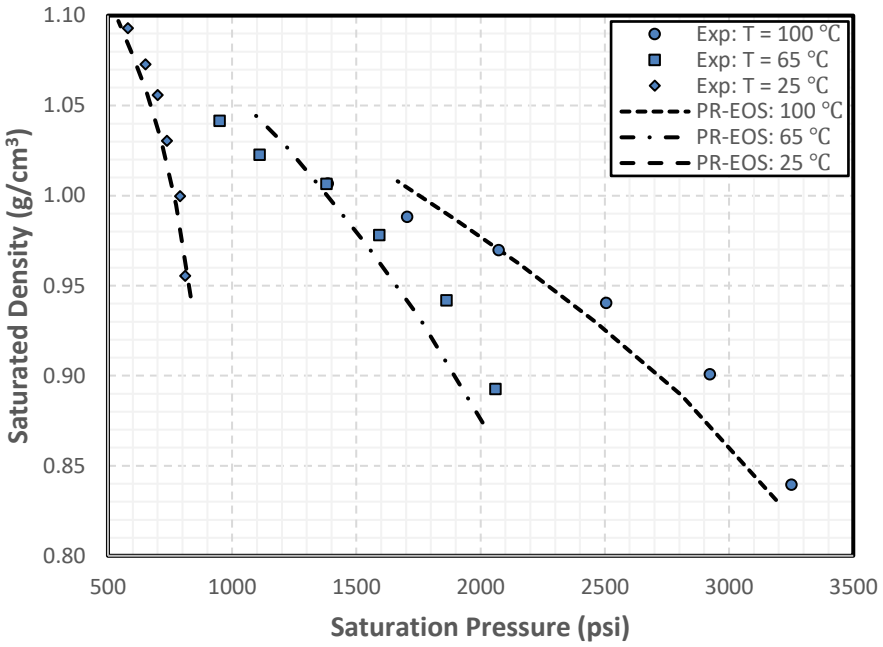

Figure 5.7: Saturation Density of CO_2-TEC Blend versus Saturation Pressure at Different Temperatures for Different CO_2 Concentrations

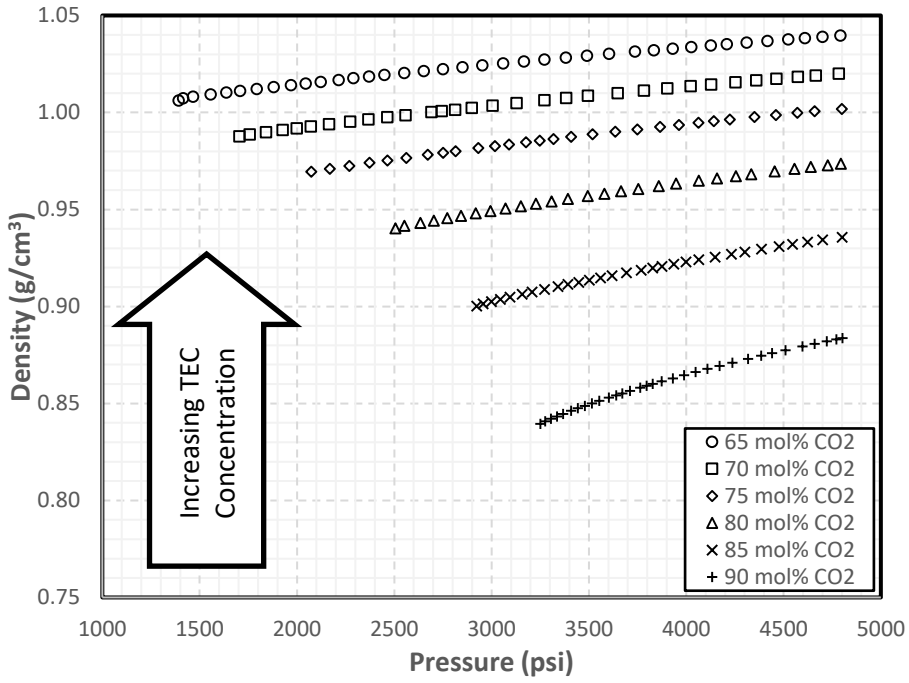

Figure 5.8: Density of CO_2-TEC Blend as a Function of Pressure at 100 °C for Different CO_2 Concentrations

5.1.2.3 Viscosity Results

For the selected CO_2-TEC blend (with 85 mol% CO_2), the viscosity at 100 °C was measured and plotted versus pressure in **Figure 5.9.** At this temperature, the blend's saturation pressure is 2,923 psia. The data shows that at the target reservoir pressure, this blend has a viscosity of the same order as reservoir fluids, which reduces the viscosity difference between the injected CO_2-TEC blend and the reservoir fluids and, thus, could result in improving sweep efficiency.

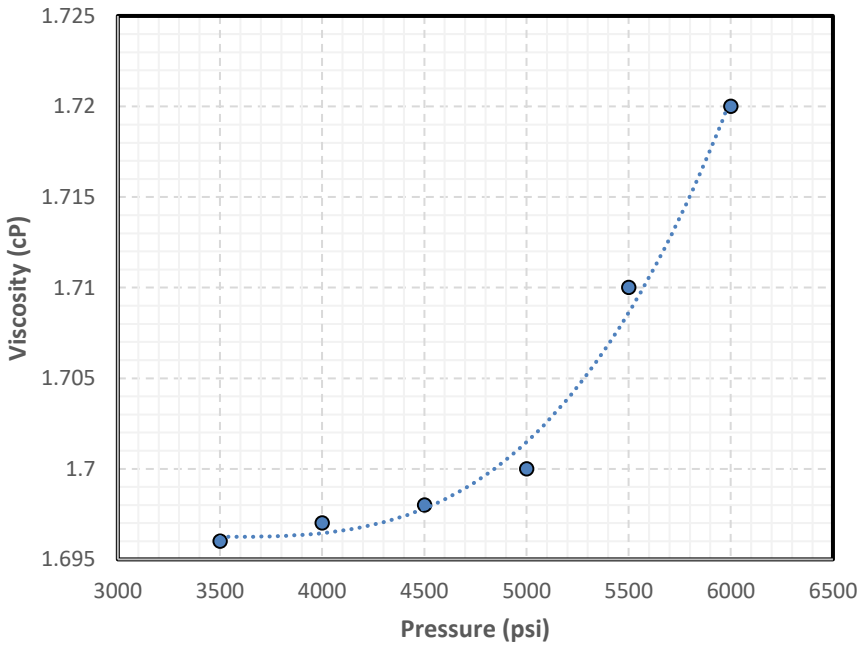

Figure 5.9: Viscosity of CO_2-TEC Blend versus Pressure at 100 °C with 85 mol% CO_2

5.1.3 Discussion of Results from Solubility Measurements

5.1.3.1 Saturation Pressure Results of CO_2-Solvent Blends

By calculating the equivalent amounts of solvent required to blend with CO_2, we can find that for the highest molar concentration of CO_2 (i.e. 90 mol% CO_2), one barrel of EB can blend with almost 7,000 SCF of CO_2 while one barrel of TEC can blend with up to 14,000 SCF of CO_2. At the lowest concentration tested (i.e. 65 mol% CO_2), one barrel of EB or TEC can blend with up to 1,500 or 2,000 SCF of CO_2, respectively. This shows that the amount of EB required to blend with CO_2 is much higher than that required by the TEC to produce the same composition. In other words, the TEC can blend with a higher volume of CO_2 to produce a given composition than with EB. This contrast is makes TEC more advantageous over EB for reservoir and practical applications.

From the saturation pressure results, we can see that at 100 ℃ and at 90 mol% CO_2, the saturation pressure of the CO_2-EB blend was about 2,850 psi while for CO_2-TEC blend it was around 3,250 psi. At room temperature, this pressure decreased to around 890 psi and 810 psi for CO_2-EB and CO_2-TEC blends, respectively. At the lowest tested concentration, the saturation pressure was decreased to around 1,980 psi for CO_2-EB blend and to about 1,385 psi for CO_2-TEC blend at 100 ℃. These results show the significant decrease in the bubble-point pressure of the CO_2-TEC blend with concentration as compared to that of CO_2-EB blend. This decrease can be attributed to the difference in the density and molecular weights and structures between EB and TEC as TEC has higher density and molecular weight than EB and, hence, the pressure required to dissolve CO_2 in the smaller molecular weight solvent is lower. It can also be attributed to the higher amount of CO_2 blended with TEC than that blended with EB.

Regardless of these differences in the amounts of solvents required and the saturation pressures of both blends, the saturation pressures at 100 ℃ are comparable to normal reservoir pressures that the blends can be used and injected into oil reservoirs.

The predicted values of the saturation pressures of the CO_2-EB blends showed some deviations from the experimental results, especially at higher temperatures and higher CO_2 concentration where PR-EOS overestimated the saturation pressures at these conditions. For the CO_2-TEC blends, the predicted values of the saturation pressure by the PR-EOS were also higher than the experimental results. This overestimation is significant at higher temperatures for all the blends. Performing regression between the experimental data and those predicted by the PR-EOS by tuning the interaction coefficients between CO_2 with either EB or TEC along with modifying the critical pressures and acentric factors of EB and TEC resulted in a better prediction of the PR-EOS. The results shown in Figures 5.1, 5.2, 5.5 and 5.6. represent those obtained after the regression was performed while the results of the prediction before the regression are shown in Appendix A along with the results of the modified parameters.

Although we could obtain better matches of the experimental results, we can still see some deviations from the experimental results. Such deviation necessitates implementation of advanced equations of state with association term to improve this prediction such as the Cubic Plus Associations (CPA) EOS which include the association term that takes into account the association due to hydrogen bonding in a self-association (between the like molecules) and cross association (between the unlike molecules) [103].

5.1.3.2 Density Results of CO_2-Solvent Blend

The density results show that the densities of the CO_2-EB blends as well as the CO_2-TEC blends are close to those of the reservoir fluids, which should help minimize the gravity override problem due to the reduced contrast in the density of injected blends and those of resident reservoir fluids.

For CO_2-EB blends, for a blend consisting of 90 mol% CO_2 and 10 mol% EB, the density ranged from almost 0.7 to 0.8 g/cm^3 at 100 ℃ and for pressures above the blend's saturation pressure. For a CO_2-TEC blend with the same composition, however, the density of the blend ranged from 0.84 to 0.87 g/cm^3 which indicates that blending CO_2 with TEC can result in higher density than that obtained by blending it with EB at the same conditions. To illustrate, to obtain a CO_2-EB blend having a density range from 0.82 to 0.86, the blend must be composed of 80 mol% CO_2 and 20 mol% EB while for the CO_2-TEC blend having the same density range, the blend must be composed of 85 mol% CO_2 and 15 mol% TEC. This indicates the high amount of EB required to obtain a blend with high density that is close to those of reservoir fluids. For both solvents, this density range increases by increasing the solvent concentrations. **Figure 5.10** shows a comparison between the density of two blends having 90 and 85 mol% CO_2 and either EB or TEC.

The trends of the saturated densities versus the saturation pressure that were predicted by PR-EOS for CO_2-EB and CO_2-TEC systems showed trends similar to the trends of the experimental results with slight deviations from the experimental results.

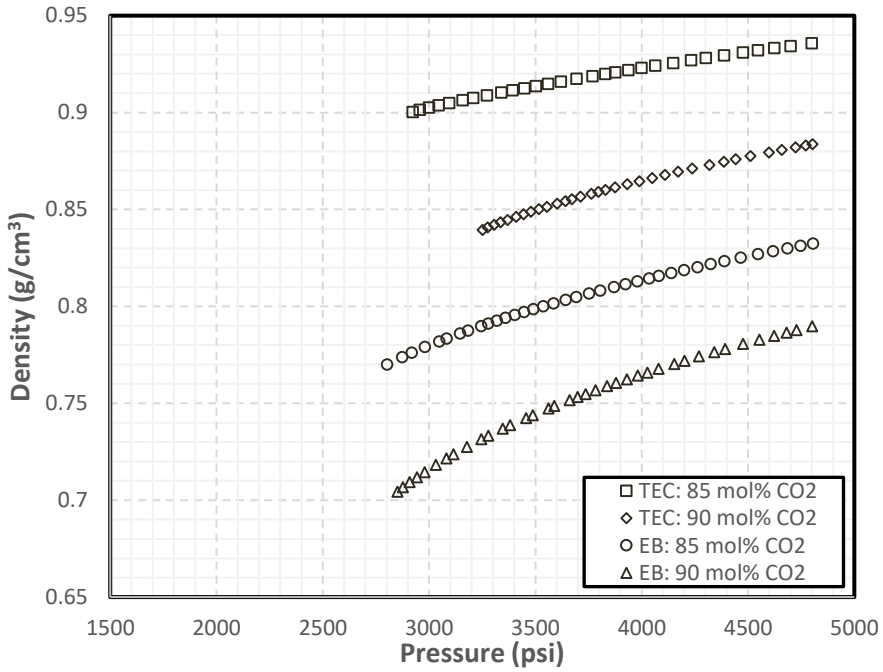

Figure 5.10: Comparison between Density Results of CO_2-TEC and CO_2-EB blends at 100 °C

5.2 Discussion of the Core Flooding Results

5.2.1 Run 1-DO: Displacing Dead Oil by Pure $scCO_2$ (Base Case)

In this run, a high-permeability Indiana core sample was used (Sample No. 4). Flooding was conducted at a pressure greater than the minimum miscibility pressure.

Table 5.3 summarizes the results of this flooding run and **Figure 5.11** shows the progress of the oil recovery and production rate with the amount of $scCO_2$ injected. The results showed that CO_2 breakthrough occurred after injecting 0.1272 PV of pure $scCO_2$. The oil recovery factor at the breakthrough moment was estimated at 14.82% of the oil initially present in the core sample. Early CO_2 breakthrough is due to the high mobility and low

density of $scCO_2$ compared to that of the oil and water initially in the core sample. The low recovery at breakthrough also indicated that there was still a high amount of oil present in the sample and more oil could be produced with continuous injection of pure $scCO_2$. The injection of the pure $scCO_2$ was continued and after injecting one pore volume of pure $scCO_2$, there was no more production of oil. The oil recovery after injecting one pore volume of pure $scCO_2$ was 60.14%. The production rate of oil was calculated from the ratio between incremental oil production to the corresponding time interval; that is:

$$q_{oil} = \frac{N_{p_{i+1}} - N_{p_{i-1}}}{t_{i+1} - t_{i-1}} \quad (5\text{-}1)$$

Where q_{oil} is the oil flow rate, $N_{p_{i+1}}$ is the cumulative oil produced at time t_{i+1} and $N_{p_{i-1}}$ is the cumulative oil produced at time t_{i-1}.

Since CO_2–oil miscibility is a multi-contact process that develops over a distance, it is somewhat difficult to estimate the fraction of the oil recovery contributed by the gas flood and that contributed by gas-oil miscibility. Nevertheless, given the relatively short length of the core sample, it is rather safe to assume that the breakthrough recovery in this run is almost entirely caused by immiscible displacement even though the flooding was conducted at pressure that is above the MMP. However, it can be said that there was solubility of $scCO_2$ in the oil, which can be discerned from the oil recovery after one PVI. The remaining oil saturation of 35.25% after the end of the flood is smaller than the residual oil saturation of 46.82% after the seawater flood, which can be due swelling of oil and reduction in its viscosity caused by the diffusivity and solubility of the $scCO_2$ into the oil.

Table 5.3: Summary of the Results Obtained from Flooding Run 1-DO

Run Name	1-DO
Back-pressure regulator (psi)	3,500
Confining pressure, P_{conf} (psi)	4,000
Flooding temperature, T_{res} (°C)	100
Pore volume, PV (cm^3)	64.87
Seawater injection rate(s) to displace oil, cc/min	0.5 & 1
Residual oil saturation after seawater flood, S_{or} (%)	46.82
Oil injection rate(s) to displace seawater, cc/min	0.5 & 1
Irreducible water saturation, S_{wi} (%)	11.56
Initial oil in place, IOIP (cm^3)	57.37
CO_2 injection rate, cc/min	0.25
Pore volumes of $scCO_2$ at breakthrough (vol/vol)	0.1272
Oil recovery at CO_2 breakthrough, RF (%)	14.82
Oil recovery after injecting one PV pure $scCO_2$ (%)	60.14
Remaining oil saturation after CO_2 flood, S_{org} (%)	35.25

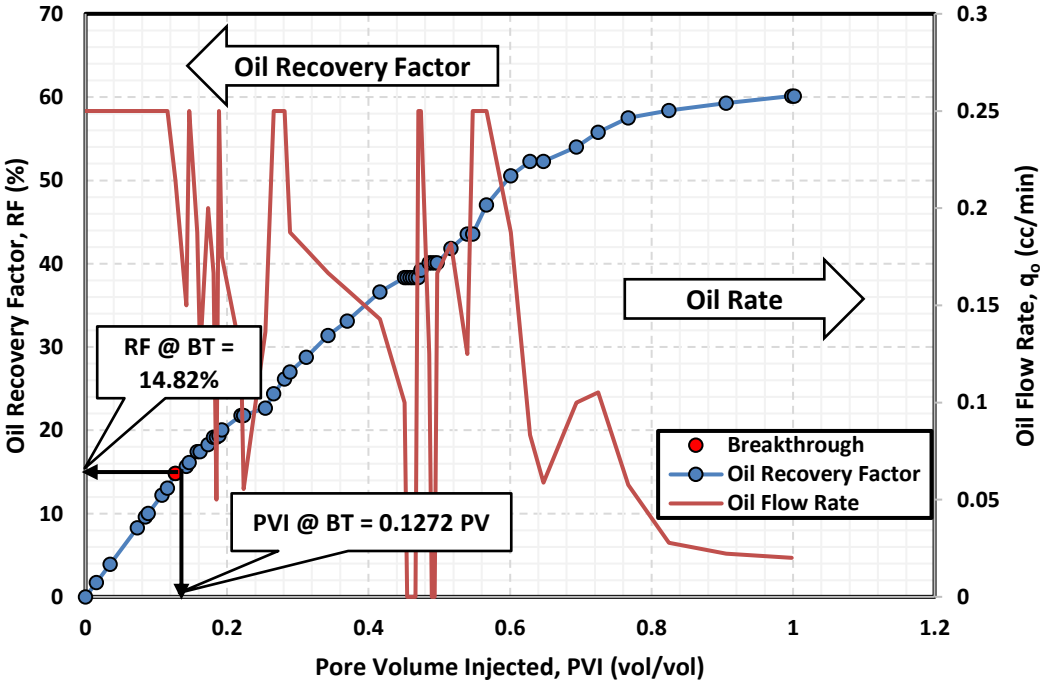

Figure 5.11: Oil Recovery Factor and Oil Flow Rate versus PV of Injected Pure $scCO_2$ (Run 1-DO)

5.2.2 Run 2-DO: Displacing Dead Oil by CO_2-TEC Blend

The results from this flooding run showed that the CO_2 breakthrough occurred after injecting 0.2722 PV of CO_2-TEC blend. The oil recovery factor at breakthrough was calculated to be 31.99% of the oil initially present in the core sample. The delay in the breakthrough and the higher oil recovery at breakthrough in this flood - compared with the pure scCO_2 flood (Run 1-DO)- indicated the effectiveness of blending CO_2 with TEC in improving the sweep efficiency of injected CO_2. Injection of the CO_2-TEC blend was continuous, and oil production ceased after injecting one pore volume of CO_2-TEC blend. The oil recovery from this run was 72.67% of the original oil in the core which is also higher than the oil recovery obtained with the pure CO_2 flood. The results obtained from this flooding run are summarized in **Table 5.4**. These results include the initial fluids' saturations, the original oil in place, the oil recovery factor at breakthrough and after injecting one pore-volume of CO_2-TEC blend. Increase in the recovery factor with pore-volumes of injected CO_2-TEC blend is shown in **Figure 5.12**. The oil production rate is also plotted on the same figure.

For comparison purposes, the performance of this run with that of run 1-DO, namely the oil recovery factors and the oil flow rate for both runs, are plotted versus the pore volumes of injected pure scCO_2 or CO_2-TEC blend as shown in **Figure 5.13** and **Figure 5.14**, respectively. Both figures show the clear improvement in the oil recovery factor and the oil production rate obtained with the CO_2-TEC blend. Furthermore, the assessment of the contribution of solubility of CO_2 in oil that was made in the previous sub-section is believed to apply to this flood as well. Therefore, the more than double increase in the breakthrough oil recovery is a clear result of the blend's larger density. The effect of CO_2 solubility is

also clear in this flood when the remaining oil saturation of 22.93% is compared with the water-flood residual oil saturation of 50.15%.

Table 5.4: Summary of the Results Obtained from Flooding Run 2-DO

Run Name	2-DO
Back-pressure regulator (psi)	3,500
Confining pressure, P_{conf} (psi)	4,000
Flooding temperature, T_{res} (°C)	100
Pore volume, PV (cm^3)	65.2
Seawater injection rate(s) to displace oil, cc/min	0.5 & 1
Residual oil saturation after seawater flood, S_{or} (%)	50.15
Oil injection rate(s) to displace seawater, cc/min	0.5 & 1
Irreducible water saturation, S_{wi} (%)	16.10
Initial oil in place, IOIP (cm^3)	54.70
CO_2-TEC blend injection rate, cc/min	0.25
Pore volumes of CO_2-TEC blend at breakthrough (vol/vol)	0.2722
Oil recovery at CO_2 breakthrough, RF (%)	31.99
Oil recovery after injecting one PV of CO_2-TEC blend (%)	72.67
Remaining oil saturation after CO_2-TEC flood, S_{org} (%)	22.93

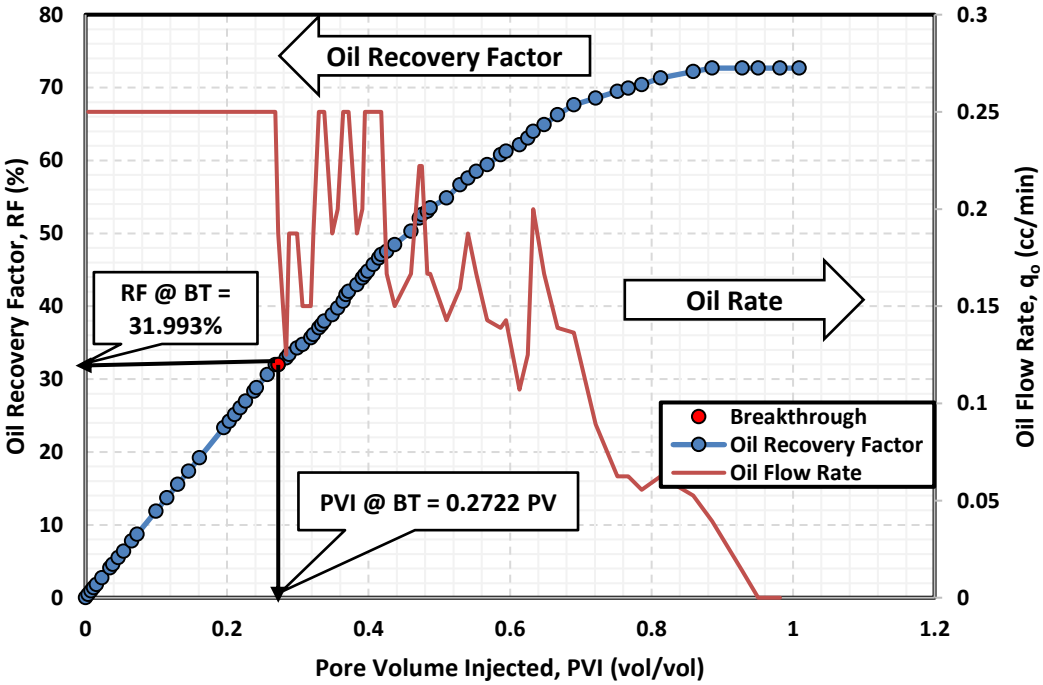

Figure 5.12: Oil Recovery Factor and Oil Flow Rate versus PV of Injected CO_2-TEC Blend (Run 2-DO)

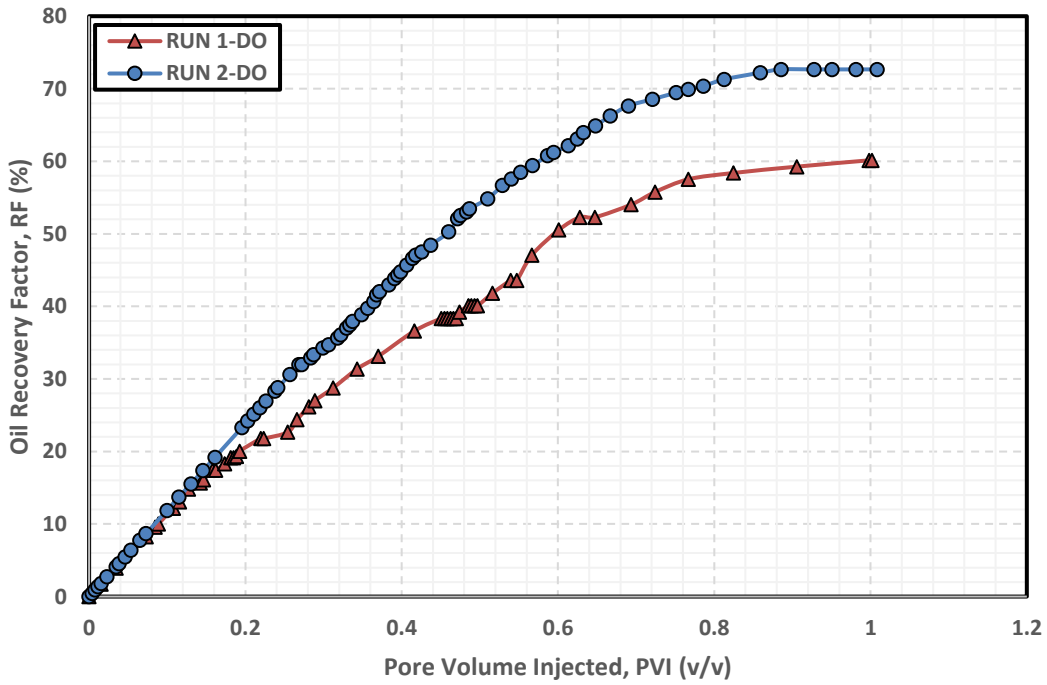

Figure 5.13: Comparison of Oil Recovery Factor Obtained from Run 1-DO and Run 2-DO

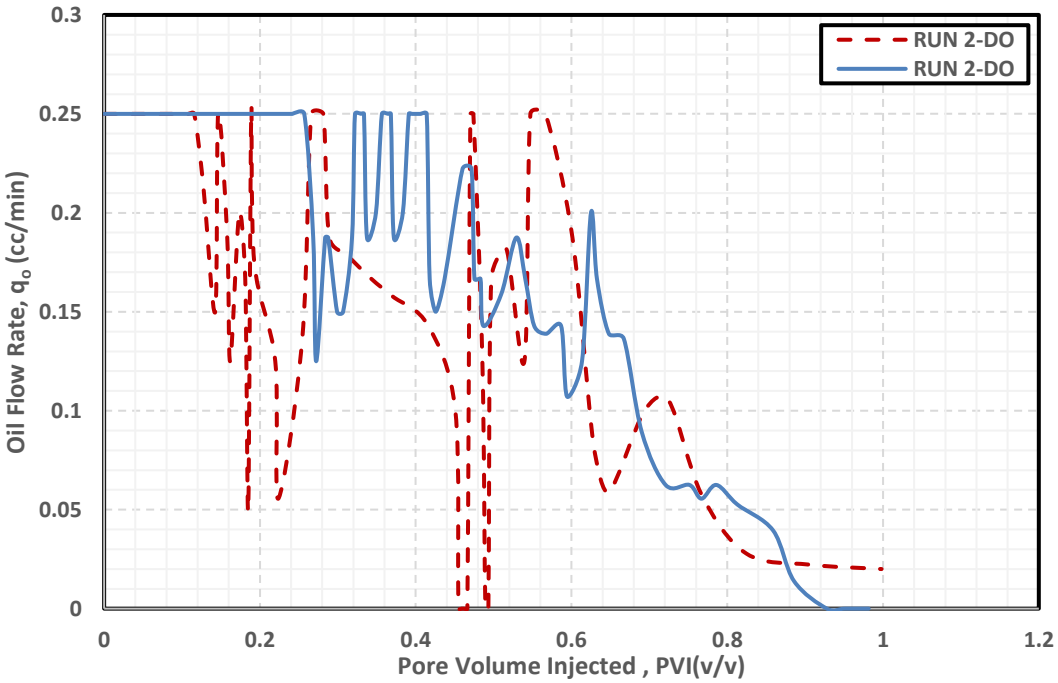

Figure 5.14: Comparison of Oil Flow Rate Obtained from Run 1-DO and Run 2-DO

5.2.3 Run 1-LO: Displacing Live Oil by Pure $scCO_2$

In this run, a high-permeability Indiana core sample was used (Sample No. 3). The flood was conducted at a pressure believed to be greater than the minimum miscibility pressure.

The CO_2 breakthrough in this run occurred after injecting 0.1329 PV of pure $scCO_2$. The oil recovery at breakthrough was 15.19% of the oil initially present in the core sample, which is almost close to that in run 1-DO. One factor could be the lower oil viscosity, which reduced the displacement mobility ratio, and the lower oil density. It was expected that this recovery factor be higher than that obtained from run 1-DO due to the very low viscosity and density of live oil compared to those of dead oil. However, due to the presence of gas in the live oil, the ability of the CO_2 to diffuse and solubilize into the oil was reduced and the effectiveness of $scCO_2$ in swelling the oil and reducing its viscosity is not present due to the diminished solubility of $scCO_2$ in the oil. This made the oil recovery at the breakthrough close to that obtained in run 1-DO where the solubility of CO_2 in the dead oil is believed, based on preliminary calculations, to reduce the density and viscosity of the oil to values less than or close to those of live oil.

The injection of the pure $scCO_2$ was continued and after injecting one pore volume of pure $scCO_2$, the production of oil ceased. The oil recovery after injecting one pore volume of pure $scCO_2$ was 49.13% of the oil initially present in the core sample. **Table 5.5** summarizes the results obtained from this flooding run. **Figure 5.15** also presents the growth in oil recovery with pore-volumes injected of $scCO_2$ along with the oil production rate.

Figure 5.16 compares the results of the first and third flooding run. The oil recovery is considerably lower than that obtained with the dead oil.

Table 5.5: Summary of the Results Obtained from Flooding Run 1-LO

Run Name	1-LO
Back-pressure regulator (psi)	3,500
Confining pressure, P_{conf} (psi)	4,000
Flooding temperature, T_{res} (°C)	100
Pore volume, PV (cm^3)	63.97
Seawater injection rate(s) to displace oil, cc/min	0.5 & 1
Residual oil saturation after seawater flood, S_{or} (%)	49.98
Oil injection rate(s) to displace seawater, cc/min	0.5 & 1
Irreducible water saturation, S_{wi} (%)	12.51
Initial oil in place, IOIP (cm^3)	55.97
CO_2 Injection Rate, cc/min	0.25
Pore volumes of CO_2 at breakthrough (vol/vol)	0.1329
Oil recovery at CO_2 breakthrough, RF (%)	15.19
Oil recovery after injecting one PV pure $scCO_2$ (%)	49.13
Remaining oil saturation after CO_2 flood, S_{org} (%)	44.51

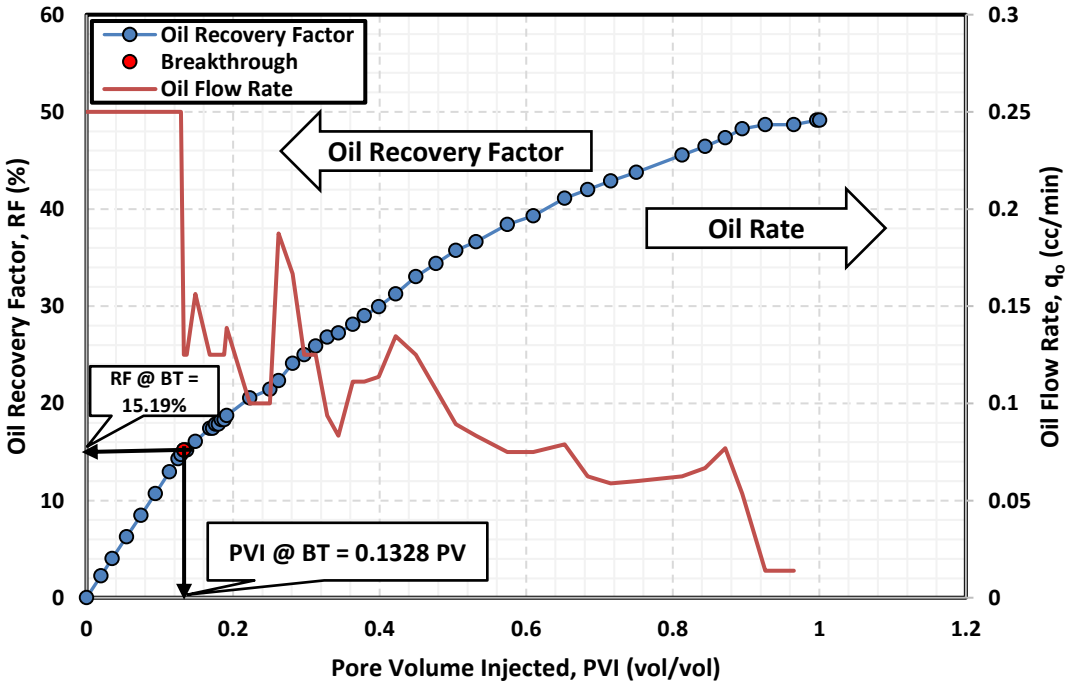

Figure 5.15: Oil Recovery Factor and Oil Flow Rate versus PV of Injected Pure $scCO_2$ (Run 1-LO)

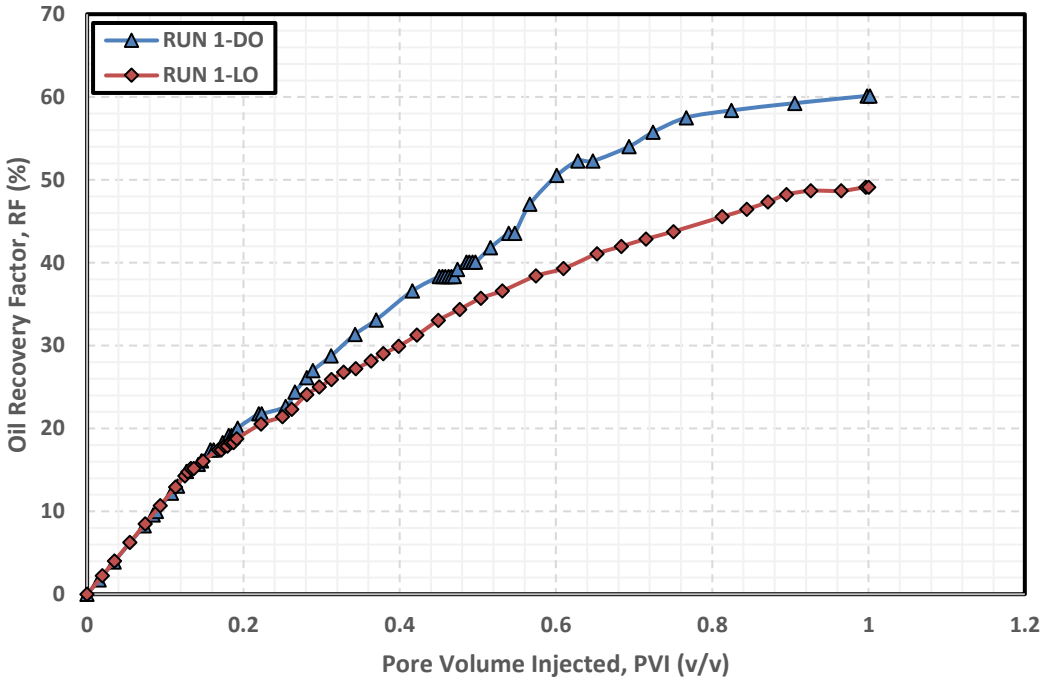

Figure 5.16: Comparison of Oil Recovery Factor Obtained from Run 1-DO and Run 1-LO

5.2.4 Run 2-LO: Displacing Live Oil by CO_2-TEC Blend

In this run, a high-permeability Indiana core sample was used (Sample No. 6). The flood with the CO_2-TEC blend was conducted at a pressure of 3,500. The results of this flooding run are summarized in **Table 5.6** and are plotted in **Figure 5.17**.

Breakthrough in this run occurred after injecting 0.2262 PV of CO_2-TEC blend. The oil recovery factor at breakthrough was calculated at 27.06% of the oil initially present in the core sample which was also expected to be higher than that in run 2-DO for the same reasons explained in run 1-LO. The injection of CO_2-TEC blend was continuous and oil production ceased after injecting one pore volume of CO_2-TEC blend. The oil recovery from this run was 67.89%, which is considerably larger than the corresponding recovery with the pure scCO_2. Comparison between the two runs is shown in **Figure 5.18**.

Table 5.6: Summary of the Results Obtained from Flooding Run 2-LO

Run Name	2-LO
Back-pressure regulator (psi)	3,500
Confining pressure, P_{conf} (psi)	4,000
Flooding temperature, T_{res} (°C)	100
Pore volume, PV (cm^3)	65.20
Seawater injection rate(s) to displace oil, cc/min	0.5 & 1
Residual oil saturation after seawater flood, S_{or} (%)	50.92
Oil injection rate(s) to displace seawater, cc/min	0.5 & 1
Irreducible water saturation, S_{wi} (%)	16.41
Initial oil in place, IOIP (cm^3)	54.50
CO_2-TEC blend injection rate, cc/min	0.25
Pore volumes of CO_2-TEC blend at breakthrough (vol/vol)	0.2262
Oil recovery at CO_2 breakthrough, RF (%)	27.06
Oil recovery after injecting one PV CO_2-TEC blend (%)	67.89
Remaining oil saturation after CO_2-TEC flood, S_{org} (%)	26.84

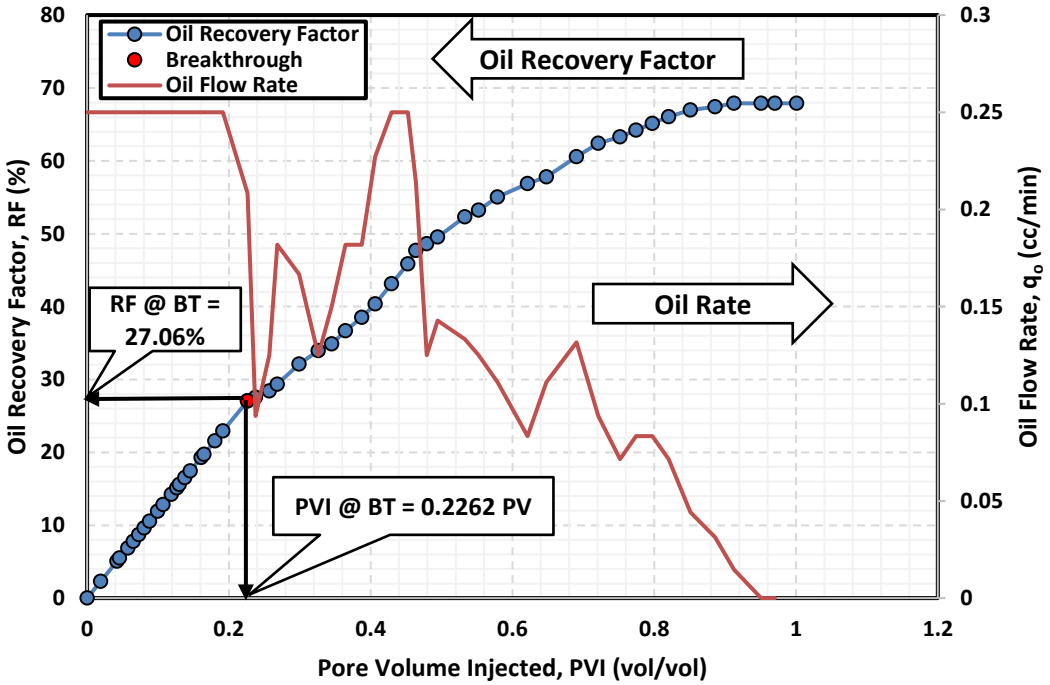

Figure 5.17: Oil Recovery Factor and Oil Flow Rate versus PV of Injected CO_2-TEC Blend (Run 2-LO)

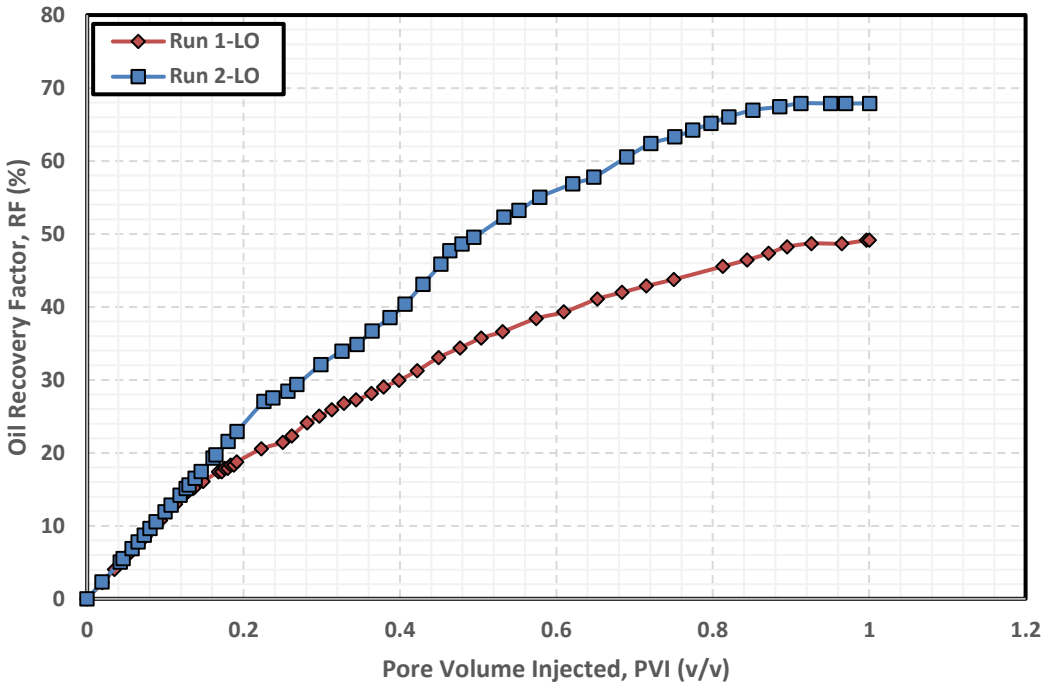

Figure 5.18: Comparison of Oil Recovery Factor Obtained from Run1-LO and Run 2-LO

5.2.5 Comparison of the Results from All Flooding Runs

For a better presentation of the core-flooding results, they are presented together for a comparison purpose. **Figure 5.19** presents a comparison of oil recovery from all the runs. This figure shows the better recovery obtained by the CO_2-TEC blend when it was injected to displace the dead oil (blue line) as compared to that obtained by pure $scCO_2$ (red line). It also demonstrates the effect of the methane on the recovery process as illustrated by the least oil recovery when pure $scCO_2$ was injected to displace the live oil (purple line). Finally, it shows the effectiveness of the CO_2-TEC blend to improve the oil recovery when it was injected to displace live oil prepared by recombining dead oil with methane-rich gas (green line). The recovery from this flooding run is higher than that of pure $scCO_2$ in both runs (i.e. dead oil and live oil by $scCO_2$) although the oil recovery after 1 PVI was slightly lower than that obtained from the second run (i.e. CO_2-TEC with dead oil) by almost 5%.

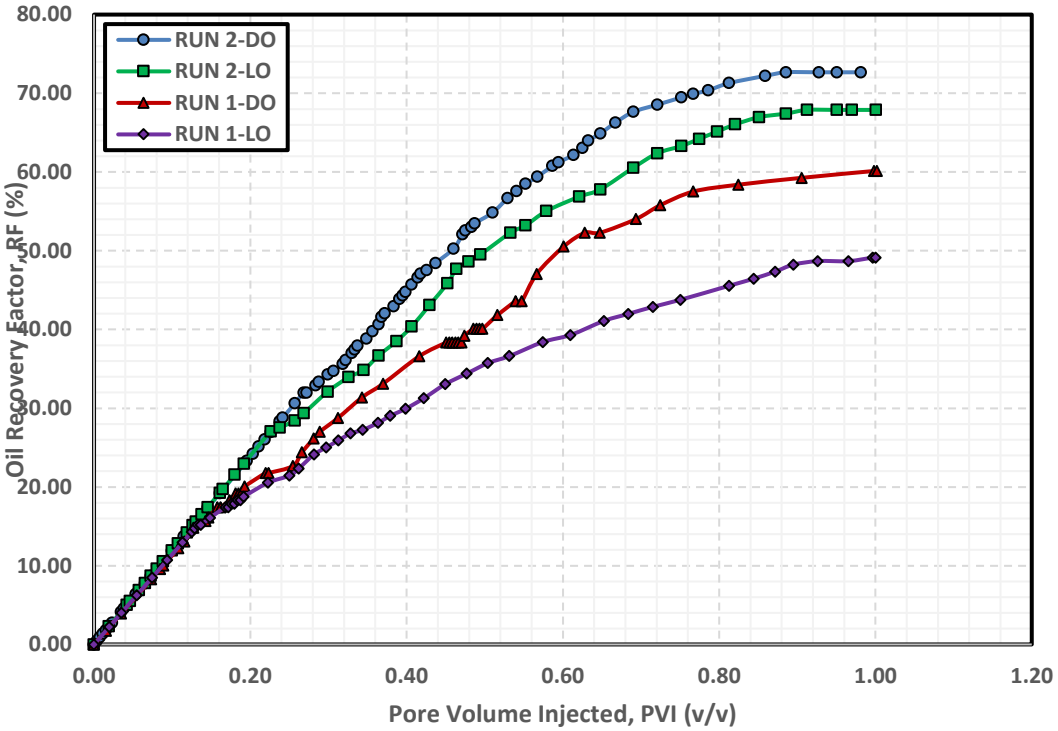

Figure 5.19: Comparison of Oil Recovery Factor from All Flooding Runs

Figure 5.20 and **Table 5.7** also summarize all the results obtained from all flooding runs. This includes the sample used for each run, the pore volume for each sample, the fluids produced by brine and oil floods (i.e. the initial fluids' saturations), the pore volumes of the $scCO_2$ or the CO_2-TEC blend to achieve breakthrough, the oil recovery factor at the breakthrough and the oil recovery from all the experiments. The results show that the initial conditions before commencing the pure $scCO_2$ or CO_2-TEC blend flood are almost the same and within the experimental error.

Looking at the recovery factors at breakthrough in the case of dead oil experiments (runs 1-DO and 2-DO), we can see that this factor in run 2-DO is almost greater than double that of run-1D. In the case of live oil experiments (runs 1-LO and 2-LO), however, the recovery factor at the breakthrough in run 2-LO is less than double of that in run 1-LO. This can be

attributed to the slight variations in the initial conditions of the flooding runs prior the CO_2 flood such as the irreducible water saturation and the volume of initial oil in place.

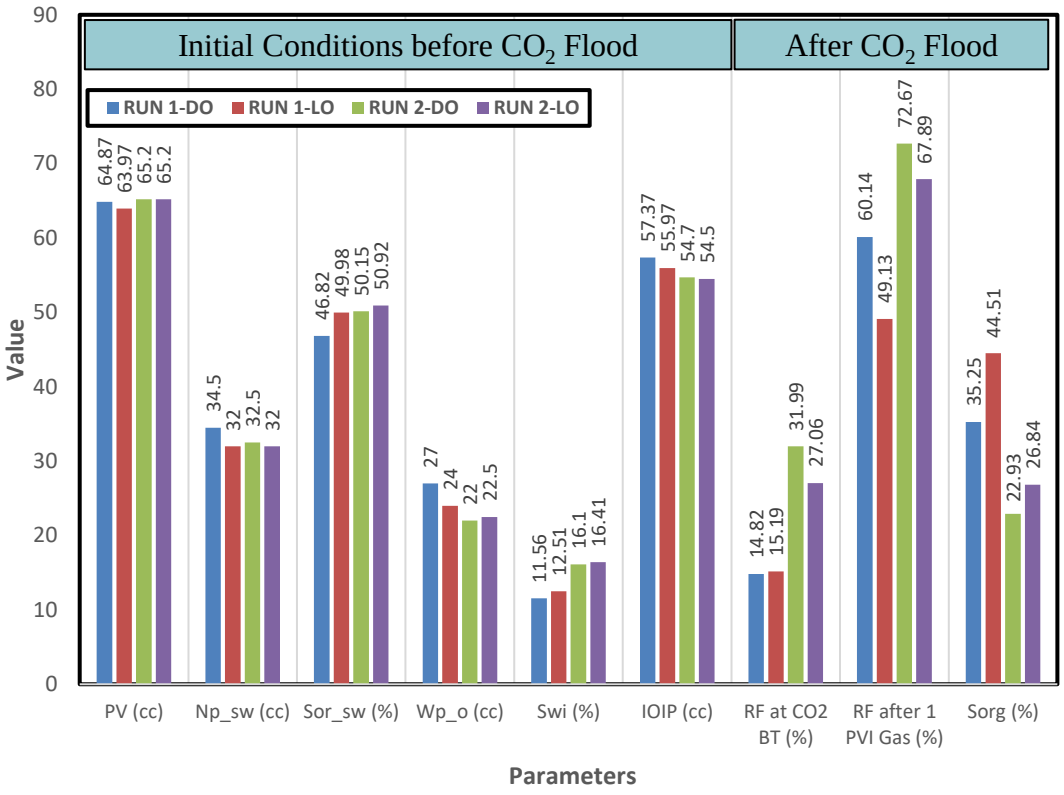

Figure 5.20: Comparison of All Parameters from All Flooding Runs

Table 5.7: Summary of the Results from All Flooding Runs

Parameters	Experimental Run			
	Run 1-DO	**Run 1-LO**	**Run 2-DO**	**Run 2-LO**
Displacement	Dead Oil by Pure $scCO_2$	Live Oil by Pure $scCO_2$	Dead Oil by CO_2-TEC Blend	Live Oil by CO_2-TEC Blend
Sample No.	4	3	5	6
Pore Volume (cm^3)	64.87	63.97	65.20	65.20
Total Oil Produced by Seawater (cm^3)	34.50	32.00	32.50	32.00
Residual Oil Saturation after Seawater Flood (%)	46.82	49.98	50.15	50.92
Total Seawater Produced by Oil (cm^3)	27.00	24.00	22.00	22.50
Irreducible Water Saturation (%)	11.56	12.51	16.10	16.41
Initial Oil in Place (cm^3)	57.37	55.97	54.70	54.50
Pore Volume Injected to Breakthrough* (vol/vol)	0.1272	0.1329	0.2722	0.2262
Recovery Factor at Breakthrough (%)	14.82	15.19	31.99	27.06
Oil Recovery after 1 PVI* (%)	60.14	49.13	72.67	67.89
Remaining Oil Saturation After CO_2 Flood (%)	35.25	44.51	22.93	26.84

* $scCO_2$ or CO_2-TEC blend

CHAPTER 6

CONCLUSIONS AND RECOMMENDATIONS

This chapter concludes the research work conducted in this study. It also presents the recommendations proposed for future work. The objective of this work was to identify different solvents that can blend with carbon dioxide and increase its density for the purpose of mitigating the effect of gravity override during $scCO_2$ enhanced oil recovery process.

6.1 Conclusions

Several conclusions can be drawn from this work. These are listed below.

1. The two selected solvents, Ethyl Benzoate (EB) and Triethyl Citrate (TEC), proved their ability to blend with carbon dioxide at conditions close to those of typical reservoirs as illustrated by the moderate saturation pressures of the resulting blends at different concentrations.
2. Blending carbon dioxide with either of the two solvents prior to the injection results in blends' density and viscosity close to those of reservoir fluids and, thus, reduces the density and viscosity difference between the injected $scCO_2$ and the reservoir fluids.
3. The amount of the CO_2 that blends with TEC is much higher than that with EB to produce the same composition although the saturation pressures of CO_2-EB

blends are lower than those of CO_2-TEC blends at the same concentrations and at the same temperatures.

4. The saturation pressure of CO_2-EB and CO_2-TEC blends predicted by PR-EOS are larger than those measured experimentally, especially at higher temperatures and higher CO_2 concentrations. Advanced and modern equations of states are, therefore, needed for better predictions.
5. The miscibility test between the crude oil and the two solvents showed that EB is not a good choice for reservoir applications due to its complete miscibility with crude oil. TEC, on the other hand, can be used for reservoir applications due to its slight miscibility with oil and water. It can also be easily separated and recovered from the produced fluids.
6. Vertical core-flooding experiments with dead oil showed the ability of the CO_2-TEC blend to improve the recovery performance of the flood and minimize the effect of gravity override. This is illustrated by the delay in the CO_2 breakthrough and the higher oil recovery by CO_2-TEC blend than that observed with pure scCO_2.
7. Vertical core-flooding experiments with live oil demonstrated the ability of the CO_2-TEC blend in improving oil recovery even with the presence of methane in the oil.
8. Given the relatively short length of core samples and since CO_2–oil miscibility is a multi-contact process that develops over a distance, it was somewhat difficult to estimate the fraction of the oil recovery contributed by the gas flood and that contributed by gas-oil miscibility. Therefore, it was rather safe to

assume that the breakthrough recovery was almost entirely caused by immiscible displacement.

9. The low remaining oil saturations after $scCO_2$ or CO_2-TEC floods compared with the residual oil saturations after the seawater flood can be attributed to the solubility of the $scCO_2$ in the oil which resulted in swelling the oil and reducing its viscosity and, thus, a better oil recovery mainly in the case of dead oil flooding runs.
10. The imbibition test by immersing the oil-saturated sample in TEC showed that the improved oil recovery by the CO_2-TEC blend is caused by the high density of the blend and that there are no changes in the rock properties caused by the TEC.

6.2 Recommendations

For further investigation, the following are recommended:

1. Conduct the flooding experiments on sandstone samples as well and study the physical and chemical interactions between TEC and the rock.
2. Other potential solvents should be investigated.
3. Conduct the flooding experiments under conditions that promote CO_2-oil miscibility.
4. Conduct a simulation study to model the laboratory results and forecast the future work of the tested solvents.
5. Examine the effectiveness of the tested solvents with other gases used for EOR purposes.
6. Implementation of advanced equations of state to improve the predictions of the saturation pressures of the CO_2-solvent blends such as Cubic Plus Associations (CPA) or Statistical Associating Fluid Theory (SAFT).

APPENDIX A

DATA FROM SOLUBILITY EXPERIMENTS

A.1 CME Data for CO_2 - Ethyl Benzoate Systems

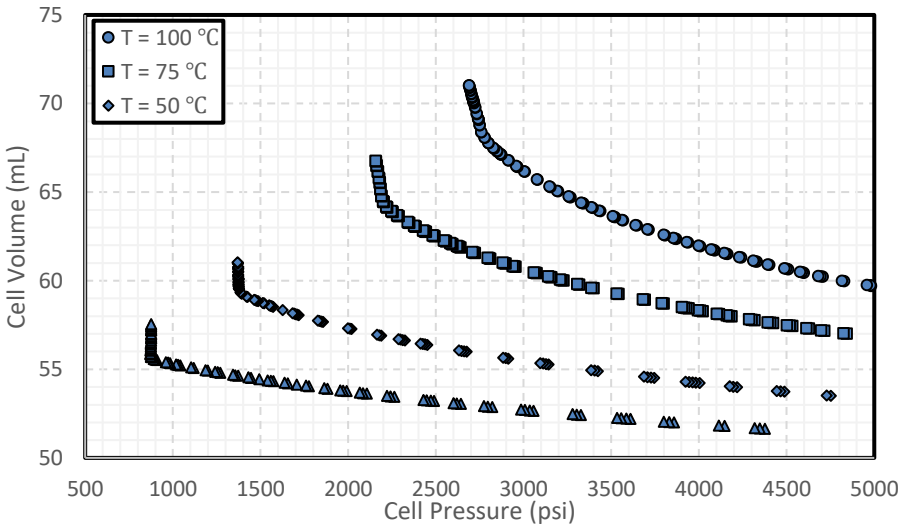

Figure A.1: CME Data for CO_2-EB Blend with 90 mol% CO_2

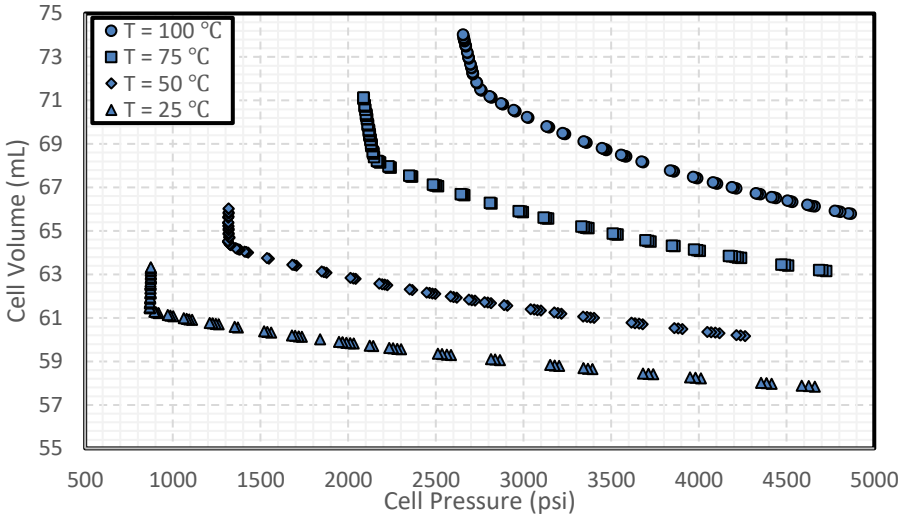

Figure A.2: CME Data for CO_2-EB Blend with 85 mol% CO_2

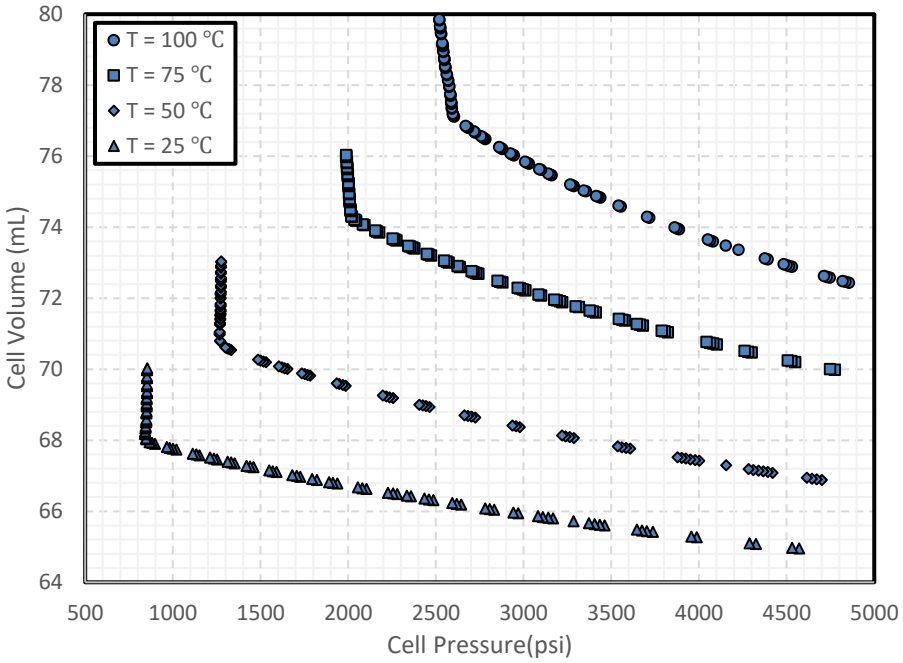

Figure A.3: CME Data for CO_2-EB Blend with 80 mol% CO_2

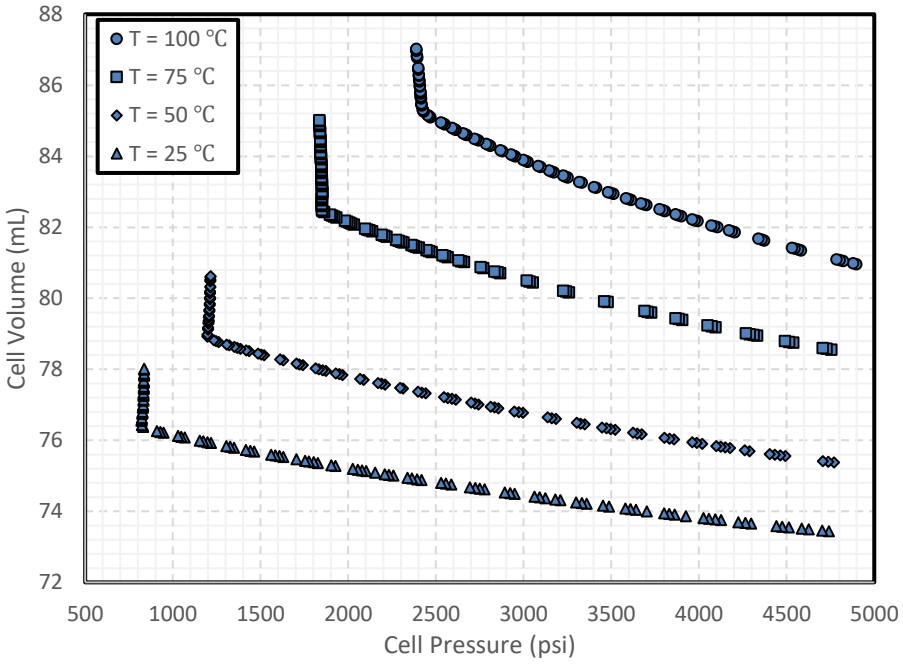

Figure A.4: CME Data for CO_2-EB Blend with 75 mol% CO_2

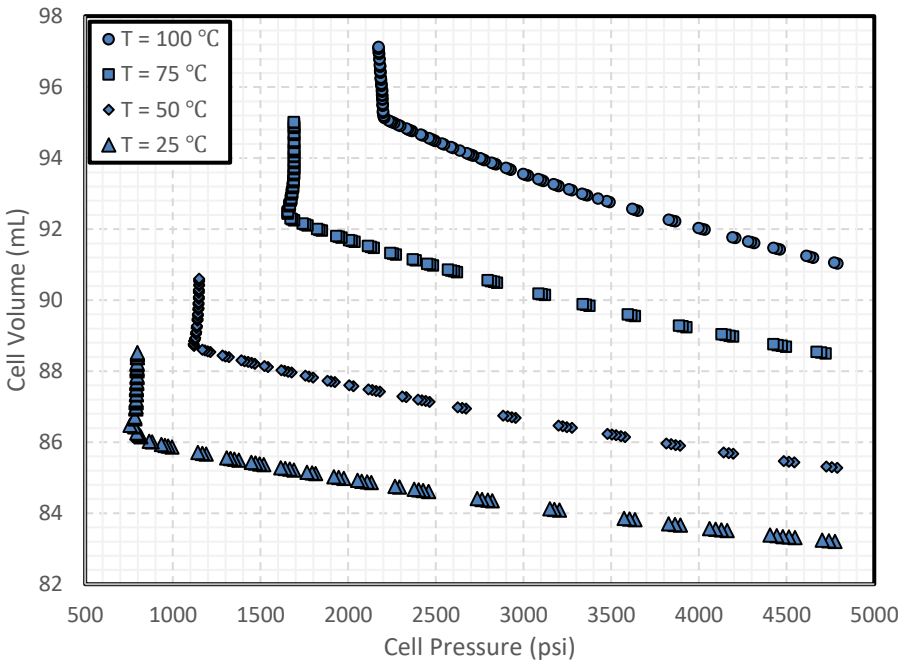

Figure A.5: CME Data for CO_2-EB Blend with 70 mol% CO_2

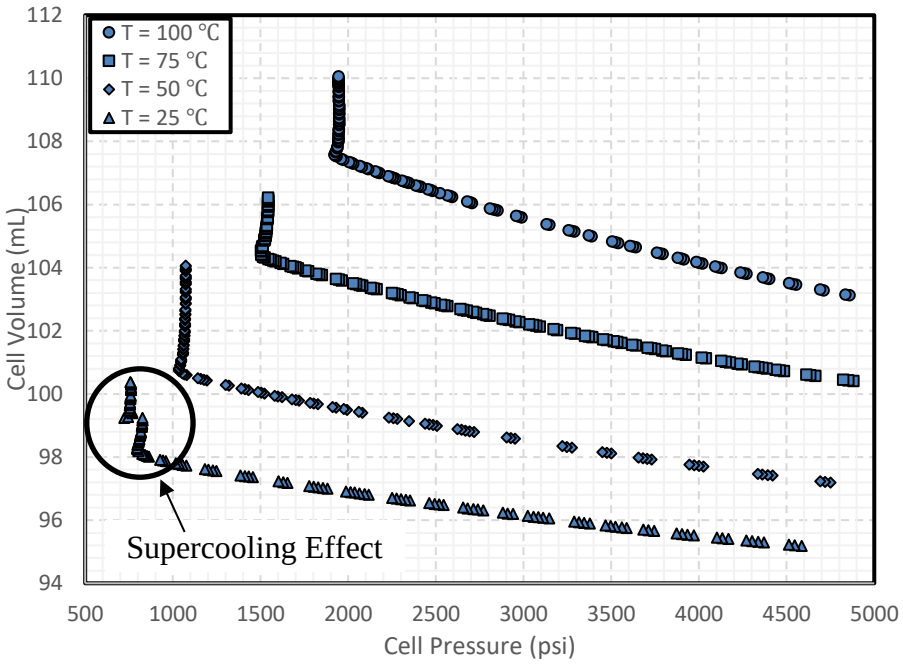

Figure A.6: CME Data for CO_2-EB Blend with 65 mol% CO_2

A.2 CME Data for CO_2 - Triethyl Citrate Systems

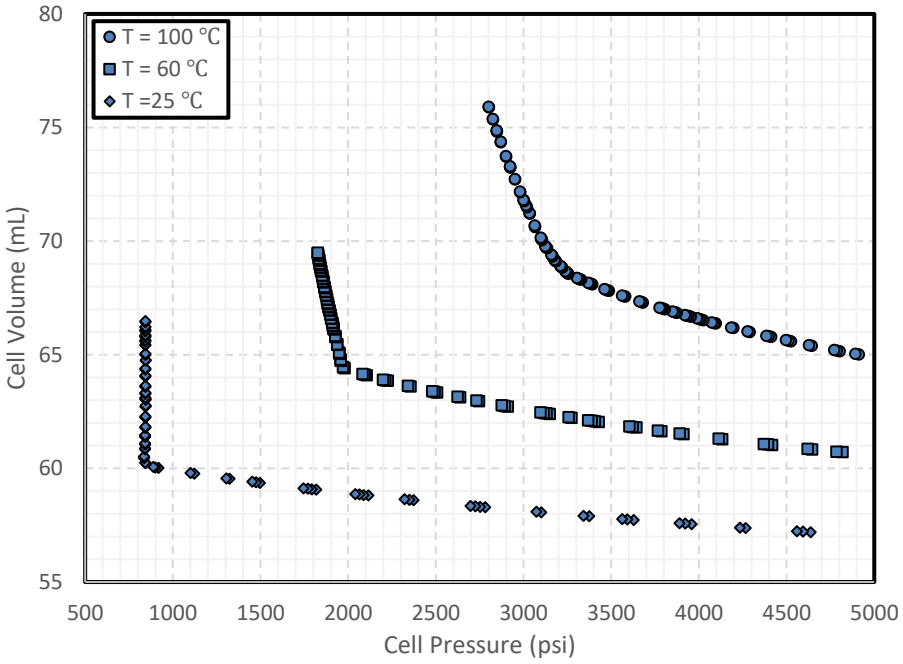

Figure A.7: CME Data for CO_2-TEC Blend with 90 mol% CO_2

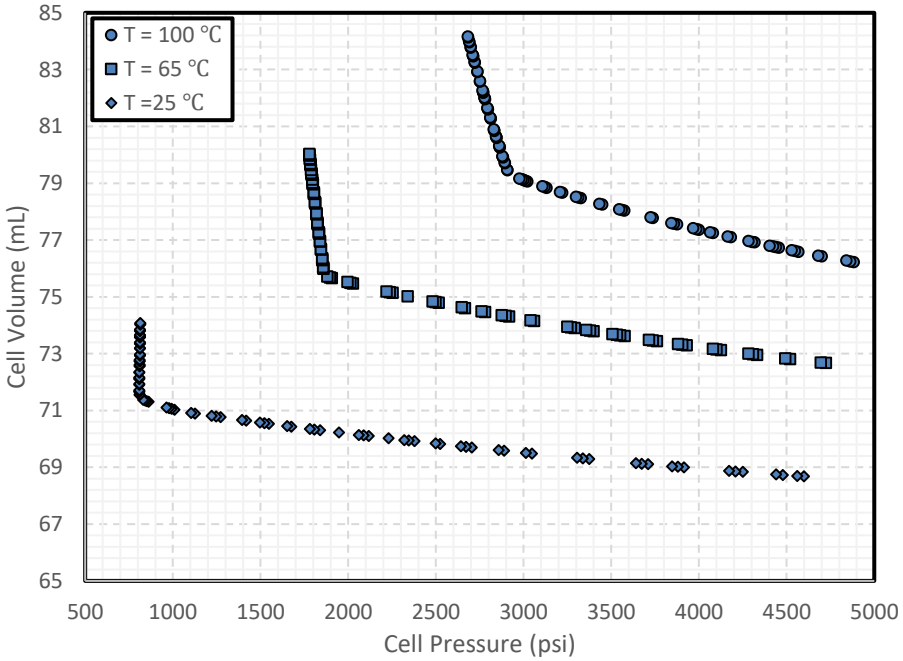

Figure A.8: CME Data for CO_2-TEC Blend with 85 mol% CO_2

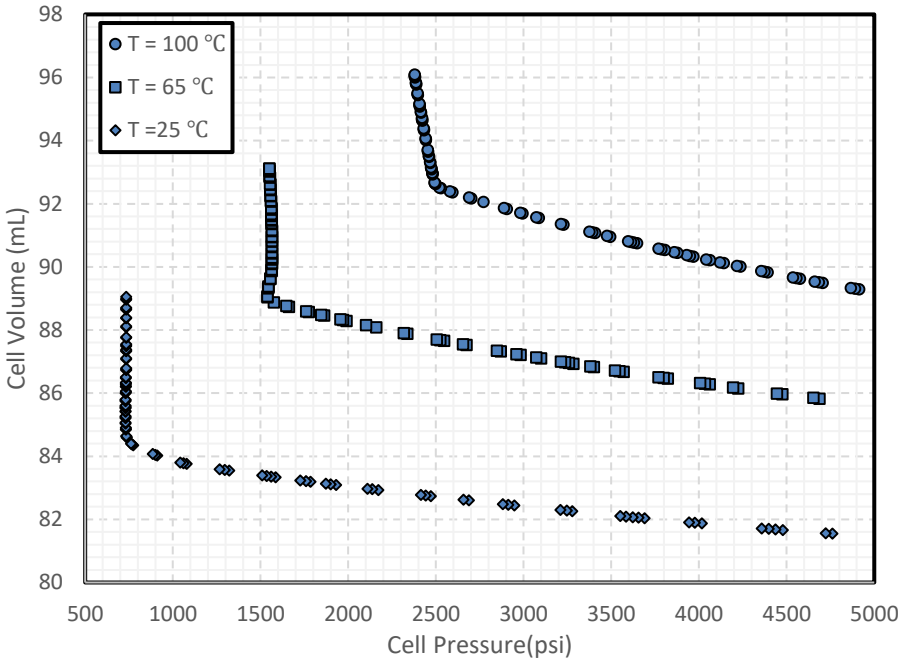

Figure A.9: CME Data for CO_2-TEC Blend with 80 mol% CO_2

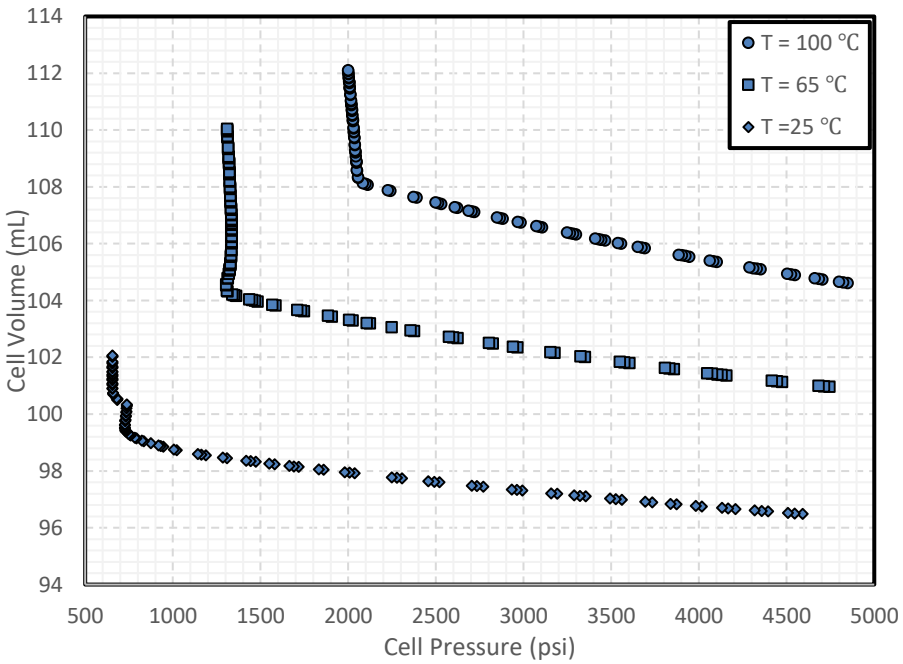

Figure A.10: CME Data for CO_2-TEC Blend with 75 mol% CO_2

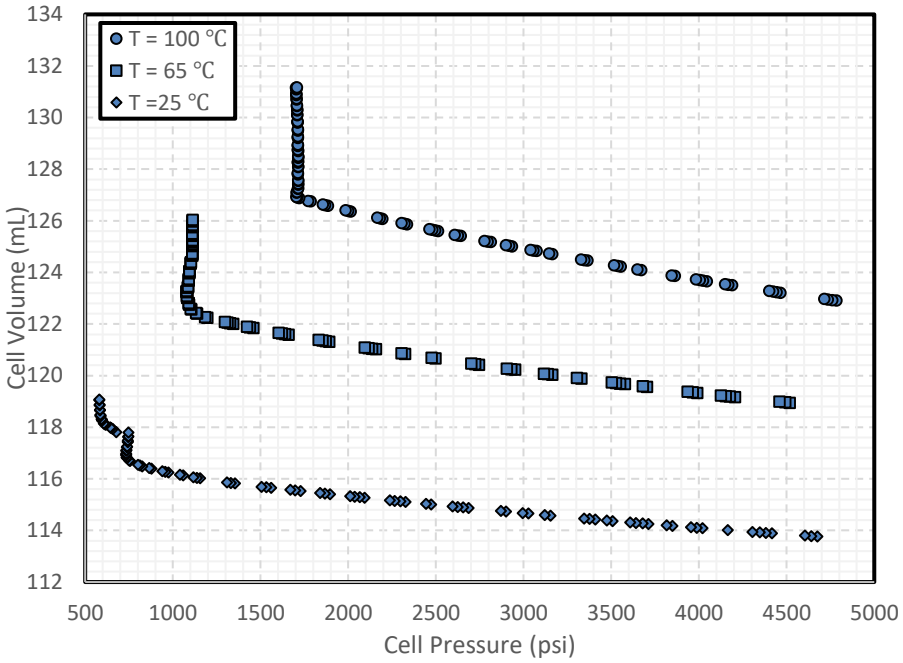

Figure A.11: CME Data for CO_2-TEC Blend with 70 mol% CO_2

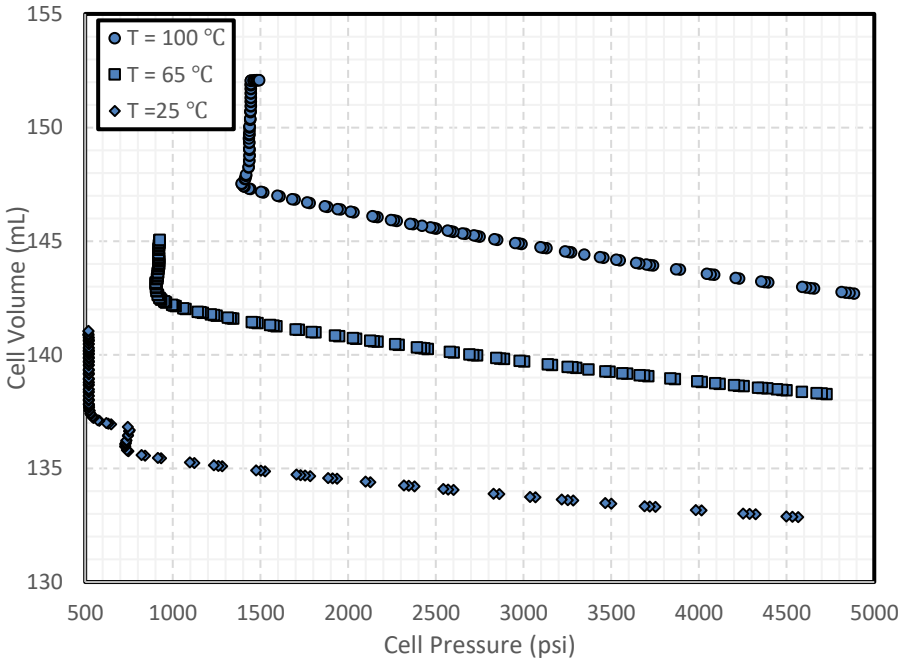

Figure A.12: CME Data for CO_2-TEC Blend with 65 mol% CO_2

A.3 Prediction of Saturation Pressure Using PR-EOS

Figures A.13 through **A.16** show the deviation of the saturation pressures predicted by PR-EOS from the experimental results. These predictions are based on the thermodynamic properties obtained from the literature, which are presented in **Table 4.7**.

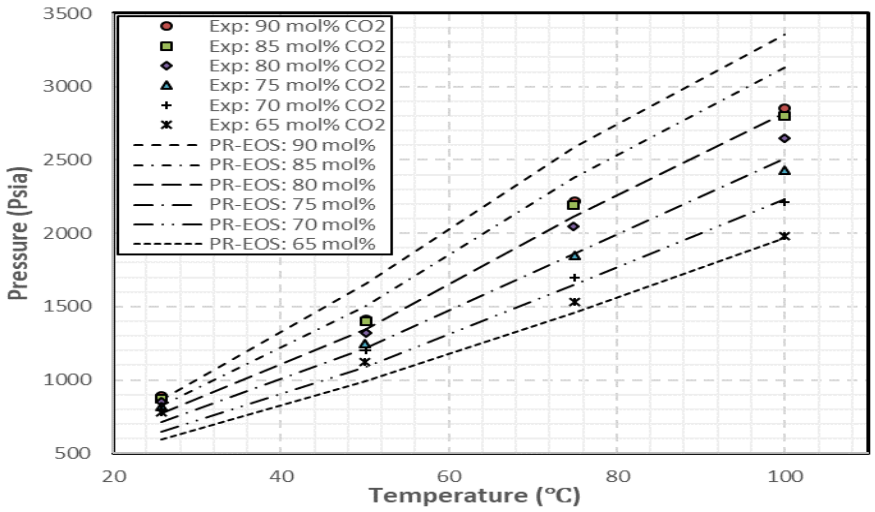

Figure A.13: Saturation Pressure of CO_2-EB Blend versus Temperature

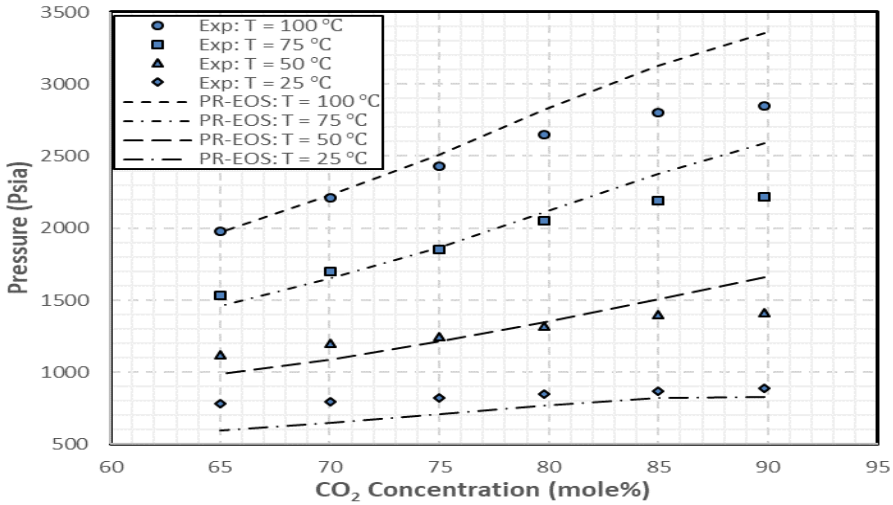

Figure A.14: Saturation Pressure of CO_2-EB Blend versus CO_2 Molar Concentration

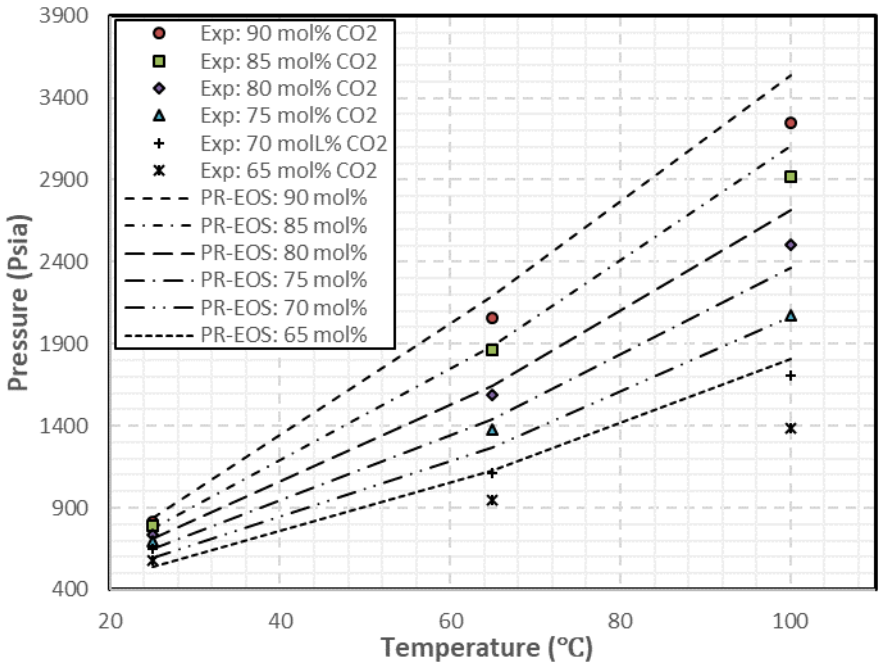

Figure A.15: Saturation Pressure of CO_2-TEC Blend versus Temperature

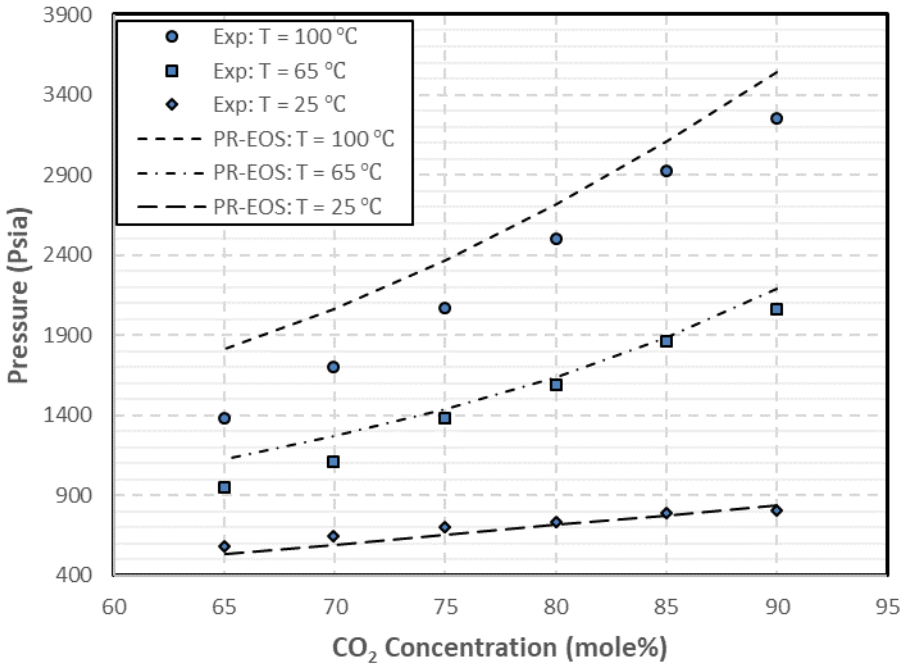

Figure A.16: Saturation Pressure of CO_2-TEC Blend versus CO_2 Molar Concentration

Table A.1 shows the parameters regressed to obtain the best prediction of the saturation pressures.

Table A.1: Regressed Parameters Obtained after Best Prediction of Saturation Pressure Using PR-EOS

Regressed Parameter	Compound			
	Ethyl Benzoate		Triethyl Citrate	
	Before Regression	After Regression	Before Regression	After Regression
Acentric Factor, ω	0.7690	0.2155	0.4140	0.4364
Critical Pressure, P_c (psia)	411.9	468.5	322.4	257.9
Interaction Coefficient	0	0.05	0	-0.012

APPENDIX B

DATA FROM CORE-FLOODING EXPERIMENTS

B.1 Data from Run 1-DO

Table B.1: Recovery Data from Run 1-DO

Time (minutes)	Total Injected CO_2 (mL)	Pore Volume Injected CO_2, PVI (vol/vol)	Cumulative Oil Produced, Np (mL)	Oil Recovery Factor, RF (%)
0	0.00	0.00	0.00	0.00
1	1.00	0.02	1.00	1.74
6	2.25	0.03	2.25	3.92
16	4.75	0.07	4.75	8.28
20	5.75	0.09	5.75	10.02
30	8.25	0.13	8.50	14.82
34	**9.25**	**0.14**	**9.00**	**15.69**
39	10.50	0.16	10.00	17.43
55	14.50	0.22	12.50	21.79
66	17.25	0.27	14.00	24.40
72	18.75	0.29	15.50	27.02
86	22.25	0.34	18.00	31.38
93	24.00	0.37	19.00	33.12
105	27.00	0.42	21.00	36.60
114	29.25	0.45	22.00	38.35
123	31.50	0.49	23.00	40.09
131	33.50	0.52	24.00	41.83
144	36.75	0.57	27.00	47.06
153	39.00	0.60	29.00	50.55
165	42.00	0.65	30.00	52.29
177	45.00	0.69	31.00	54.04
185	47.00	0.72	32.00	55.78
196	49.75	0.77	33.00	57.52
211	53.50	0.82	33.50	58.39
232	58.75	0.91	34.00	59.26
256	64.75	1.00	34.50	60.14
257	65.00	1.00	34.50	60.14

B.2 Data from Run 2-DO

Table B.2: Recovery Data from Run 2-DO

Time (minutes)	Total Injected CO_2-TEC Blend (mL)	Pore Volume Injected CO_2-TEC Blend, PVI (vol/vol)	Cumulative Oil Produced, Np (mL)	Oil Recovery Factor, RF (%)
0	0.00	0.00	0.00	0.00
1	0.25	0.00	0.25	0.46
10	2.50	0.04	2.50	4.57
19	4.75	0.07	4.75	8.68
30	7.50	0.12	7.50	13.71
42	10.50	0.16	10.50	19.20
51	12.75	0.20	12.75	23.31
62	15.50	0.24	15.50	28.34
70	**17.50**	**0.27**	**17.50**	**31.99**
80	20.00	0.31	19.00	34.73
91	22.75	0.35	21.25	38.85
93	23.25	0.36	21.75	39.76
95	23.75	0.36	22.25	40.68
96	24.00	0.37	22.75	41.59
97	24.25	0.37	23.00	42.05
100	25.00	0.38	23.50	42.96
111	27.75	0.43	26.00	47.53
120	30.00	0.46	27.50	50.27
133	33.25	0.51	30.00	54.84
141	35.25	0.54	31.50	57.59
153	38.25	0.59	33.25	60.79
160	40.00	0.61	34.00	62.16
169	42.25	0.65	35.50	64.90
174	43.50	0.67	36.25	66.27
188	47.00	0.72	37.50	68.56
196	49.00	0.75	38.00	69.47
200	50.00	0.77	38.25	69.93
212	53.00	0.81	39.00	71.30
224	56.00	0.86	39.50	72.21
231	57.75	0.89	39.75	72.67
242	60.50	0.93	39.75	72.67
248	62.00	0.95	39.75	72.67
256	64.00	0.98	39.75	72.67
263	65.75	1.01	39.75	72.67

B.3 Data from Run 1-LO

Table B.3: Recovery Data from Run 1-LO

Time (minutes)	Total Injected CO_2 (mL)	Pore Volume Injected CO_2, PVI (vol/vol)	Cumulative Oil Produced, Np (mL)	Oil Recovery Factor, RF (%)
0	0.00	0.000	0.00	0.000
5	1.25	0.020	1.25	2.233
9	2.25	0.035	2.25	4.020
14	3.50	0.055	3.50	6.253
24	6.00	0.094	6.00	10.720
29	7.25	0.113	7.25	12.953
34	**8.50**	**0.133**	**8.50**	**15.187**
45	11.25	0.176	10.00	17.867
57	14.25	0.223	11.50	20.547
64	16.00	0.250	12.00	21.440
72	18.00	0.281	13.50	24.120
80	20.00	0.313	14.50	25.907
88	22.00	0.344	15.25	27.247
93	23.25	0.363	15.75	28.140
102	25.50	0.399	16.75	29.927
115	28.75	0.449	18.50	33.053
122	30.50	0.477	19.25	34.393
129	32.25	0.504	20.00	35.733
136	34.00	0.531	20.50	36.627
147	36.75	0.574	21.50	38.413
156	39.00	0.610	22.00	39.307
167	41.75	0.653	23.00	41.093
175	43.75	0.684	23.50	41.987
183	45.75	0.715	24.00	42.880
192	48.00	0.750	24.50	43.773
208	52.00	0.813	25.50	45.560
216	54.00	0.844	26.00	46.453
223	55.75	0.872	26.50	47.347
229	57.25	0.895	27.00	48.240
237	59.25	0.926	27.25	48.687
247	61.75	0.965	27.25	48.687
255	63.75	0.997	27.50	49.133
256	64.00	1.000	27.50	49.133

B.4 Data from Run 2-LO

Table B.4: Recovery Data from Run 2-LO

Time (minutes)	Total Injected CO_2-TEC Blend (mL)	Pore Volume Injected CO_2-TEC Blend, PVI (vol/vol)	Cumulative Oil Produced, Np (mL)	Oil Recovery Factor, RF (%)
0	0.00	0.000	0.00	0.000
5	1.25	0.019	1.25	2.294
11	2.75	0.042	2.75	5.046
19	4.75	0.073	4.75	8.716
26	6.50	0.100	6.50	11.927
31	7.75	0.119	7.75	14.220
38	9.50	0.146	9.50	17.431
42	10.50	0.161	10.50	19.266
50	12.50	0.192	12.50	22.936
59	**14.75**	**0.226**	**14.75**	**27.064**
62	15.50	0.238	15.00	27.523
70	17.50	0.268	16.00	29.358
78	19.50	0.299	17.50	32.110
85	21.25	0.326	18.50	33.945
95	23.75	0.364	20.00	36.697
106	26.50	0.406	22.00	40.367
112	28.00	0.429	23.50	43.119
121	30.25	0.464	26.00	47.706
129	32.25	0.495	27.00	49.541
139	34.75	0.533	28.50	52.294
144	36.00	0.552	29.00	53.211
151	37.75	0.579	30.00	55.046
162	40.50	0.621	31.00	56.881
169	42.25	0.648	31.50	57.798
180	45.00	0.690	33.00	60.550
188	47.00	0.721	34.00	62.385
196	49.00	0.752	34.50	63.303
202	50.50	0.775	35.00	64.220
208	52.00	0.798	35.50	65.138
214	53.50	0.821	36.00	66.055
222	55.50	0.851	36.50	66.972
231	57.75	0.886	36.75	67.431
248	62.00	0.951	37.00	67.890
253	63.25	0.970	37.00	67.890
261	65.25	1.001	37.00	67.890

REFERENCES

[1] D. W. Green and G. P. Willhite, *Enhanced oil recovery*. Henry L. Doherty Memorial Fund of AIME, Society of Petroleum Engineers, 1998.

[2] I. Sandrea and R. Sandrea, "Global Oil Reserves – Recovery Factors Leave Vast Target for EOR Technologies .," *Oil Gas J.*, vol. 105, no. 45, pp. 1–8, 2007.

[3] V. Alvarado and E. Manrique, "Enhanced oil recovery: An update review," *Energies*, vol. 3, no. 9. pp. 1529–1575, 2010.

[4] G. Moritis, "CO2 sequestration adds new dimension to oil, gas production," *Oil gas J.*, vol. 101, no. 9, pp. 39–44, 2003.

[5] D. F. Martin and J. J. Taber, "Carbon Dioxide Flooding," *J. Pet. Technol.*, vol. 44, no. 04, pp. 396–400, Apr. 1992.

[6] L. W. Lake, R. T. Johns, W. R. Rossen, and G. A. Pope, *Fundamentals of enhanced oil recovery*. Richardson, TX: Society of Petroleum Engineers, 2014.

[7] J. J. Taber, F. D. Martin, and R. S. Seright, "EOR Screening Criteria Revisited - Part 1: Introduction to Screening Criteria and Enhanced Recovery Field Projects," *SPE Reserv. Eng.*, vol. 12, no. 3, pp. 189–198, 1997.

[8] J. J. Taber, F. D. Martin, and R. S. Seright, "EOR Screening Criteria Revisited—Part 2: Applications and Impact of Oil Prices," *SPE Reserv. Eng.*, vol. 12, no. 03, pp. 199–206, Aug. 1997.

[9] M. Kulkarni, "Immiscible and miscible gas-oil displacements in porous media," *LSU Master's Theses*, Jan. 2003.

[10] H. Yongmao and W. Zenggui, "Laboratory Investigation of CO2 Flooding," *SPE Int. Tech. Conf. Exhib.*, p. 6, 2004.

[11] R. B. Grigg and D. S. Schechter, "State of the Industry in CO2 Floods," in *SPE Annual Technical Conference and Exhibition*, 1997.

[12] J. Han, M. Lee, W. Lee, Y. Lee, and W. Sung, "Effect of gravity segregation on CO2 sequestration and oil production during CO2 flooding," *Appl. Energy*, vol. 161, pp. 85–91, Jan. 2016.

[13] P. M. Jarrell, C. Fox, M. Stein, and S. Webb, *Practical aspects of CO_2 flooding*. Richardson, TX USA: Society of Petroleum Engineers, 2002.

[14] A. M. Amao and S. Siddiqui, "Permian Basin: Historical Review of CO2 EOR Processes, Current Challenges and Improved Optimization Possibilities," in *The International Symposium of the Society of Core Analysts* , 2009.

[15] “Uthmaniyah Carbon Dioxide Enhanced Oil Recovery (CO2-EOR) Demonstration Project | CSLForum.” [Online]. Available: https://www.cslforum.org/cslf/Projects/Uthmaniyah.

[16] S. Kokal, M. Sanni, and A. Alhashboul, “Design and Implementation of the First CO2-EOR Demonstration Project in Saudi Arabia,” in *SPE Annual Technical Conference and Exhibition*, 2016.

[17] S. B. Dyer and S. M. F. Ali, “Linear Model Studies of the Immiscible CO2 WAG Process for Heavy-Oil Recovery,” *SPE Reserv. Eng.*, vol. 9, no. 02, pp. 107–111, May 1994.

[18] “Thermophysical Properties of Fluid Systems.” [Online]. Available: https://webbook.nist.gov/chemistry/fluid/.

[19] H. Sim Yeoh, G. Hean Chong, N. Mohd Azahan, R. Abdul Rahman, and T. S. Yaw Choong, “Solubility measurement method and mathematical modeling in supercritical fluids,” *Engineering Journal*, vol. 17, no. 3. pp. 67–78, 2013.

[20] L. W. Holm and V. A. Josendal, “Effect of Oil Composition on Miscible-Type Displacement by Carbon Dioxide,” *Soc. Pet. Eng. J.*, vol. 22, no. 01, pp. 87–98, Feb. 1982.

[21] Y. Wang and F. M. Orr, “Analytical calculation of minimum miscibility pressure,” *Fluid Phase Equilib.*, vol. 139, no. 1, pp. 101–124, 1997.

[22] F. S. Kovarik, “A Minimum Miscibility Pressure Study Using Impure CO2 and West Texas Oil Systems: Data Base, Correlations, and Compositional Simulation,” in *SPE Production Technology Symposium*, 1985.

[23] F. I. Stalkup, *Miscible displacement*. Henry L. Doherty Memorial Fund of AIME, Society of Petroleum Engineers of AIME, 1983.

[24] R. L. Christiansen and H. K. Haines, “Rapid Measurement of Minimum Miscibility Pressure With the Rising-Bubble Apparatus,” *SPE Reserv. Eng.*, vol. 2, no. 04, pp. 523–527, Nov. 1987.

[25] A. M. Elsharkawy, F. H. Poettmann, and R. L. Christiansen, “Measuring Minimum Miscibility Pressure: Slim-Tube or Rising-Bubble Method?,” in *SPE/DOE Enhanced Oil Recovery Symposium*, 1992.

[26] Y.-C. Song *et al.*, “Magnetic Resonance Imaging Study on the Miscibility of a CO2/n-Decane System,” *Chinese Phys. Lett.*, vol. 28, no. 9, p. 096401, Sep. 2011.

[27] Y. Liu, L. Jiang, Y. Song, Y. Zhao, Y. Zhang, and D. Wang, “Estimation of minimum miscibility pressure (MMP) of CO2 and liquid n-alkane systems using an improved MRI technique,” *Magn. Reson. Imaging*, vol. 34, no. 2, pp. 97–104, Feb. 2016.

[28] A. S. Al-Netaifi, “Experimental Investigation of CO2-Miscible Oil Recovery at

Different Conditions," King Saud University (KSU), 2008.

[29] C. Cronquist, "Carbon dioxide dynamic miscibility with light reservoir oils," in *Proc. Fourth Annual US DOE Symposium, Tulsa*, 1978, vol. 1, pp. 28–30.

[30] M. M. Oskay, D. A. Al-Shehri, S. A. Abu-khamsin, and M. A. Al-Marhoun, "Carbon-Dioxide Minimum Miscibility Pressure for Saudi-Arabian Crudes," *Arab. J. Sci. Eng.*, vol. 14, no. 2, pp. 169–180, 1989.

[31] A. Arshad, A. A. Al-Majed, H. Menouar, A. M. Muhammadain, and B. Mtawaa, "Carbon Dioxide (CO2) Miscible Flooding in Tight Oil Reservoirs: A Case Study," in *Kuwait International Petroleum Conference and Exhibition*, 2009.

[32] M. S. A. Perera, R. P. Gamage, T. D. Rathnaweera, A. S. Ranathunga, A. Koay, and X. Choi, "A Review of CO2-Enhanced oil recovery with a simulated sensitivity analysis," *Energies*, vol. 9, no. 7. p. 481, 2016.

[33] S. Haynes Jr and R. B. Alston, "Study of the Mechanisms of Carbon Dioxide Flooding and Applications to More Efficient EOR Projects," *SPE/DOE Enhanced Oil Recovery Symposium*. 1990.

[34] A. A. Zick, "A Combined Condensing/Vaporizing Mechanism in the Displacement of Oil by Enriched Gases," in *SPE Annual Technical Conference and Exhibition*, 1986.

[35] S. S. Alian, A. F. Alta'ee, A. A. Omar, and I. Hani, "Study of asphaltene precipitation during CO2 injection for Malaysian light oil reservoirs," in *2011 National Postgraduate Conference*, 2011, pp. 1–5.

[36] A. S. Al-Netaifi, "Experimental Investigation of CO2 -Miscible Oil Recovery at Different Conditions," King Saud University, 2008.

[37] J. Kim, J. Kim, J. Seo, H. Park, H. Seomoon, and W. Sung, "Effect of Miscibility Condition for CO2 Flooding on Gravity Drainage in 2D Vertical System," *J. Pet. Environ. Biotechnol.*, vol. 05, no. 03, pp. 1–4, Jul. 2014.

[38] D. J. Stephenson, A. G. Graham, and R. W. Luhning, "Mobility Control Experience in the Joffre Viking Miscible CO2 Flood," *SPE Reserv. Eng.*, vol. 8, no. 03, pp. 183–188, 1993.

[39] Z. Li and Y. Gu, "Soaking effect on miscible CO2 flooding in a tight sandstone formation," *Fuel*, vol. 134, pp. 659–668, 2014.

[40] J. M. Nordbotten, M. A. Celia, and S. Bachu, "Injection and storage of CO2 in deep saline aquifers: Analytical solution for CO2 plume evolution during injection," *Transp. Porous Media*, vol. 58, no. 3, pp. 339–360, 2005.

[41] J. B. Moortgat, A. Firoozabadi, Z. Li, and R. O. Espósito, "CO2 Injection in Vertical and Horizontal Cores: Measurements and Numerical Simulation," *SPE J.*, vol. 18, no. 02, pp. 331–344, 2013.

[42] R. M. Enick, D. K. Olsen, J. R. Ammer, and W. Schuller, “Mobility and Conformance Control for CO2 EOR via Thickeners, Foams, and Gels -- A Literature Review of 40 Years of Research and Pilot Tests,” in *SPE Improved Oil Recovery Symposium*, 2012.

[43] R. M. Enick and D. K. Olsen, “Mobility and Conformance Control for Carbon Dioxide Enhanced Oil Recovery (CO2-EOR) via Thickeners, Foams, and Gels–A Detailed Literature Review of 40 Years of Research,” 2012.

[44] M. Liu, A. Andrianov, and W. R. Rossen, “Sweep Efficiency in CO2 Foam Simulations with Oil,” *SPE Eur. Annu. Conf. Exhib.*, no. April 2011, pp. 1–18, 2013.

[45] X. Duan, J. Hou, F. Zhao, Y. Ma, and Z. Zhang, “Determination and controlling of gas channel in CO2 immiscible flooding,” *J. Energy Inst.*, vol. 89, no. 1, pp. 12–20, Feb. 2016.

[46] F. Friedmann, W. H. Chen, and P. A. Gauglitz, “Experimental and Simulation Study of High-Temperature Foam Displacement in Porous Media,” *SPE Reserv. Eng.*, vol. 6, no. 01, pp. 37–45, Feb. 1991.

[47] W. R. Rossen and W. J. Renkema, “Success of Foam SAG Processes in Heterogeneous Reservoirs,” in *SPE Annual Technical Conference and Exhibition*, 2007.

[48] N. F. Djabbarah, “Miscible oil recovery process using carbon dioxide and alcohol,” US4899817A, 15-Dec-1988.

[49] F. Al-Otaibi, S. Kokal, H. Schmidt, and Y. Chang, “Densifying carbon dioxide with a dispersion of carbon dioxide-philic water capsules,” US20180258341A1, 11-May-2018.

[50] S. Babamohammadi, A. Shamiri, and M. K. Aroua, “A review of CO2 capture by absorption in ionic liquid-based solvents,” *Reviews in Chemical Engineering*, vol. 31, no. 4. pp. 383–412, 2015.

[51] J. L. Anthony, E. J. Maginn, and J. F. Brennecke, “Solution thermodynamics of imidazolium-based ionic liquids and water,” *J. Phys. Chem. B*, vol. 105, no. 44, pp. 10942–10949, 2001.

[52] S. G. Kazarian, N. Sakellarios, and C. M. Gordon, “High-pressure CO2-induced reduction of the melting temperature of ionic liquids.,” *Chem. Commun.*, no. 12, pp. 1314–1315, 2002.

[53] L.-C. Feng, K.-W. Cheng, M. Tang, and Y.-P. Chen, “Vapor–liquid equilibria of carbon dioxide with ethyl benzoate, diethyl succinate and isoamyl acetate binary mixtures at elevated pressures,” *J. Supercrit. Fluids*, vol. 21, no. 2, pp. 111–121, Oct. 2001.

[54] S. Shen, Y. Yang, Y. Wang, S. Ren, J. Han, and A. Chen, “CO2 absorption into aqueous potassium salts of lysine and proline: Density, viscosity and solubility of

CO2," *Fluid Phase Equilib.*, vol. 399, pp. 40–49, Aug. 2015.

[55] H.-Y. Chiu, A. H. Tiwikrama, Y.-R. Gou, H. Lin, and M.-J. Lee, "Phase equilibria of ternary systems of carbon dioxide + ethanol, dimethyl sulfoxide, or N,N-dimethyl formamide + water at elevated pressures including near critical regions," *Fluid Phase Equilib.*, vol. 429, pp. 84–92, Dec. 2016.

[56] P. Ilieva, A. Kilzer, and E. Weidner, "Measurement of solubility, viscosity, density and interfacial tension of the systems tristearin and CO 2 and rapeseed oil and CO 2," *J. Supercrit. Fluids*, vol. 117, pp. 40–49, Nov. 2016.

[57] X. Li, X. Liu, Y. Jiang, and D. Deng, "Solubilities and Thermodynamic Properties of Carbon Dioxide in Some Biobased Solvents," *J. Chem. Eng. Data*, vol. 61, no. 9, pp. 3355–3362, Sep. 2016.

[58] T. Kegl, G. Kravanja, Ž. Knez, and M. Knez Hrnčič, "Effect of addition of supercritical CO2 on transfer and thermodynamic properties of biodegradable polymers PEG 600 and Brij52," *J. Supercrit. Fluids*, vol. 122, pp. 10–17, Apr. 2017.

[59] A. Bera and H. Belhaj, "Ionic liquids as alternatives of surfactants in enhanced oil recovery—A state-of-the-art review," *Journal of Molecular Liquids*, vol. 224. pp. 177–188, 2016.

[60] K. E. Johnson, "What's an Ionic Liquid?," *Electrochemistry*, vol. Spring, pp. 38–41, 2007.

[61] S. Lago, H. Rodríguez, M. K. Khoshkbarchi, A. Soto, and A. Arce, "Enhanced oil recovery using the ionic liquid trihexyl(tetradecyl)phosphonium chloride: phase behaviour and properties," *RSC Adv.*, vol. 2, no. 25, p. 9392, 2012.

[62] S. Keskin, D. Kayrak-Talay, U. Akman, and Ö. Hortaçsu, "A review of ionic liquids towards supercritical fluid applications," *Journal of Supercritical Fluids*, vol. 43, no. 1. pp. 150–180, 2007.

[63] M. Ramdin, T. W. De Loos, and T. J. H. Vlugt, "State-of-the-art of CO 2 capture with ionic liquids," *Industrial and Engineering Chemistry Research*, vol. 51, no. 24. pp. 8149–8177, 2012.

[64] A. P. Abbott, D. Boothby, G. Capper, D. L. Davies, and R. K. Rasheed, "Deep Eutectic Solvents formed between choline chloride and carboxylic acids: Versatile alternatives to ionic liquids," *J. Am. Chem. Soc.*, vol. 126, no. 29, pp. 9142–9147, 2004.

[65] D. Carriazo, M. C. Serrano, M. C. Gutiérrez, M. L. Ferrer, and F. del Monte, "Deep-eutectic solvents playing multiple roles in the synthesis of polymers and related materials," *Chem. Soc. Rev.*, vol. 41, no. 14, p. 4996, 2012.

[66] M. Althuluth, M. T. Mota-Martinez, M. C. Kroon, and C. J. Peters, "Solubility of carbon dioxide in the ionic liquid 1-ethyl-3- methylimidazolium tris(pentafluoroethyl)trifluorophosphate," *J. Chem. Eng. Data*, vol. 57, no. 12, pp.

3422–3425, 2012.

[67] S. G. Nam and B. C. Lee, “Solubility of carbon dioxide in ammonium-based ionic liquids: Butyltrimethylammonium bis(trifluoromethylsulfonyl)imide and methyltrioctylammonium bis(trifluoromethylsulfonyl)imide,” *Korean J. Chem. Eng.*, vol. 30, no. 2, pp. 474–481, 2013.

[68] T. Makino, M. Kanakubo, T. Umecky, and A. Suzuki, “CO2 solubility and physical properties of N-(2-hydroxyethyl)pyridinium bis(trifluoromethanesulfonyl)amide,” *Fluid Phase Equilib.*, vol. 357, pp. 64–70, Nov. 2013.

[69] P. J. Carvalho *et al.*, “High pressure density and solubility for the CO2 + 1-ethyl-3-methylimidazolium ethylsulfate system,” *J. Supercrit. Fluids*, vol. 88, pp. 46–55, Apr. 2014.

[70] Y. Chen, N. Ai, G. Li, H. Shan, Y. Cui, and D. Deng, “Solubilities of carbon dioxide in eutectic mixtures of choline chloride and dihydric alcohols,” *J. Chem. Eng. Data*, vol. 59, no. 4, pp. 1247–1253, 2014.

[71] G. Li, D. Deng, Y. Chen, H. Shan, and N. Ai, “Solubilities and thermodynamic properties of CO2 in choline-chloride based deep eutectic solvents,” *J. Chem. Thermodyn.*, vol. 75, pp. 58–62, Aug. 2014.

[72] D. Deng, Y. Jiang, X. Liu, Z. Zhang, and N. Ai, “Investigation of solubilities of carbon dioxide in five levulinic acid-based deep eutectic solvents and their thermodynamic properties,” *J. Chem. Thermodyn.*, vol. 103, pp. 212–217, 2016.

[73] Y. Ji, Y. Hou, S. Ren, C. Yao, and W. Wu, “Phase equilibria of high pressure CO2and deep eutectic solvents formed by quaternary ammonium salts and phenol,” *Fluid Phase Equilib.*, vol. 429, pp. 14–20, 2016.

[74] N. da P. M. Zakrzewska, M., “Volumetric and phase behaviour of mixtures of fluoroalkylphosphate-based ionic liquids with high pressure carbon dioxide,” *J. Supercrit. Fluids*, vol. 113, pp. 61–65, 2016.

[75] F. M. Orr, M. K. Silva, C. L. Lien, and M. T. Pelletier, “Laboratory Experiments To Evaluate Field Prospects for CO2 Flooding,” *J. Pet. Technol.*, vol. 34, no. 04, pp. 888–898, Apr. 1982.

[76] E. T. S. Huang and J. H. Tracht, “The Displacement of Residual Oil By Carbon Dioxide,” in *SPE Improved Oil Recovery Symposium*, 1974.

[77] G. C. Wang, “Microscopic Investigation of CO2, Flooding Process,” *J. Pet. Technol.*, vol. 34, no. 08, pp. 1789–1797, Aug. 1982.

[78] Y. Sun, Q. Li, D. Yang, and X. Liu, “Laboratory core flooding experimental systems for CO2 geosequestration: An updated review over the past decade,” *Journal of Rock Mechanics and Geotechnical Engineering*, vol. 8, no. 1. pp. 113–126, 2016.

[79] D. L. Tiffin and V. J. Kremesec, “Mechanistic Study of Gravity-Assisted CO2

Flooding," *SPE Reserv. Eng.*, vol. 3, no. 02, pp. 524–532, May 1988.

[80] K. Asghari and F. Torabi, "Effect of Miscible and Immiscible CO2 Injection on Gravity Drainage: Experimental and Simulation Results," in *SPE Symposium on Improved Oil Recovery*, 2008.

[81] A. A. Hamouda and V. A. Tabrizy, "The effect of light gas on miscible CO2 flooding to enhance oil recovery from sandstone and chalk reservoirs," *J. Pet. Sci. Eng.*, vol. 108, pp. 259–266, 2013.

[82] "Ostwald's Viscometer," *Croatian-English Chemistry Dictionary & Glossary*. [Online]. Available: https://glossary.periodni.com/glossary.php?en=Ostwald's+viscometer.

[83] A. M. Hassan and H. S. Al-Hashim, "Cost Effective Chelating Agent EOR Fluid System for Carbonate Reservoirs," in *SPE Kingdom of Saudi Arabia Annual Technical Symposium and Exhibition*, 2016.

[84] "Critical properties and acentric factor—Organic compounds," pp. 1–95, Jan. 2009.

[85] "Ethyl citrate," pp. 2–3, 2018.

[86] D. Y. Peng and D. B. Robinson, "A New Two-Constant Equation of State," *Ind. Eng. Chem. Fundam.*, vol. 15, no. 1, pp. 59–64, 1976.

[87] "Core Laboratories: PVT Cell 300 ml 700 bar Full Visibility Educational," 2018. [Online]. Available: https://www.corelab.com/sanchez/pvt-studies/pvt-300-700-fv-edu. [Accessed: 21-Dec-2018].

[88] M. Hassan, R. N. Gajbhiye, A. S. Sultan, and S. Abu-Khamsin, "Measurement of Bubble Point Pressures of n-Decane, CO2 and N2 Mixtures," in *SPE Kingdom of Saudi Arabia Annual Technical Symposium and Exhibition*, 2016.

[89] J.-H. Yim and J. S. Lim, "CO2 solubility measurement in 1-hexyl-3-methylimidazolium ([HMIM]) cation based ionic liquids," *Fluid Phase Equilib.*, vol. 352, pp. 67–74, Aug. 2013.

[90] D. Peng and D. Robinson, *The characterization of the heptanes and heavier fractions*. Tulsa, Okla.: Gas Processors Association, 1978.

[91] T. Ahmed, *Equations of State and PVT Analysis: Applications for Improved Reservoir Modeling: Second Edition*. 2016.

[92] "EOR Coreflood System for Gas Injection - Vindum Engineering." [Online]. Available: https://vindum.com/product-category/eor-coreflood-system-for-gas-injection/. [Accessed: 28-Dec-2018].

[93] A. R. Adebayo, A. A. Barri, and M. S. Kamal, "Effect of Flow Direction on Relative Permeability Curves in Water/Gas Reservoir System: Implications in Geological CO2 Sequestration," *Geofluids*, vol. 2017, pp. 1–10, Jul. 2017.

[94] M. S. Kamal, A. R. Adebayo, L. T. Fogang, and A. A. Barri, “Improving Gas Sequestration by Surfactant-Alternating-Gas Injection: A Comparative Evaluation of the Surfactant Type and Concentration,” *J. Surfactants Deterg.*, vol. 21, no. 5, pp. 667–675, Sep. 2018.

[95] “Model 906 CO2 Analyzer for Process & Research.” [Online]. Available: http://www.quantekinstruments.com/model-906-co2-analyzer/. [Accessed: 01-Jan-2019].

[96] M. A. Al-Marhoun, “PVT Correlations for Middle East Crude Oils,” *J. Pet. Technol.*, vol. 40, no. 05, pp. 650–666, May 1988.

[97] M. B. Standing, *Volumetric and Phase Behavior of Oil Field Hydrocarbon System*, 9th ed. Dallas, TX.: Society of Petroleum Engineers, 1981.

[98] S. A. Abu-Khamsin and M. A. Al-Marhoun, “Development of a New Correlation for Bubble-Point Oil Viscosity,” *Arab. J. Sci. Eng.*, vol. 16, pp. 99–106, 1991.

[99] S. A. Khan, M. A. Al-Marhoun, S. O. Duffuaa, and S. A. Abu-Khamsin, “Viscosity Correlations for Saudi Arabian Crude Oils,” in *Middle East Oil Show*, 1987.

[100] Z. Al Yousef, “Study of CO2 Mobility Control in Heterogeneous Media Using CO2 Thickening Agents,” Texas A & M University, 2012.

[101] O. S. Hjelmeland and L. E. Larrondo, “Experimental Investigation of the Effects of Temperature, Pressure, and Crude Oil Composition on Interfacial Properties,” *SPE Reserv. Eng.*, vol. 1, no. 04, pp. 321–328, Jul. 1986.

[102] A. Graue, B. G. Viksund, T. Eilertsen, and R. Moe, “Systematic wettability alteration by aging sandstone and carbonate rock in crude oil,” *J. Pet. Sci. Eng.*, vol. 24, no. 2–4, pp. 85–97, Dec. 1999.

[103] G. M. Kontogeorgis, E. C. Voutsas, I. V. Yakoumis, and D. P. Tassios, “An Equation of State for Associating Fluids,” *Ind. Eng. Chem. Res.*, vol. 35, no. 11, pp. 4310–4318, 1996.

Vitae

Name	: Khaled Hussein Muhammed Al-Azani
Nationality	: Yemeni
Data of Birth	: 04/01/1992
Email	: g201080760@gmail.com
Address	: Rada'a, Al-Baydha'a, Yemen

Academic Background : **Master's in petroleum engineering**

April, 2019

King Fahd University of Petroleum & Minerals

Dhahran, Saudi Arabia

BS in Petroleum Engineering

May, 2016

King Fahd University of Petroleum & Minerals

Dhahran, Saudi Arabia

GPA: 3.92/4.00 (1st honor)